UNIVERSITY OF CALIFORNIA

Santa Barbara

Structural Evolution of an Extensional Terrane Margin: Case Studies from the Colorado River Extensional Corridor, Southeastern California, USA

A Thesis submitted in partial satisfaction of the

requirements for the degree Master of Science

in Earth Science

by

Justin Ronald Newmann

Committee in charge:

Professor Phillip B. Gans, Chair

Professor Zachary C. Eilon

Professor Kristin D. Morell

December 2019

The thesis of Justin Ronald Newmann is approved.

_____

Zachary C. Eilon

_____

Kristin D. Morell

_____

Phillip B. Gans, Committee Chair

December 2019

Structural Evolution of an Extensional Terrane Margin: Case Studies from the Colorado River Extensional Corridor, Southeastern California, USA

by

Justin Ronald Newmann

ACKNOWLEDGEMENTS

Thank you first and foremost to my inimitable advisor Dr. Phillip B. Gans, who has taught me more in the last six years than I ever could've imagined. Phil, your guidance, leadership, patience, and care has enabled my growth as a scientist and person, and set me up for a lifetime of curiosity driven experience. Thank you. I would also like to thank Dr. Zachary Eilon and Dr. Kristin Morell for serving on my committee and giving me feedback and advice whenever I sought it. Special thanks to Mom and Dad for their constant support and for exposing me to the wonders of the Earth from the very beginning. Extra special thanks to Dad for making me walk across the Grand Canyon when I was 15, sparking my interest in the natural sciences. Thanks also to Evan Monroe and Alex Wrobel for all the good times across the Basin and Range, the stimulating conversations, and the dusty jam sessions; and to Alaina Rosenthal-Guillot for assisting me in the field. Thanks to the entire Earth Science department for making me into a geologist and to my family at the Cheetah House for their love and support. Finally, special thanks to my guitar, bandmates, and the power of music for keeping me sane in trying times and allowing me to express myself in ways scientific writing never will.

ABSTRACT

Structural Evolution of an Extensional Terrane Margin: Case Studies from the Colorado River Extensional Corridor, Southeastern California, USA

by

Justin Ronald Newmann

The lower Colorado River extensional corridor (CREC) is an area of extreme crustal extension (>100%) which borders areas of moderate to minimal (<15%) extension. Regionally extensive detachment (low-angle normal) fault models commonly applied to the CREC define the margin of the extensional terrane as a discrete "breakaway" where the detachment fault originally intersected the surface. Results of field investigations along the CREC margin reveal locally complex deformation histories inconsistent with simple detachment models. In the Little Piute and northwest Piute Mountain areas, the dominant extension direction (NW-SE) is orthogonal to the commonly observed extension direction in the CREC (SW-NE), multiple generations of strike slip and oblique normal faults are present, and deformation occurred after roughly 17.7 Ma. These observations suggest a complex strain field evolved throughout the Miocene along the western margin of the CREC. Westward tilting of the Piute Mountain block indicates extensional deformation persisted beyond the previously hypothesized

CREC breakaway. In the Piute Range, west-directed normal faults dip steeply (60°) and have cutoff angles near 90° showing no obvious relationship to east-dipping detachment faults documented to the south (Homer Mountain) and east (Newberry Mountains). In all study areas the observed deformation history is more complex than expected in simple detachment fault breakaway models, suggesting current models are inadequate in describing deformation patterns along the margin of highly extended terranes.

TABLE OF CONTENTS

LIST OF FIGURES

1. Introduction and Geologic Background

1.1 Introduction

The Basin and Range Province (B&R) of western North America (Fig. 1.1) is a classic natural laboratory for the study of extensional tectonics and intracontinental extensional processes. Decades of study across the vast province (>800,000 km^2) have informed understanding of the mechanics, timing, and tectonic significance of extensional deformation and related magmatic processes. Extension in the B&R is not uniformly distributed. Increasingly detailed studies continue to reveal significant complexity in the space-time pattern of extension, the magnitude and distribution of localized extension, and the relationship between magmatism and extension.

Many of the more highly extended regions of the B&R contain metamorphic core complexes (MCCs) and associated low angle normal faults (LANFs, also called detachment faults). MCCs and LANFs are topics of considerable controversy and have been disproportionally studied relative to less extended regions. One such highly extended region within the B&R is the lower Colorado River extensional corridor (CREC, Fig. 1.2), home to a series of well-known MCCs (Buckskin-Rawhide, Whipple, Chemehuevi, and Sacramento Mountains). Debate has raged in the CREC over topics such as the geometry, original orientation, and areal extent of detachment faults, the relationship between extension, magmatism, and sedimentation, and the kinematic evolution of extension within the corridor.

Areas which may shed considerable light on the tectonic evolution of highly extended regions and MCCs are the “transition zones” between highly extended and

neighboring much less extended crust. These less extended areas may preserve a more complete record of the deformation field and fault history in the early stages of extension, thus providing insight into the initial conditions of deformation in highly extended domains. In particular, predictions made by models that invoke a large scale detachment fault underlying highly extended regions and surfacing at a "breakaway" can be tested against the observed deformation history. Structures along the margin of highly extended domains provide an opportunity to better understand the geometry and kinematics of upper crustal deformation in such areas, subjects which are difficult to constrain in MCCs due to the extreme magnitude of extension.

This project clarifies the history and kinematics of deformation along the western margin of the central CREC through a combination of detailed geologic mapping, cross section construction, sedimentary basin analysis, and structural analysis of mesoscopic faults. Study sites in the Little Piute Mountains, northwest Piute Mountains, and Piute Range (Fig. 1.2) are selected because they lie close to the inferred western margin of the CREC and contain well preserved accumulations of Miocene sedimentary and volcanic rocks associated with extension. Mapping was carried out between October, 2017 and March, 2019 on satellite and topographic base maps (1:5000 scale) with assistance of handheld GPS. Structural data are analyzed using Faultkin and Stereonet programs first published by Allmendinger et al. (1992). New observations presented here call into question the validity of large scale detachment models for highly extended regions and suggest greater complexity and heterogeneity in the deformational strain field than previously considered.

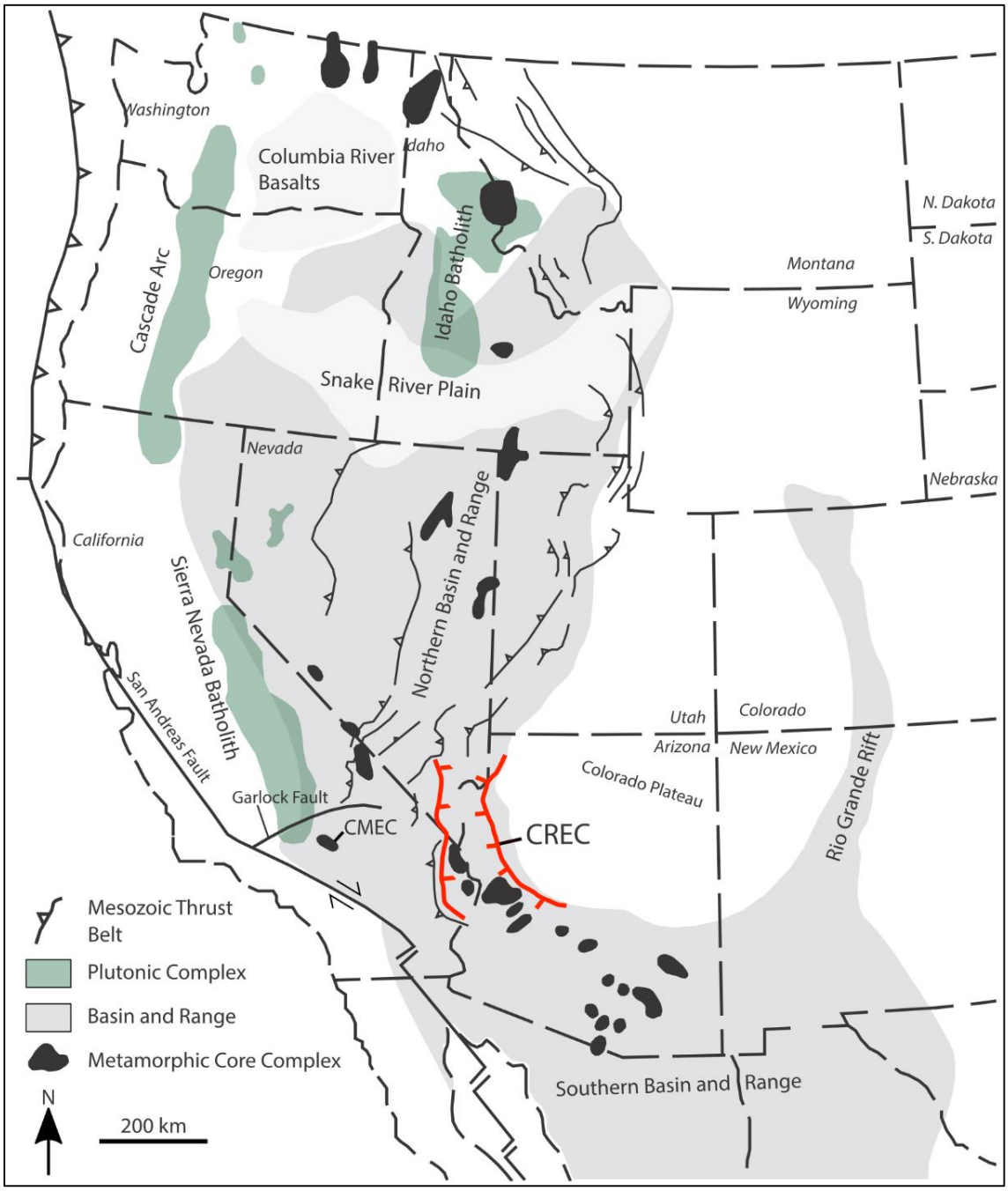

Figure 1.1: Tectonic overview map of western North America showing approximate location of Colorado River extensional corridor within Basin and Range Province. Modified from Gans and Bohrson, 1998.

1.2 Geologic Background

The CREC is an approximately 200 km long, 50–100 km wide zone of large magnitude extension centered around the California-Nevada-Arizona border region and stretching from the latitude of Las Vegas, NV to the latitude of Parker, AZ. The corridor borders the unextended Colorado Plateau to the east and the moderately extended Mojave Desert to the west. Mountain ranges along the Colorado River (Whipple, Chemehuevi, Sacramento, etc.) expose mid-crustal mylonites and are the site of localized extreme extension up to 400% (Lister and Davis, 1988). The domal uplifts which expose these mid-crustal rocks beneath extensive low-angle "detachment" faults are considered classic cordilleran metamorphic core complexes. Other major ranges within the corridor expose a variety of upper crustal rocks ranging from Proterozoic to Quaternary in age.

1.2.1 General Geologic History

The CREC lies near the edge of the North American craton and contains rocks which span much of the tectonic history of western North America. Proterozoic crystalline basement of the eastern Mojave formed c. 2.3–2.0 Ga (Bennett and DePaolo, 1987) and was highly metamorphosed from 1.7–1.3 Ga (Wooden and Miller, 1990). Regionally metamorphosed, deformed Paleozoic strata—correlative with the classic cratonal section of the western Grand Canyon, AZ and spanning from Cambrian to Permian time—unconformably overlie pЄ rocks and are exposed in isolated outcrops scattered throughout the eastern Mojave region (Stone et al., 1983). The CREC lies near the eastern edge of the Jurassic-Cretaceous magmatic arc and contains abundant plutonic rocks of that age owing to subduction beneath the west coast of ancestral North America

(Hamilton, 1969; Kistler, 1974). Virtually no rocks of early Cenozoic age have been identified in the CREC region, suggesting a prolonged period of erosion and external drainage with no magmatism.

The oldest Cenozoic rocks in the CREC are latest Oligocene sedimentary and volcanic accumulations associated with the onset of tectonic extension in the southernmost corridor c. 26 Ma (Lucchitta and Suneson, 1996). Oligocene to late Miocene sedimentary, volcanic, and plutonic rocks are found throughout the corridor in isolated centers (e.g. Old Woman-Piute Mountains) and continuous preserved expanses (e.g. Piute Range, Black Mountains). Quaternary alluvium covers most of the area of the eastern Mojave Desert and CREC such that mountain ranges represent islands of bedrock in a sea of alluvial deposits. Although pre-Miocene events in the CREC are not the focus of this study, the long and complex tectonic history of the region may have exerted profound influence on the location and geometry of subsequent extensional deformation in the Miocene and is an important consideration when evaluating more recent tectonic events.

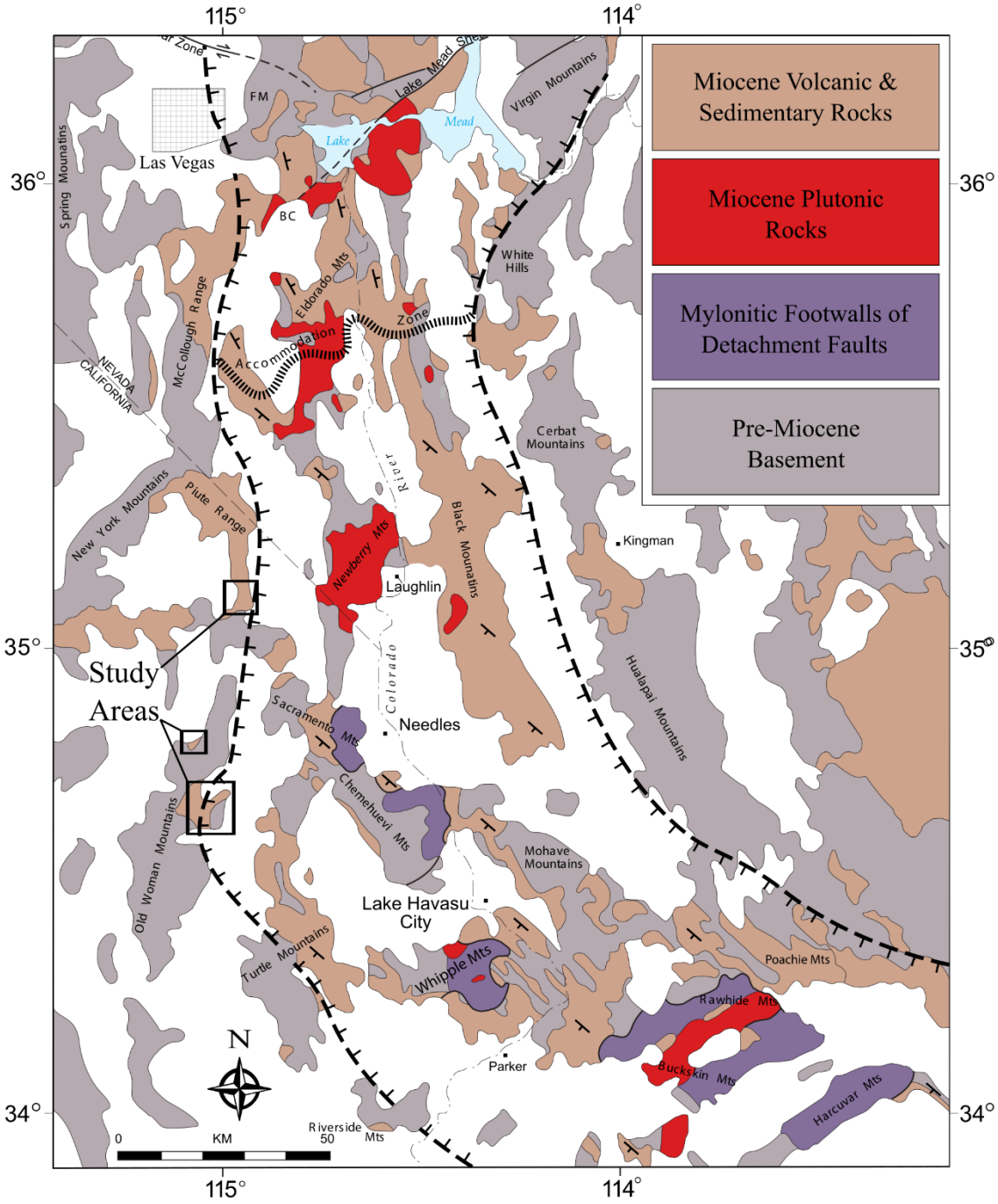

Figure 1.2: Overview map of Colorado River extensional corridor showing distribution of rock types, approximate boundaries of corridor (dashed lines), and location of study areas. Modified from Gans and Gentry, 2016.

1.2.2 Miocene Evolution of the CREC

The CREC was originally defined as the west-southwest tilt domain (region of uniform fault block tilt direction, see Stewart, 1980) around the lower Colorado River from roughly Parker, AZ to Laughlin, NV and centered on the axial trace of the belt of MCCs running from the Buckskin-Rawhide Mountains to the Sacramento Mountains (Howard and John, 1987). The corridor has since been expanded northward to include highly extended east-northeast tilted Miocene rocks between Laughlin and Lake Mead, NV (Faulds et al., 2001). The present conception of the CREC is a zone of large magnitude extension which contains two oppositely dipping tilt domains separated by an accommodation zone (see Faulds and Varga, 1998), characterized by detachment fault and MCC exposure in the southern portion and abundant Miocene magmatism and high-angle normal faulting in the northern portion.

In the southern portion of the corridor the dominant documented extension direction is northeast-southwest (030–050°; see Fig. 1.3). Extension directions are determined based on tilting of Miocene rocks, slickenlines on detachment faults, and kilometer scale corrugations in detachment surfaces (Howard and John, 1987; Lister and Davis, 1989; Spencer and Reynolds, 1991). Recent work has called into question the uniformity of extension direction across the southern ranges (e.g. Ferguson et al., 2013). In the northern portion of the corridor (latitude 35°–36° N) extension directions are variable. North of the accommodation zone, fault motion is west directed (~260°) with rocks tilted to the east. The accommodation zone between the northern and southern

portions of the corridor is an area of complex faulting and folding, like accommodation zones observed in other parts of the Basin and Range (Faulds et al., 2001).

Intracontinental rifting in the CREC occurred primarily from 22 Ma to 12 Ma (Fig. 1.3), propagating from south to north (Glazner and Bartley, 1984). Thermochronologic studies in the southern corridor suggest detachment fault slip began in the Buckskin-Rawhide Mountains c. 21 Ma (Singleton et al., 2014), in the Whipple and Chemehuevi Mountains c. 20 Ma (John and Foster, 1993; Gans and Gentry, 2016), and in the Sacramento Mountains c. 18.5 Ma (Foster and John, 1999). The regionally distributed Peach Spring Tuff (PST; of Young and Brennan, 1974; see also Glazner et al., 1986) provides an important temporal marker (age = 18.8 Ma, Ferguson et al., 2013) and corroborates northward propagation of extensional deformation in the southern CREC. In the Whipple Mountains the PST is near flat lying, undeformed, and overlies the entirety of the volcanic section while in the Sacramento Mountains the tuff dips as much as 70° and is located near the base of the volcanic section, suggesting upper plate block rotation in the Whipple Mountains had ceased by 18.8 Ma but was just beginning in the Sacramento Mountains. Magmatism and extension continued to propagate northward, with extension initiating in the Newberry and Black Mountains c. 16 Ma (Faulds et al., 1995), El Dorado Mountains c. 14.5 Ma (Gans and Bohrson, 1998), and terminating near Lake Mead, NV by 11.3 Ma (Faulds et al., 1995).

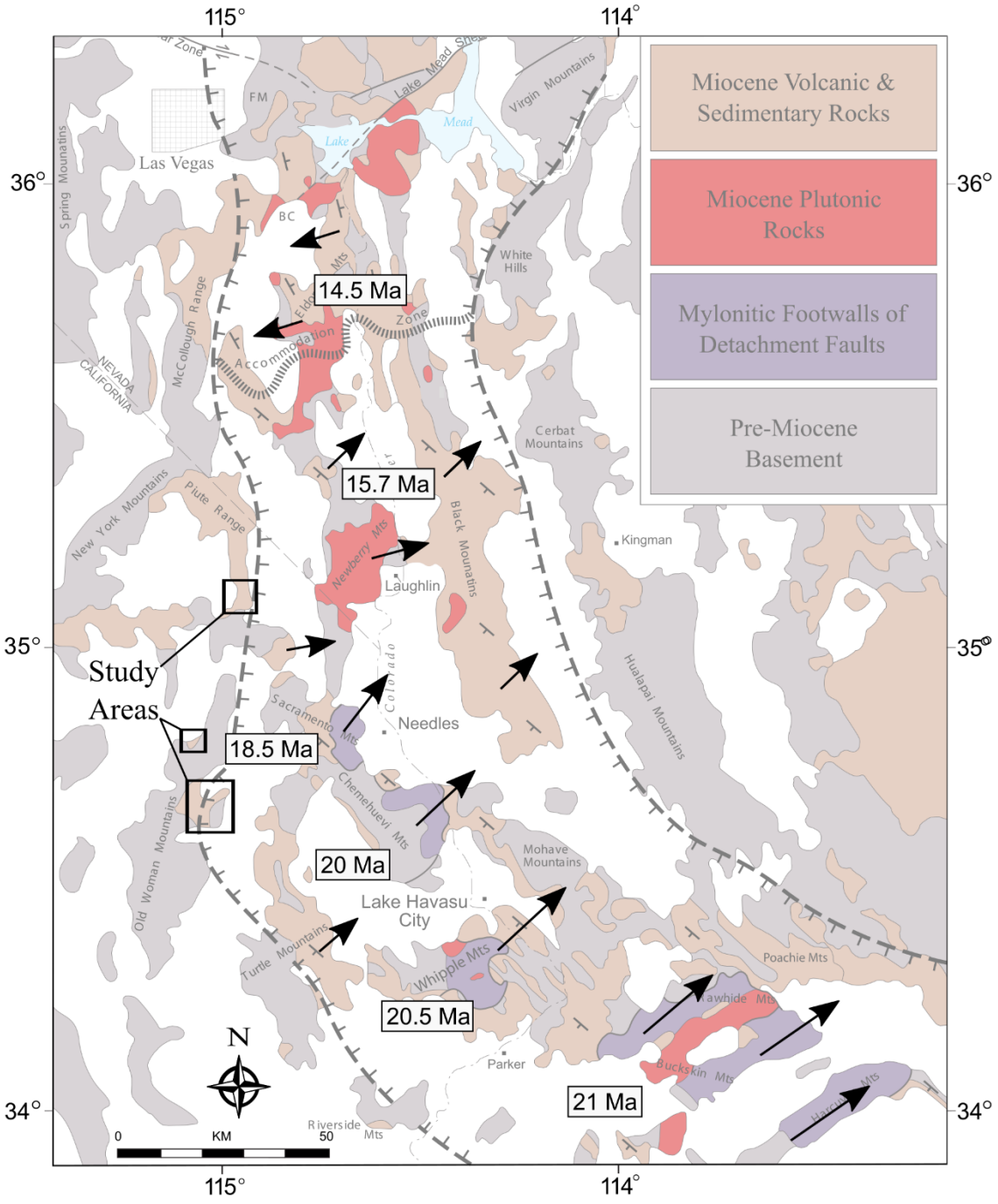

Figure 1.3: Overview map of CREC showing dominant extension direction and approximate age of onset of extension for ranges in the corridor. Arrow length represents relative magnitude of extension. Note transition to west directed extension north of the accommodation zone in northern CREC. See in text citations for sources.

1.2.3 Margins of the CREC

Although the central axis of the CREC is clearly defined by exposed MCCs and Miocene volcanic and plutonic rocks, the margins of the corridor are somewhat ambiguous. There is no accepted definition for the margin of an extensional domain making where the boundary should be placed unclear and somewhat subjective. The eastern margin of the CREC is generally considered a gradational boundary through the moderately (<20%) extended "transition zone" into the unextended Colorado Plateau, and is conveniently drawn beneath alluvial cover for much of its length (Fig. 1.2).

The western margin was originally defined by Howard and John (1987) as following the trace of Tertiary faults that dip east at low angles (5-35°) into the corridor, above footwalls of crystalline basement rocks. They suggested areas west of this trace are relatively unbroken, contain no large detachment faults, and exhibit inconspicuous or variable Tertiary tilting. They also considered the regional trace of these "gently dipping basal faults" to approximate the original position of the "headwall breakaway" where a regional detachment fault—connected at depth with detachment faults presently exposed in the Chemehuevi Mountains—initially surfaced. Exposures of possible breakaway faults are rare, and the western margin of the CREC is also typically drawn beneath alluvium for the majority of its length.

Transitions from highly extended domains of uniform tilt identified elsewhere in the Basin and Range Province have been interpreted differently. Gans and Miller (1983) evaluated a belt of highly extended ranges in east-central Nevada and interpreted the

transition to lesser extended neighboring areas as occurring across “sharp supracrustal boundaries” but not necessarily discreet fault planes.

Thus the margins of the CREC can be defined in three ways:

1. A gradual transition from highly to moderately extended upper crust.
2. A discrete transition at the surficial intersection of the “breakaway” associated with a regional detachment fault.
3. A gradual (or discreet) transition from SW tilted blocks to another tilt domain.

Which form of transition is actually occurring along the western edge of the CREC has important implications for models of extensional deformation across the corridor.

1.2.4 Fault Models in the CREC

The most popular geometric model proposed for MCC evolution in the CREC is one of a regionally continuous detachment fault surface that accommodates >50 km of shear (Howard and John, 1987) and is isostatically upwarped (Spencer, 1984) over exposed core complexes (Fig. 1.4A). This regional detachment is thought to dip into the subsurface west of exposed MCCs and resurface far up-dip in the fault headwall or “breakaway” zone. A series of smaller synthetic normal faults in the hanging wall also accommodate some shear and thin the upper crust. Regional detachment models make several key predictions about deformation in the corridor and breakaway zone.

1. Motion in the hanging wall of the breakaway fault should be dominantly unidirectional and parallel to down-dip extension direction.

2. Synthetic fault blocks should progressively young down dip, away from the point where the breakaway intersects the surface.
3. In the breakaway zone, fault blocks should be closely spaced and sole into the master detachment at relatively shallow depths. Block spacing should increase down dip as the depth to the master detachment increases.

As discussed above, the detachment fault model necessitates a sharp transition between two neighboring extensional domains.

Alternatively, large magnitude extension in the CREC can be modeled as a consequence of a system of concentrated high angle imbricate normal faults (Fig. 1.4B), each individually rooted in the brittle-ductile transition and possibly active at any time in the rift history. This model is commonly applied to the northern CREC (e.g. Faulds et al., 2001) and other highly extended domains within the Basin and Range (e.g. Great Basin, Gans and Miller, 1983). The high angle imbricate fault model differs fundamentally from the detachment model in that it does not require any consistent pattern in deformation timing or magnitude. The model also allows for transitions to less extended terranes to occur gradually, as fault magnitude and frequency decrease.

Fault models for the CREC also make predictions about sedimentation patterns. In the detachment model, small isolated sedimentary basins are expected to form first in the upper plate fault blocks of the breakaway zone. Sediments should display progressively lower dips up section associated with growth faulting, and basins should grow larger and younger toward the root of the detachment. In the high angle imbricate

fault model synkinematic sedimentary accumulations with fanning dips are expected proximal to any major normal fault capable of producing a closed basin.

Fault models are not inherently linked to magmatism, but extended domains almost always exhibit some degree of magmatic activity. In detachment fault models magmatic activity should initiate near the root of the detachment, where decompression is greatest and melting is most likely. In a high angle system, magmatism could be induced beneath any major fault where sufficient decompression occurs. Alternatively,

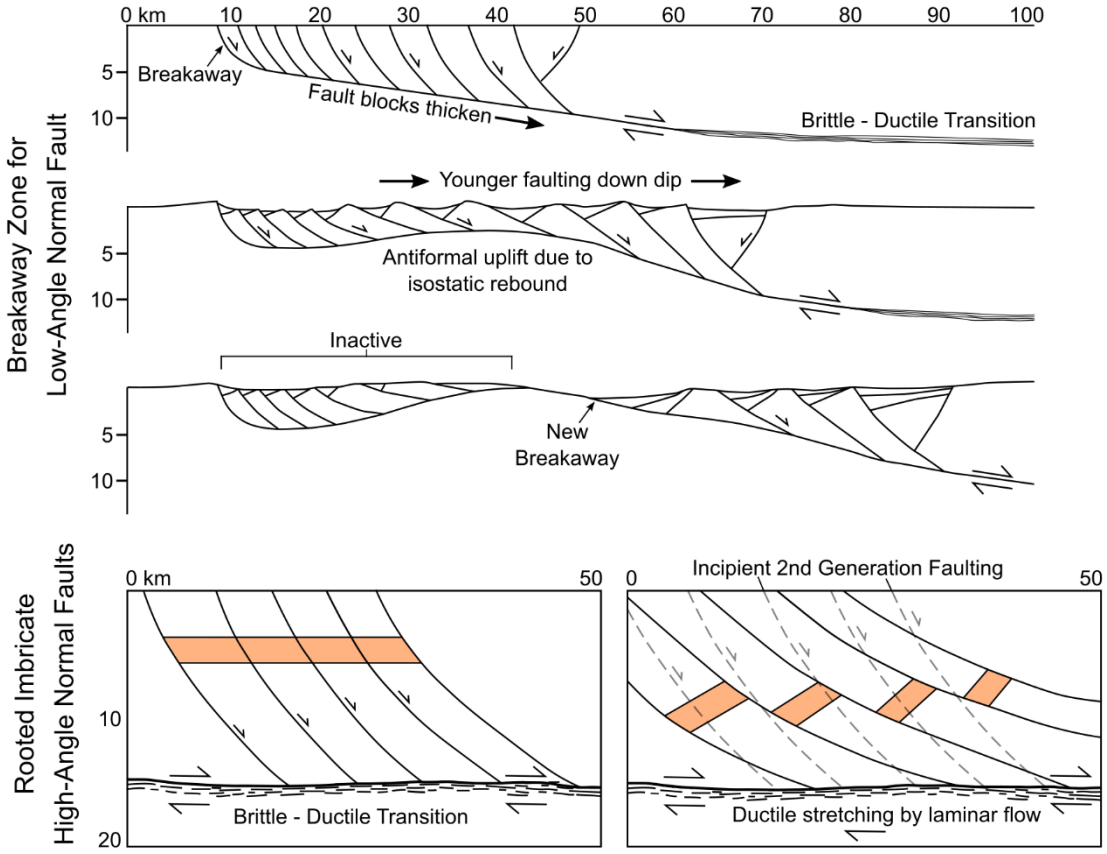

Figure 1.4: Schematic diagrams showing two end member models for large magnitude crustal extension. The low angle normal fault model consists of a single through going master detachment rooted in the brittle-ductile transition. The high-angle fault model consists of a series of steep normal faults individually rooted in the mid-crust. Breakaway model after Spencer, 1984. High-angle model after Proffett, 1977; Gans and Miller, 1983.

extension and normal faulting by either model may be a consequence of magmatic activity (e.g. Gans et al., 1985; Faulds et al., 2001).

1.3 Objectives of this Study

This study utilizes geologic mapping and associated observations and analyses to describe and interpret the western margin of the CREC in three distinct study areas. Each of the selected sites preserves a unique Miocene structural, volcanic, and sedimentary history which, when combined with observations from throughout the CREC, helps inform the overall evolution of the corridor.

Mapping and structural data from the Little Piute Mountains illustrates a polyphase deformation history of strike-slip faulting, normal faulting, sedimentary basin formation, and active volcanism from just inside the supposed breakaway margin of the corridor. Volcanism and some sedimentation in the Little Piute Mountains clearly predates east directed faulting along the CREC margin, complicating the history of the Old-Woman Piute area. Observations from the northwest Piute Mountains suggest a similarly complex history west of the CREC margin, with faulting and sedimentation prior to the onset east-west extension. In the Piute Range, faults dip away from the CREC, calling into question the unidirectional nature of faulting in the corridor and raising questions about how quickly an extensional terrane can change dip direction without the presence of a transform structure.

Data presented and discussed in the following chapters provides insight into the tectonic history of the western CREC and helps to improve understanding of tectonic processes marginal to an intracontinental rift zone.

1.4 Old Woman-Piute Mountains Region

1.4.1 Area Overview

The Old Woman-Piute Mountains (OWPM) are an approximately 100 km long, 15 km wide N-S trending crest located ~50 km west of Needles, CA. The range is underlain primarily by Precambrian to Cretaceous crystalline rocks (Bishop, 1963; Howard et al., 1987). Metamorphosed Paleozoic strata are preserved in isolated exposures, commonly associated with Mesozoic thrust faults (Howard et al., 1987). The range is locally flanked by Miocene sedimentary and volcanic rocks (including the Peach Spring Tuff) in the Piute, Little Piute, and Ship Mountains. These sections preserve a history of local basin filling and upper-crustal deformation (Knoll, 1988; Hileman et al., 1990). Miocene rocks generally strike north-northeast and dip moderately to the west. The northern part of the OWPM area is divided into three crustal blocks (Piute, Little Piute, Old Woman) separated by major Miocene structures discussed at length by Hileman et al. (1990).

1.4.2 Major Structures in OWPM Area

The Little Piute Fault (LPF) separates the Piute and Little Piute blocks (Fig. 1.5), placing Miocene clastic sediments in the hanging wall against crystalline basement rocks in the footwall. The fault is exposed for ~15 km, strikes northeast, and, where measurable, dips from 35° to 45° SE (Hileman et al., 1990). Hanging wall strata dip 10°–20° NW, toward the fault, except directly adjacent to the fault where strata dip gently SE apparently as a result of drag. Down dip striae are reported by Hileman et al. (1990).

The Carson Wash Fault (CWF) separates the Piute and Little Piute blocks on the north from the Old Woman block on the south. It is generally obscured by Quaternary deposits but forms a sharp lineament (trend=125°) on aerial imagery. In sparse exposures the fault is a subvertical zone of highly altered, brecciated basement rock (Hileman et al., 1990). The fault marks the southern exposure of Miocene sediments in the Little Piute block, and truncates both the strata and the LPF at an approximately 90° angle. The CWF bifurcates at its SE end, with one strand running through the southernmost Little Piute Mountains and the other running further south (Fig. 1.6) The length of the fault is unclear as it is obscured by Quaternary alluvium at both ends.

A major normal fault is inferred in the Fenner Valley NW of the Piute Mountains (Fig. 1.5). This fault must be present to account for ~20° tilting of Miocene rocks in the Piute Mountain block (Hileman et al., 1990; Foster et al., 1991). An additional normal fault is inferred to lie under alluvium in the Ward Valley, east of the OWPM (Howard et al., 1987).

Mesozoic thrust faults have been identified in pЄ and Pz rocks throughout the region (Miller et al., 1982; Howard et al., 1997) and correlated across structural blocks forming possible offset markers across the LPF and CWF (Howard et al., 1987; Howard et al., 1997).

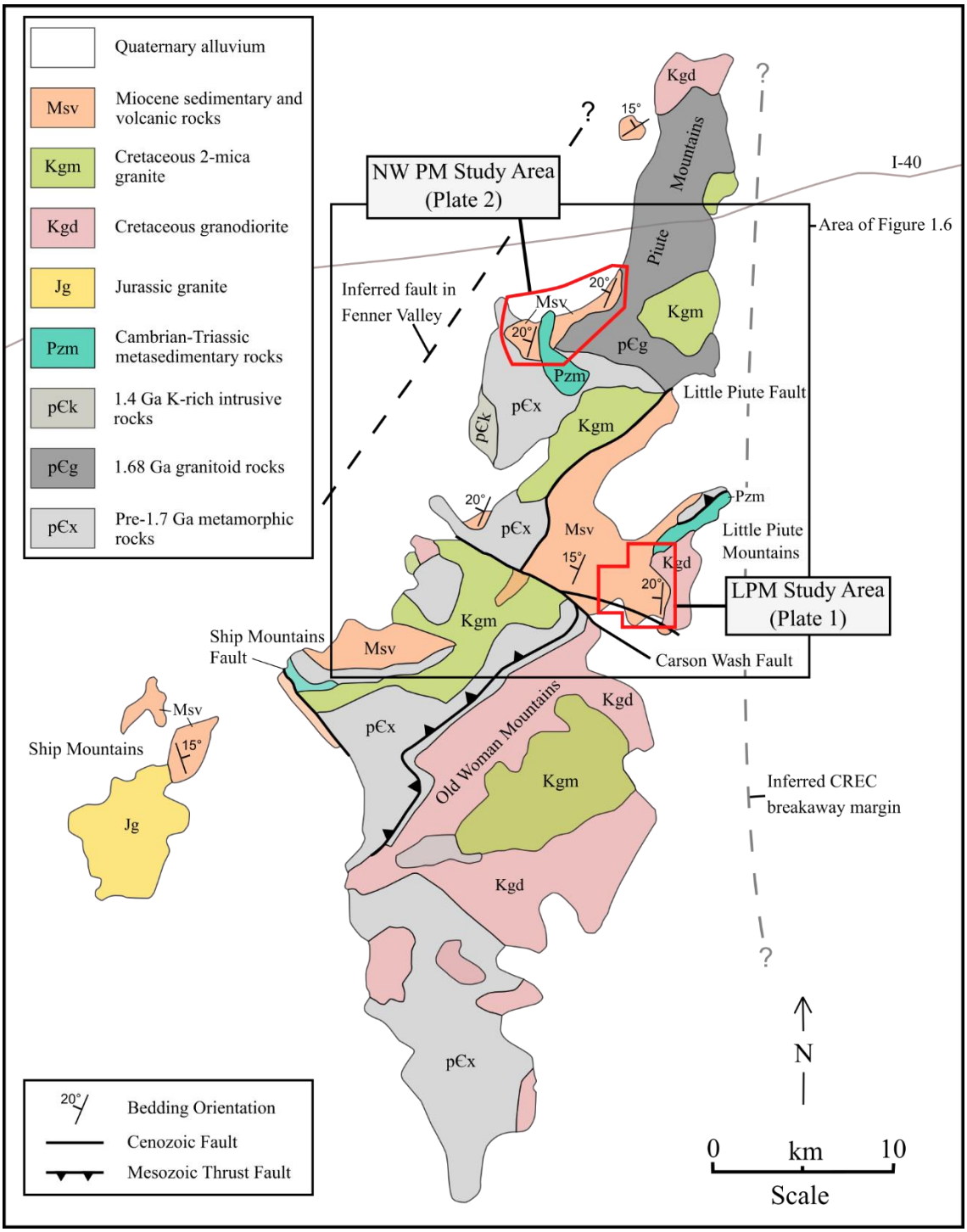

Figure 1.5: Simplified geologic map of Old Woman-Piute Mountain area showing distribution of rocks, major structures, and location of study areas. Data from Hileman et al., 1990; Foster et al., 1991; Miller et al., 1998.

1.4.3 Previous Interpretations of Major Structures

The LPF has been interpreted by previous workers as a major down to the southeast normal fault. Hileman et al. (1990) estimate 3 km of vertical displacement on the LPF based on projection of the Peach Spring Tuff, and offset of the projected trace of Mesozoic shortening structures. Sediments in the hanging wall are interpreted as synkinematic basin fill (Knoll, 1988). Howard and John (1987) interpreted the LPF as an exposed segment of the CREC detachment fault breakaway. They inferred the breakaway fault to continue under Ward Valley to the north and south, east of the OWPM (see Fig. 1.5). Alternatively, Hileman et al. (1990) and Miller et al. (1998) interpret the fault as lying in the footwall of the CREC detachment breakaway, suggesting the breakaway is actually located somewhere east of the Little Piute Mountains beneath Ward Valley.

The CWF is interpreted by Hileman et al. (1990) as a steeply dipping down to the north normal and/or right lateral fault with approximately 1 km vertical displacement. This interpretation is drawn based on juxtaposition of a Cretaceous pluton on the south side (Old Woman block) of the fault against pЄ rocks on the north side (Piute block) of the fault which are identical to those that form the pluton roof (Howard et al., 1987). Hileman et al. (1990) also consider the CWF a transfer fault, accommodating differential extension between the Little Piute block and the Old Woman block. They make this interpretation based on two points: the LPF apparently terminates against the CWF and is not offset by it, and the CWF separates the moderately extended Piute and Little Piute blocks from the unextended Old Woman block.

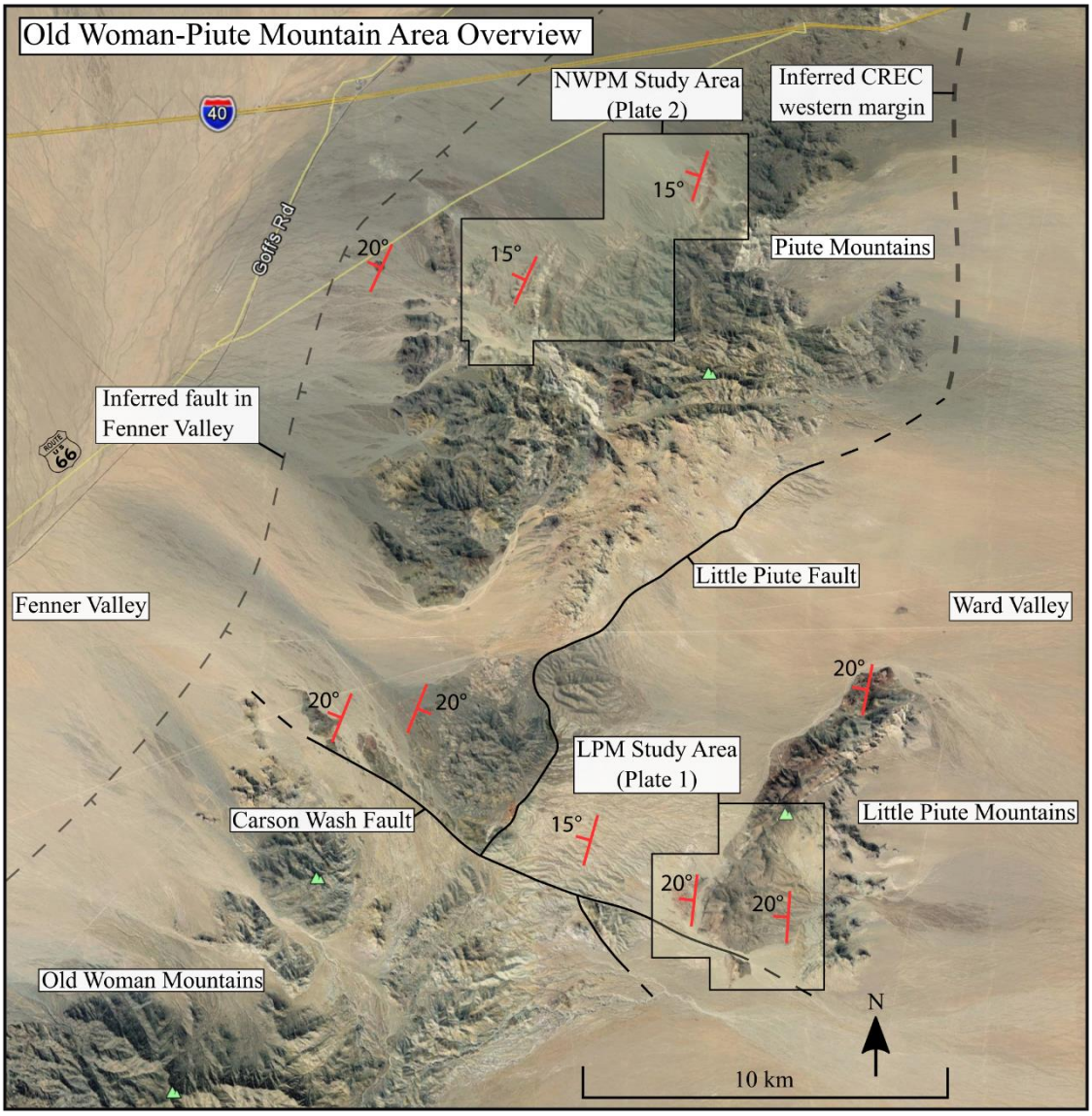

Figure 1.6: Satellite overview map of Piute Mountains and Little Piute Mountains area showing location of study areas, Little Piute and Carson Wash faults, and inferred CREC boundary from Howard and John, 1987.

The inferred fault in the Fenner Valley NW of the OWPM was first proposed by Hileman et al. (1990) on the basis of uniform 20°–30° rotation of Miocene strata in the Piute block. Apatite fission track analysis of crystalline basement rocks in the Piute block also indicates 20°–30° rotation to the NW in the middle Miocene (Foster et al., 1991). This fault is interpreted as a listric normal fault in the footwall of the CREC detachment breakaway fault.

1.4.4 Miocene Stratigraphy of OWPM area

Miocene stratigraphy in the northern OWPM area consists of a mix of volcanic and clastic sedimentary rocks exposed along the flanks of the range (Fig. 1.5). The thickest and best preserved sections are found in the Little Piute and NW Piute Mountain areas. Coarse conglomeratic rocks are typically deposited nonconformably on pЄ and K basement. Clastic sediments contain a mix of young volcanic and old basement detritus and range from medium grain sandstone to boulder conglomerate. The Peach Spring Tuff is typically found in the middle or near the top of Miocene sections. Locally erupted volcanic rocks range from basalt lavas to rhyolite tuff and are interbedded in sedimentary sections. Detailed stratigraphy and sedimentology of the OWPM area is described by Knoll (1988). Volcanic rocks are described geochemically and petrographically by Miller and Miller (1991).

1.4.5 Timing of Volcanism and Deformation

The timing of volcanism and deformation in the Piute and Little Piute Mountains is constrained by $^{40}Ar/^{39}Ar$ geochronology of Miocene volcanic rocks. Tilting of the Piute Mountain block is constrained to between 18.8 Ma (age of PST, Ferguson et al., 2013)

and 16.6 ± 0.4 Ma (eruption of flat lying Barrel Springs Dacite, Miller et al., 1998). In the Little Piute Mountains tilting is thought to have occurred after 17.8 ± 0.1 Ma (emplacement of tuff above PST, Miller et al., 1998). Tilting in this time period overlaps the timing of extension at the same latitude in the central CREC (Chemehuevi and Sacramento Mountains).

1.4.6 Relationship to CREC

The OWPM area lies along the western margin of the CREC, approximately 50 km west of the central MCC belt (Fig. 1.2). Howard and John (1987) infer the trace of the CREC detachment fault breakaway to run under alluvium along the east side of the OWPM. They interpret the LPF as an exposed portion of the breakaway based on the moderate eastward dip of the fault and the presence of Miocene fanglomerates and other apparently synkinematic sediments in its hanging wall. If the LPF does represent the CREC detachment breakaway, the predictions laid out in sections 1.2.3 and 1.2.4 should hold true throughout the OWPM area. The LPF should represent the margin of the CREC tilt domain and the transition to a less extended neighboring domain. The Little Piute Mountains should reside in the first tilted block of the detachment terrane, and the Piute Mountains should lie outside the detachment terrane. The LPF is the only potential exposed structure identified as part of the breakaway by Howard and John (1987). Therefore, the understanding the history of the fault and surrounding areas is critical to understanding the geometry and evolution of the margin of the CREC extensional domain.

1.4.7 Study Areas

Study sites in the Little Piute Mountain (LPM) and northwest Piute Mountain (NWPM) areas provide an opportunity to assess the history of sedimentation, volcanism, and deformation along the only proposed exposure of the CREC detachment breakaway. This report now presents new data from detailed mapping in the LPM and NWPM study areas which reveals greater complexity in the extensional strain field and sedimentation history than previously described, with implications for the development of the LPF, OWPM area, and the margin of the central CREC as a whole.

2. Geology of the Southern Little Piute Mountains Study Area

2.1 Area Overview

The Little Piute Mountains (LPM) form an isolated ~30 km^2 range approximately 10 km east-southeast of the Old Woman-Piute Mountain crest (see Fig. 1.5). The southern LPM sedimentary and volcanic section represents the most complete record of Miocene basin formation, sedimentation, volcanism, and deformation in the OWP area. The LPM crustal block sits in the hanging wall of the Little Piute Fault to the northwest and is bounded by the Carson Wash fault to the south (see Fig. 1.5). Following interpretations by Howard and others the LPM block should thus represent the first in a series of increasingly tilted synthetic fault blocks in the hanging wall of the CREC detachment fault. Geologic mapping, sedimentary and volcanic stratigraphy, and structural data presented here indicate the Miocene deformation history of the LPM block and CREC margin at this latitude is more complex and protracted than suggested by previous workers.

2.2 Miocene stratigraphy

2.2.1 Overview

An approximately 2 km thick section of sedimentary and volcanic rocks are exposed in the LPM block and are tilted 10°–20° NW (Fig. 1.5). The lower portion of the section is deposited directly on Cretaceous and Precambrian crystalline rocks and is well exposed along active drainages throughout the map area. There is significant oxidation in the uppermost 10 m of crystalline basement below the unconformity confirming surficial exposure during the Miocene (Fig. 2.2).

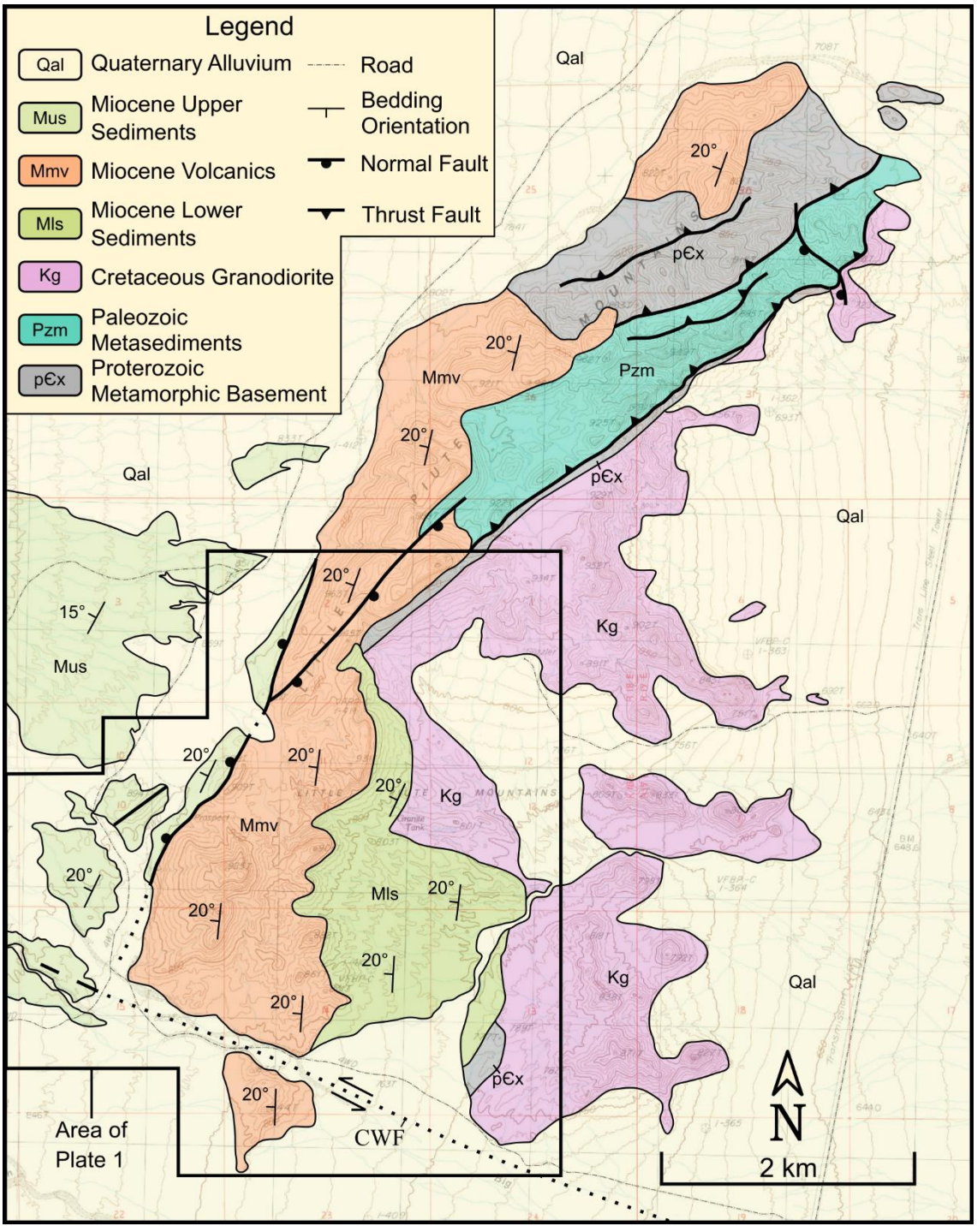

Figure 2.1: Geologic overview map of Little Piute Mountains showing study area (plate 2). Compiled from Hileman et al., 1990, Howard et al., 1997, and new mapping. See Figure 1.3 for location.

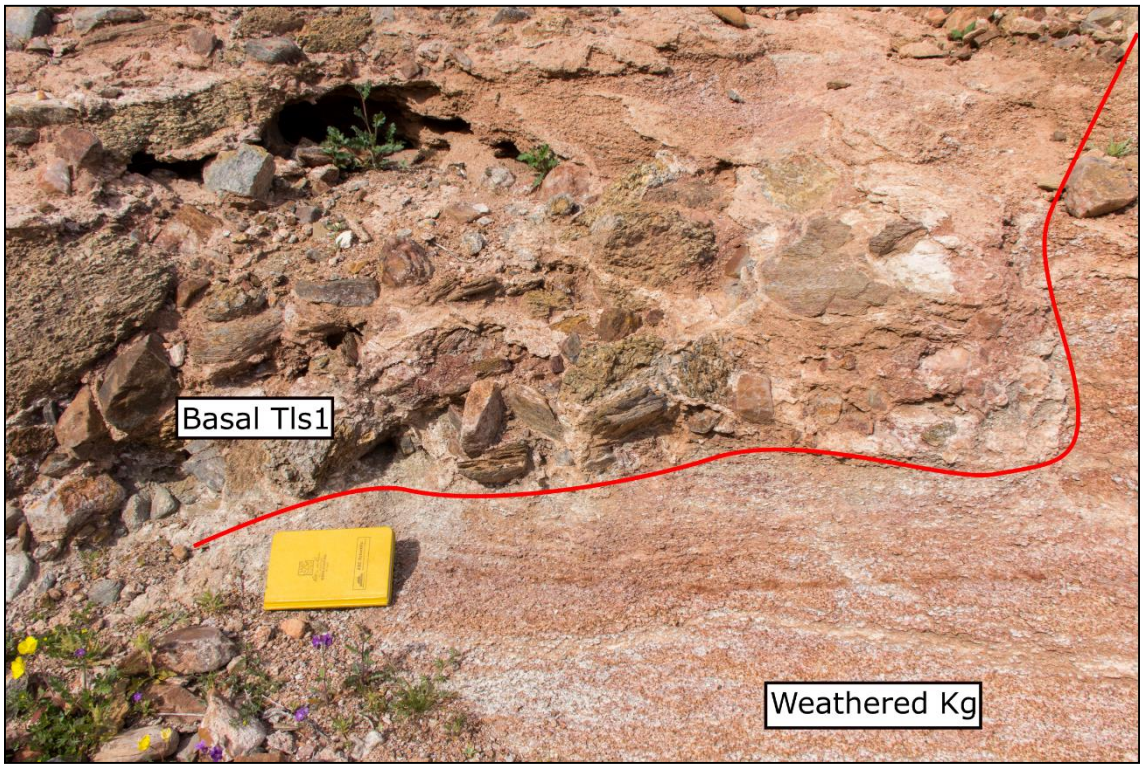

Figure 2.2: Field photo showing basal Miocene unconformity (red line). Polymict crystalline conglomerate (Tls1) is deposited on red weathered Cretaceous granodiorite which must have been exposed at the surface at the time of deposition.

The Miocene section is divided into a lower sedimentary section, middle mixed volcanic and sedimentary section, and upper sedimentary section (Fig. 2.1). The lower sedimentary section (Tls) is exposed for roughly 2.5 km along strike, thinning and terminating abruptly against Kg to the north and covered by alluvium to the south (Plate 1). Knoll (1988) and Hileman et al. (1990) interpreted the lower section as channel filling debris flows deposited in a paleovalley. This interpretation is based on east-directed paleocurrent indicators (Fig. 2.6) and plutonic detritus inferred to be sourced from the OWPM area to the west. The middle volcanic section (Tmv) is thickest (300–500 m) in the southernmost ~4 km of the LPM and thins rapidly northward. Sediments in the middle section represent local accumulations in and around an active volcanic center (Knoll,

1988; Miller and Miller, 1991). The Peach Spring Tuff is exposed for ~8.5 km along strike and caps the middle Miocene section. The upper sedimentary section (Tus) consists of sandstones and debris flow deposits interpreted as an alluvial fan sequence shed from the OWPM area to the west, in response to motion on the LPF (Knoll, 1988). Generalized stratigraphic relationships are shown in Fig. 2.3. Detailed descriptions of all map units are found in Appendix A.

2.2.2 Lower Sedimentary Section

The lower sedimentary section consists of three distinct sedimentary units (Tls1,2,3) with interstratified basalt flows (Tlb) near its top. The section ranges from <50 m thick at its northern limit to 430 m thick in southern and central exposures. Lower sediments dip uniformly 20° to the west and are restricted to an approximately 2.5 km by 1.2 km area of low topography in the southeastern LPM study area (Plate 1).

Tls1 sediments are dominated by cobble conglomerates with mixed sandstone and gravel beds (Fig. 2.2) and form the lowest ~150 m of section. Conglomerate clasts are angular to sub-rounded and consist of pЄx, Pzm, and Kg crystalline and metasedimentary rocks in roughly equal proportion, sourced from local basement exposures. The unit generally coarsens northward and contains lenses of boulder conglomerate in its northernmost exposures (Fig. 2.3).

Tls2 is a coarse conglomerate with occasional sandstone/gravel beds dominated by plutonic clasts (Fig. 2.4A). The unit forms the middle ~150 m of the lower section and contains ~10% pЄx and Pzm clasts and ~90% plutonic clasts which are correlative with exposed basement in both the LPM and the OWPM areas (Knoll, 1988). Clasts are sub-

rounded to rounded and range from cobble to boulder size. The unit thins to <30 m in its northernmost exposures.

Olivine basalt (Tlb) lava flows are interbedded with and deposited on Tls2 and Tls3. Individual lava flows of a'a and pahoehoe are exposed along active drainages and range from 1–5 m thick with vesicular margins. Northern exposures of Tlb are thin (<10 m) and discontinuous with interbedded Tls3. Southern exposures are close to the eruptive center and are thicker (up to 50 m). Phenocrysts consist of olivine (commonly altered to iddingsite), clinopyroxene, and plagioclase up to ~3 mm, constituting 7–10% of the total rock volume.

Tls3 is a pebble to cobble conglomerate with rounded plutonic and angular volcanic clasts. The unit contains from 3–25% volcanic detritus and has a sand to gravel matrix. The unit is interbedded with and overlies Tlb and contains some clasts of Tlb as well as some andesitic clasts in its uppermost sections (Fig. 2.4B). Unlike other lower sedimentary units, Tls3 maintains uniform thickness (~80 m) along strike before pinching out in the northern part of Plate 1.

Map patterns in the lower sedimentary section reveal important aspects of the early sedimentation history. The sharp truncation of Tls1 and abrupt thinning of Tls2 and Tlb occur along a ~1 km long lineament traced by the contact between Miocene and Cretaceous rocks. The contact is never exposed but can be tightly constrained, and based on map relations can be interpreted in two ways:

1. As a south facing, east-west trending buttress unconformity along the wall of a deep channel incised into basement prior to deposition of Tls1.

2. As a south side down, east-west trending fault that was active prior to and during deposition of Tls1 and the lower part of Tls2 and ceased moving during deposition of Tls2.

Knoll (1988) prefers the first interpretation, suggesting that early sedimentation in the LPM area was driven by unroofing of the OWPM to the west and coeval extension in the lower CREC to the east. The reason for deposition in the intermediate LPM area is unclear.

The second interpretation is preferred here due to several lines of evidence. The implied height (~350 m) and steep dip (~70°) of the escarpment (Plate 1, XS E) would constitute a buttress far steeper than the angle of repose expected in an unfaulted drainage; Tls1 coarsens northward toward the Kg contact and contains lenses of boulder conglomerate; and the pЄx-Kg intrusive contact appears to be offset at least 1.5 km across the lineament. The trace of the fault does not continue into the middle volcanic section, implying the fault stopped moving and whatever basin remained filled in completely with deposits of Tls2, Tlb, and Tls3. Thinner deposits of these units exposed north of the fault trace do form a buttress unconformity against Kg (Fig. 2.3), suggesting sedimentation continued post-faulting.

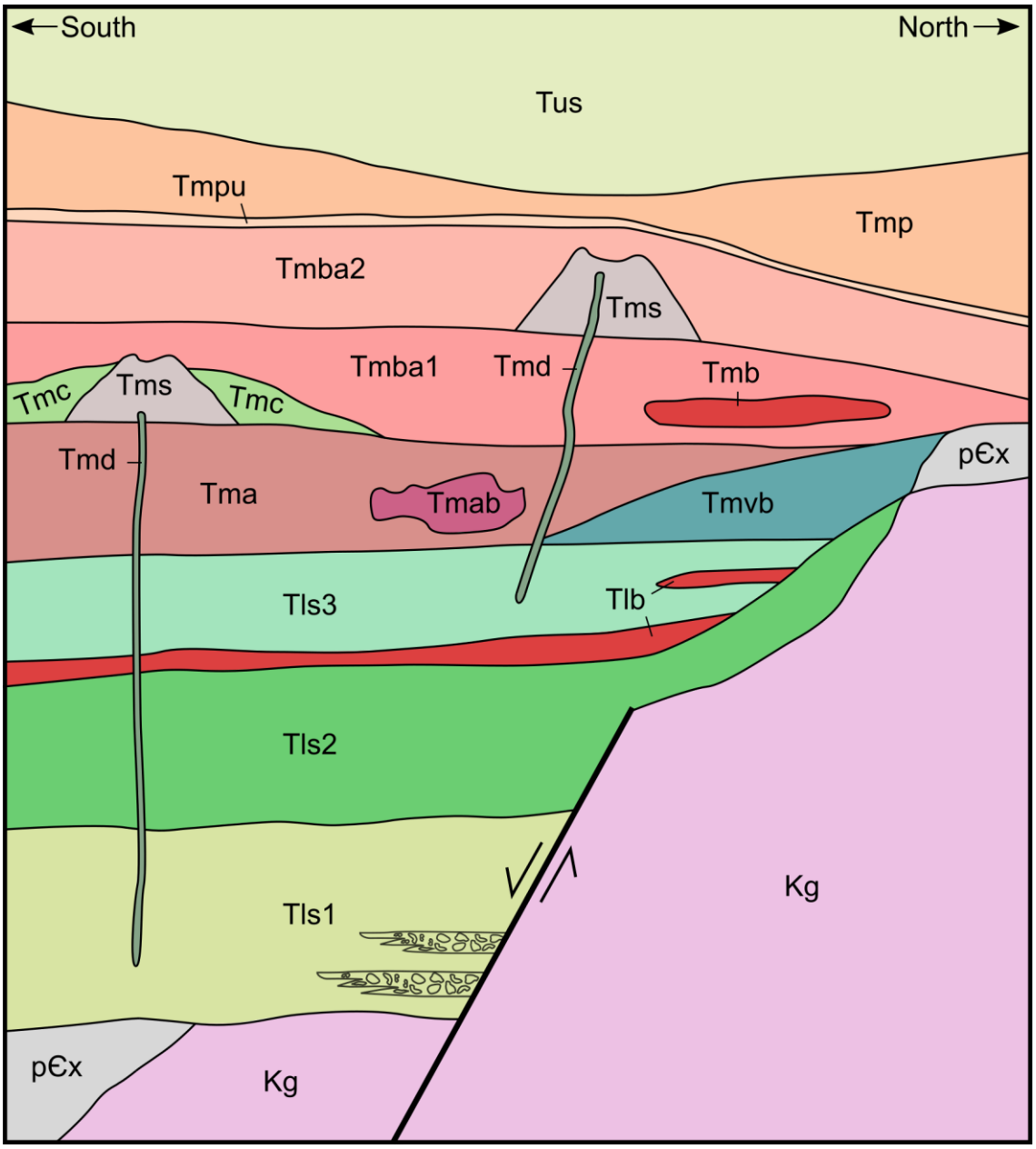

Figure 2.3: Schematic cross section showing stratigraphic relationships in LPM area. Tls1 and lower Tls2 deposited in hanging wall of basement normal fault. Upper Tls2 covers fault and forms buttress unconformity against Kg. Lower middle section (Tm) forms buttress against basement. Upper middle section deposited on basement and capped by regionally extensive PST. Upper section deposited on PST.

2.2.3 Middle Volcanic Section

The middle volcanic section consists of lava flows, volcanic breccias, and interbedded sediments dominated by volcanic clasts. Lavas range in composition from basalt to andesite and are overlain by the Peach Spring Tuff, a regionally extensive rhyolite ignimbrite which erupted from a caldera ~80 km northeast of the LPM study area. The middle section is thickest in the south central map area (~550 m), thins to the north (~180 m), and is covered by alluvium to the south. Lavas and sediments dip an average of 20° to the west, similar to the underlying sedimentary section. Individual lava flows range from 10s of meters to >1 km long and from 50 cm to >4 m thick. Map units are generally composed of 3-10 individual flows or breccia layers, grouped by estimated composition and phenocrysts content. All lavas appear to have been erupted locally, from at least two neighboring vents.

Throughout most of the map area the base of the middle section is a two-pyroxene andesite (Tma) that contains 10-15% phenocrysts of clinopyroxene, orthopyroxene, and plagioclase. The unit is exposed for 2.6 km along strike and ranges from 20 m to 80 m thick with autobrecciated lenses (Tmab, Fig. 2.4C) up to 200 m long contained within at least five distinct lava flows. In the north-central study area the base of the middle section consists of a volcaniclastic breccia (Tmvb) dominated by angular clasts of basalt and basaltic andesite ranging from pebble to cobble size with a dark sandy matrix. Tmvb forms a buttress unconformity against pЄx rocks but contains <10% basement clasts and appears to be derived almost entirely from the oldest locally erupted lavas.

Vent facies volcanic rocks (Tms) are preserved in two localities in the map area (Plate 1) and consist of lapilli to bomb scoria fragments in an ashy red matrix of similar material. Fragments are commonly flattened or tube shaped with vesicular interiors and quenched margins. Dips in Tms are irregular and steeper than surrounding rocks, probably owing to original dips of rocks around the vent. The southern exposures of Tms are clearly preserved remnants of a cinder cone. Although original vent geometry has been modified by erosion and faulting, current exposure suggests a diameter of at least 300 m. Red and green clast supported conglomerates and breccias (Tmc) are present around the flank of southern Tms exposures and consist of angular to sub-angular volcanic fragments ranging from pebble to cobble size. Tmc deposits are poorly sorted and are derived almost entirely from surrounding volcanic deposits, especially Tms. The uppermost portions of Tmc contain some plutonic detritus apparently derived from the west based on paleocurrent indicators (Fig. 2.6; Knoll, 1988). A single discontinuous ash flow tuff bed (~2 m thick) is exposed near the top of Tmc.

A 30–150 m thick sequence of basaltic andesite lava flows (Tmba1/2) overlie Tms and Tma deposits, capping the locally erupted section. These lavas contain 3–15% phenocrysts of olivine, clinopyroxene, orthopyroxene, plagioclase, and iron-titanium oxides ranging from ~0.5–3 mm in a groundmass that varies from glassy to holocrystalline. Basaltic andesite lavas are separated into lower (Tmba1) and upper (Tmba2) members. Tmba1 flows are glassy, contain <10% phenocrysts, and form thin ledges. Tmba2 flows have are devitrified and show signs of vapor phase alteration, contain 10-15% phenocrysts and form cliffs up to 15 m high. Tmba lavas flowed over

and around the southern vent and are thickest in the central part of the map area, thinning to the north where they form a buttress unconformity against pЄx basement.

Olivine bearing basalts (Tmb) are present in the north-central part of the volcanic section. Several individual lava flows ranging from 1–3 m thick form this isolated exposure which is most similar to olivine basalts observed in the lower sedimentary section. Mafic dikes (Tmd) containing are also found in several localities in the lower and middle section. Dikes range from <1 m to ~4 m thick and ~5–200 meters long (see Fig. 2.4D) and have a distinct holocrystalline groundmass of plagioclase and clinopyroxene. Tmd rocks intrude Tmba1, Tms, Tlb, and Tls2 and contain ~15–20% plagioclase and clinopyroxene with minor orthopyroxene and Fe-Ti oxides, compositionally similar to Tmba lavas.

The volcanic section is capped by Peach Spring Tuff (Tmp) which is exposed along the crest of the LPM. The basal unwelded (Tmpl) and vitrophyric portions of the tuff are generally covered by talus from the overlying devitrified cliff forming interior member. The devitrified and moderately vapor phase altered interior of the tuff forms the uppermost exposures of PST. The upper vitrophyre and unwelded top are not preserved. The tuff is deposited on Tmba2 and pЄx basement in the map area, ranges from <10 m to 110 m thick, and dips uniformly 20° to the west (see Plate 1, XS A-D). Through magnetic analysis, Hillhouse and Wells (1991) determined the PST flowed from southwest to northeast in the LPM area, orthogonal to the dominant sediment transport direction inferred by Knoll (1988).

Miller (1989) and Miller and Miller (1991) provide petrographic and geochemical descriptions of some volcanic rocks in the LPM area. Sampled rocks range from 48 to 70% SiO_2 and contain magmatic inclusions, xenoliths, and evidence for textural and mineralogical disequilibrium. They find samples are in general calc-alkaline to alkaline and interpret both assimilation of solid material and magma mixing to have played a role in the genesis of volcanic rocks in the LPM area. The age of volcanism in the LPM area is poorly constrained. Volcanism in the LPM area entirely predates emplacement of the 18.8 Ma PST. $^{40}Ar/^{39}Ar$ geochronology on single grains of plagioclase from an ash flow tuff near the base of the middle section gives a rather uncertain age of ~19.7 ± 1.5 Ma (Miller et al., 1998). Because this tuff lies above the base of the section and has an unknown source, the initiation of local volcanic activity is poorly constrained.

The middle volcanic section in the LPM exposes a cross sectional view of a basaltic to andesitic volcanic center with multiple vent sites (Fig. 2.5). Lavas buttress against basement rocks, and vary significantly in thickness over ~3 km of along strike exposure. The preservation of volcanic vent features and dikes and lava flows of similar composition indicate lavas erupted locally. The volcanic center constructed cinder cones and likely a shield or stratovolcano. Thickness variations in the PST suggest the presence of a volcanic edifice at least 100 m high at the time of emplacement.

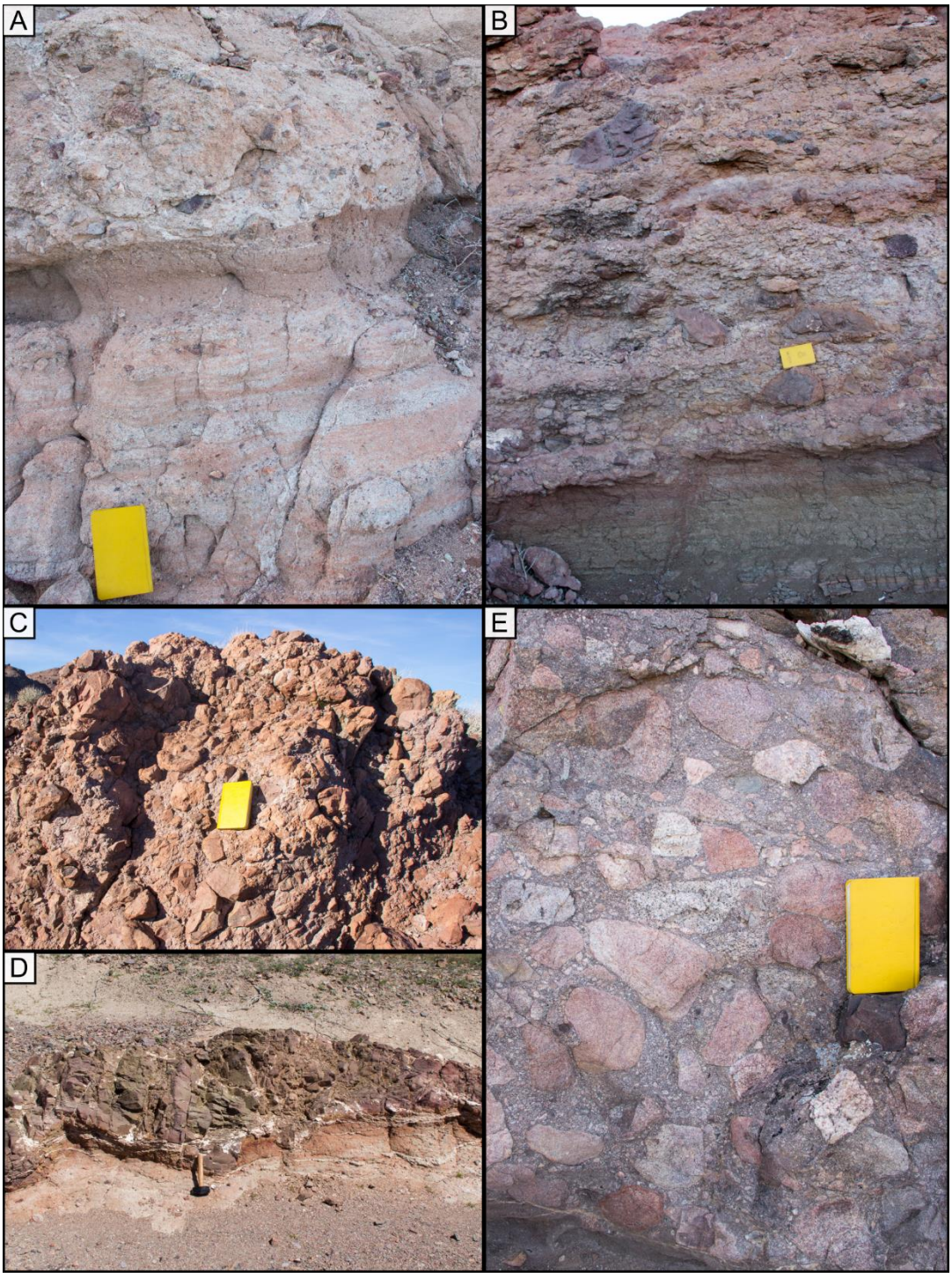

Figure 2.4: Field photos showing representative outcrops of Miocene rocks in LPM study area. (A) Tls2 mixed sandstone and conglomerate. (B) Tls3 conglomerate with mixed plutonic and volcanic clasts. (C) Outcrop of Tmab showing autobrecciation. (D) Mafic dike (Tmd) intruded into Tls2. (E) Clast rich horizon in Tus.

2.2.4 Upper Sedimentary Section

The upper sedimentary section (Tus) consists of a mix of sandstone and gravel to cobble conglomerate (Fig. 2.4E). The section is exposed for ~3 km along strike in the LPM study area and for ~10 km along strike in the low-lying topography between the LPM block and the LPF (see Fig. 1.5). Beds are mostly well sorted, contain tabular cross stratification, and range from <5 cm to ~2 m thick. The lower portion of Tus contains angular volcanic clasts up to 1.5 m across as well as euhedral sanidine, plagioclase, biotite, and chlorite grains, derived from PST and other underlying volcanic rocks. The upper portions of Tus consist entirely of plutonic and metamorphic basement and yield east directed paleocurrent indicators and rounded clasts in a quartz dominated matrix. These observations suggest a shift from locally derived sediment near the base of the Tus section to sediment derived from the OWPM crest area to the west.

Exposures of the upper sedimentary section are faulted against the PST along a system of relatively small displacement, steep northwest dipping normal faults, precluding accurate determination of the thickness and character of its lowest clastic members. The presumed depositional contact is never exposed and the lowest part of the section is covered by alluvium throughout most of the map area. The amount of section omitted by and offset on NW dipping normal faults cannot be determined, although the presence of abundant coarse volcanic detritus in the lower Tus section suggests offset is 10s to 100s of meters at most. It is also unclear how much of the PST eroded away prior to deposition of the base of Tus. A single ash bed approximately 30 m stratigraphically above the PST has an age of 17.8 ± 0.1 Ma (Miller et al., 1998).

The upper sedimentary section is interpreted by Knoll (1988) and others as a sequence of alluvial fan deposits shed from the OWPM crest into a hanging wall basin formed by normal sense motion on the Little Piute Fault. Sediments display moderate fanning of dips starting about 150 m above the PST, from ~20° westward dips in the study area to ~10° westward dip near the LPF (Hileman et al., 1990). Flat lying boulder conglomerates overlie the section and the LPF approximately 8 km northwest of the LPM study area, interpreted as post-kinematic deposits (Hileman et al., 1990).

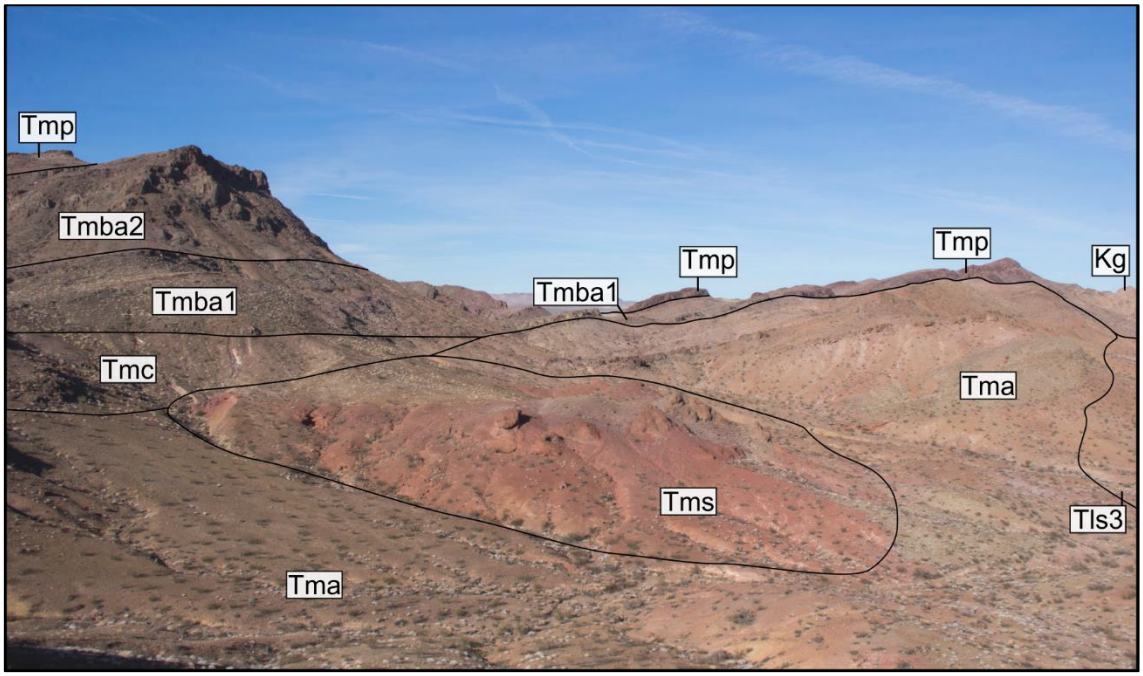

Figure 2.5: Field photo showing preserved cinder cone (Tms) and surrounding rocks in southern map area. Tmba1 appears to have flowed around the vent. Tmp caps ridges in background.

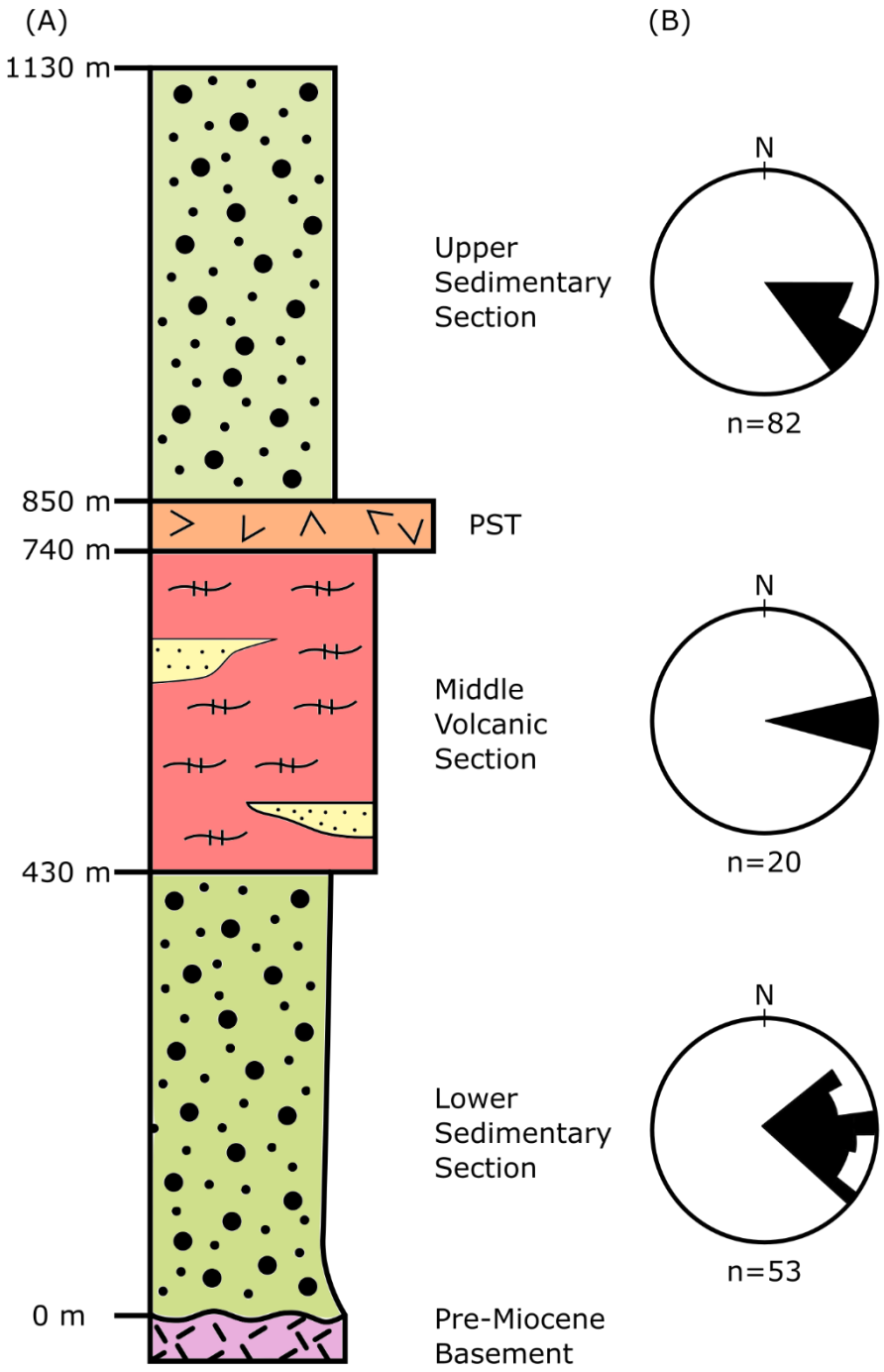

Figure 2.6: (A) Generalized stratigraphic column of Miocene section in Little Piute Mountains, as measured by Knoll, 1988. (B) Rose diagrams showing paleocurrent directions measured by Knoll (1988) for lower, middle, and upper sedimentary sections.

2.2.5 Tectono-stratigraphic Summary

The Miocene section in the LPM block preserves a history of sedimentation, volcanism, and deformation from c. 20–17 Ma. The lower sedimentary section consists of 400 m of localized coarse clastic sediments which appear to have accumulated in an east-west trending depression, bound by a buttress unconformity/south dipping normal fault to the north and possibly bound by the Carson Wash Fault to the south. This section largely predates volcanism and may be associated with an early episode of N-S directed extension (see discussion below). The middle section (Tmv) records the onset of local magmatism. Although the volcanic section is not well dated, local eruptions clearly predate emplacement of the PST (18.78 Ma). Volcanism appears to have built a broad composite edifice of basalt to andesite lavas, breccias, and minor pyroclastic deposits which created significant local topography within the pre-existing lowland at the time of PST arrival. Clastic sedimentation resumed post-PST emplacement, with sediment mostly derived from the OWPM area to the west. Over 1 km of syntectonic coarse clastic sediment accumulated in the hanging wall basin of the Little Piute Fault.

2.3 Structural geology

2.3.1 Overview

Fault plane surfaces, slip direction indicators, and sense of offset indicators preserved in the LPM area provide insight into the kinematics and evolution of deformation in the LPM block. Analysis of mesoscopic fault slip data allows for determination of the strain field distribution and evaluation of kinematic compatibility between observed faults (e.g. Angelier, 1984; Allmendinger et al., 1992). Data presented

in this section illustrate a complex, polyphase deformation history in the LPM study area which may be compatible with sedimentation patterns described in the previous section.

Miocene brittle fault features are preserved throughout the LPM study area. Deformation in the LPM block appears to be related to the two major structures which bound the block. The northern strand of the Carson Wash Fault is inferred to run under alluvium in the southern map area, and the Little Piute Fault is exposed ~8 km northwest of the study area (see Fig. 1.5). Several map scale faults cut the study area with ~10–100 m of offset (Plate 1). Abundant small (cm to m scale) faults are also preserved in the area, and are better exposed than larger faults.

Miocene rocks in the study area are uniformly tilted ~20° westward from the basal unconformity through the mapped portion of the upper sedimentary section (Fig. 2.7) indicating tilting occurred entirely after deposition and eruption of these rocks. Knoll (1988) and Hileman et al. (1990) report westward dips between 10° and 15° in the upper sedimentary section closer to the LPF suggesting some growth faulting and syntectonic deposition during early titling in the uppermost sedimentary section.

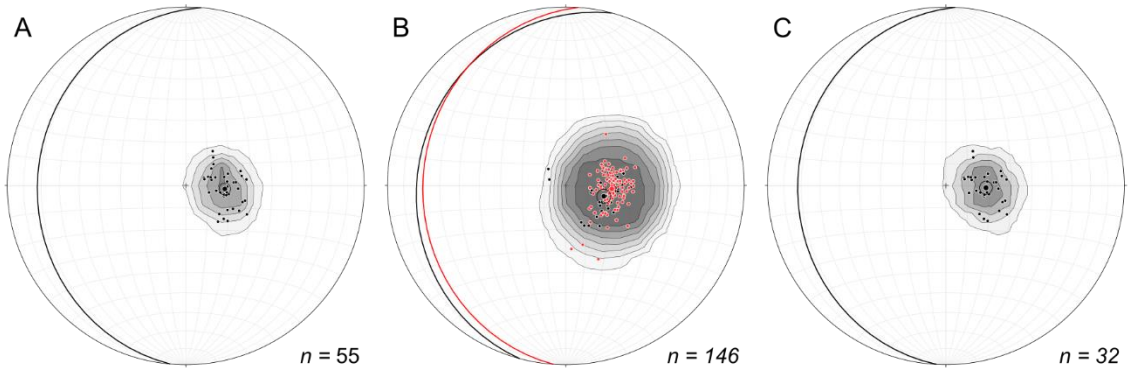

Figure 2.7: (A) Poles to bedding for lower sedimentary section with contour, mean vector (095°,72°), and plane to mean vector (185°,18°). (B) Poles to bedding for middle volcanic (red, mean vector = 094°,69°, plane to mean vector = 184°,21°) and sedimentary (black, mean vector = 105°,72°, plane to mean vector = 195°,18°) section. (C) Poles to bedding for upper sedimentary section with contour, mean vector (093°,72°), and plane to mean vector (183°,18°). Equal-area lower hemisphere stereographic projection plots. n = number of measurements.

2.3.2 Description of Fault Slip Data

Fault planes are best preserved in densely welded Peach Spring Tuff and to a lesser extent in clastic rocks. Evidence for fluid-flow in some fault zones is recorded by secondary calcite, chalcedony, and quartz which aid in fault plane preservation. Many smaller offset (<10 m) fault planes preserve slickenlines and Riedel shears, allowing assessment of direction and sense of slip. Most map scale faults (>10 m) are not as well exposed but can be easily traced based on offset rock units and their slip histories are inferred from geometrically similar minor faults. A total of 70 fault planes and 43 sets of slickenlines have been measured in the LPM study area (Fig. 2.8). 39% of fault plane measurements are from the PST, 22% are from other Tm units, and 39% are from Tls and Tus. Faults strike in all quadrants but most commonly strike NE-SW or E-W (Fig. 2.8B). Slickenlines also trend in all quadrants but most commonly trend NW-SE or E-W (Fig. 2.8C).

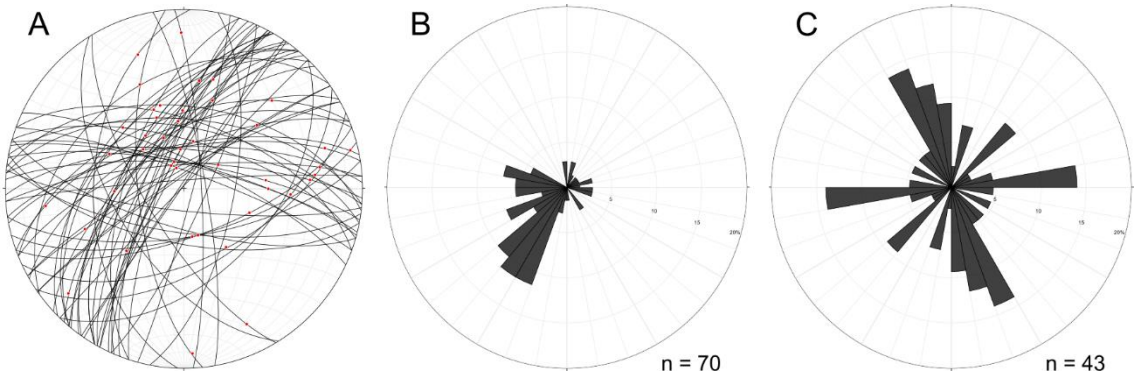

Figure 2.8: (A) All fault planes (great circles) with slip vectors (red lines).
(B) Rose diagram of all fault planes by strike (bin size = 10%).
(C) Rose diagram showing all slickenlines by trend (bidirectional, bin size = 10%).

Fault data from the LPM area are divided into two populations (FP1 and FP2). The relative age of these two fault populations cannot be definitively established, but based on field and map relations FP2 faults appear to cut FP1 faults and are inferred to be younger. The less abundant, older population (FP1) strikes roughly east-west (range = 056°–081°, 248°–290°) and dips steeply (range = 52°–86°, Fig. 2.7A). Two sets of slickenlines are observed on FP1 planes. One set trends NW-SE and is near dip slip (average rake = 76°, Fig. 2.9B). The other trends E-W and indicates strike slip motion (average rake = 37°, Fig. 2.9E). Exposures of FP1 faults are concentrated in the south-central part of the map area, close to the CWF (Plate 1). Map scale FP1 faults display apparent normal, left lateral, and right lateral offset, with the largest offsets being left lateral and closest to the CWF at the southern edge of the map area. Thus, FP1 faults are similarly oriented and have apparent offsets similar to the CWF, especially in the southernmost map area.

The more abundant, younger fault set (FP2) strikes mostly NE-SW (range = 180°–240°) and dips steeply NW (average = 70°). The majority of slickenlines are oriented

~335° (average rake = 105°), roughly parallel to the dip slip FP1 population. A minor group (n = 4) of slickenlines in FP2 faults trend NE-SW suggesting a possible component of strike slip motion on FP2 faults. Map scale FP2 faults show consistent dextral-normal offset and are distributed evenly throughout the study area. Additional minor faults strike N-S and NW-SE with steep dips but do not clearly fit into either population.

2.3.3 Description of Fault Kinematic Data

Incremental shortening and extension axes (P- and T-axes) derived from fault data are used to assess the distribution and compatibility of strain patterns between fault populations. Kinematically compatible fault populations are characterized through fault plane solutions constructed from linked Bingham P- and T- axes using Faultkin software (Allmendinger et al., 1992; Allmendinger, 2015). Fault plane solutions and contoured P- and T- axes illustrate the variation in strain field geometry between fault populations, suggesting deformation in the LPM block occurred in at least two distinct phases.

FP1 fault planes are separated into two subpopulations: those with NW-SE trending slickenlines, and those with E-W trending slickenlines. For the first group, shortening axes (P-axes) are clustered near vertical, and extension axes (T-axes) are clustered near north-south (Fig. 2.9C). The mean fault plane solution from linked Bingham axes for this subset has a nodal plane which strikes near E-W and dips ~45° to the north with normal sense motion. FP1 faults with E-W trending slickenlines have near horizontal P-axes concentrated in the SE quadrant. T-axes trend NE-SW and are also near horizontal (Fig. 2.9F). The nodal plane of the linked Bingham fault plane solution strikes 290°, dips 65° NE, and suggests dominantly oblique right lateral slip (Fig. 2.9G).

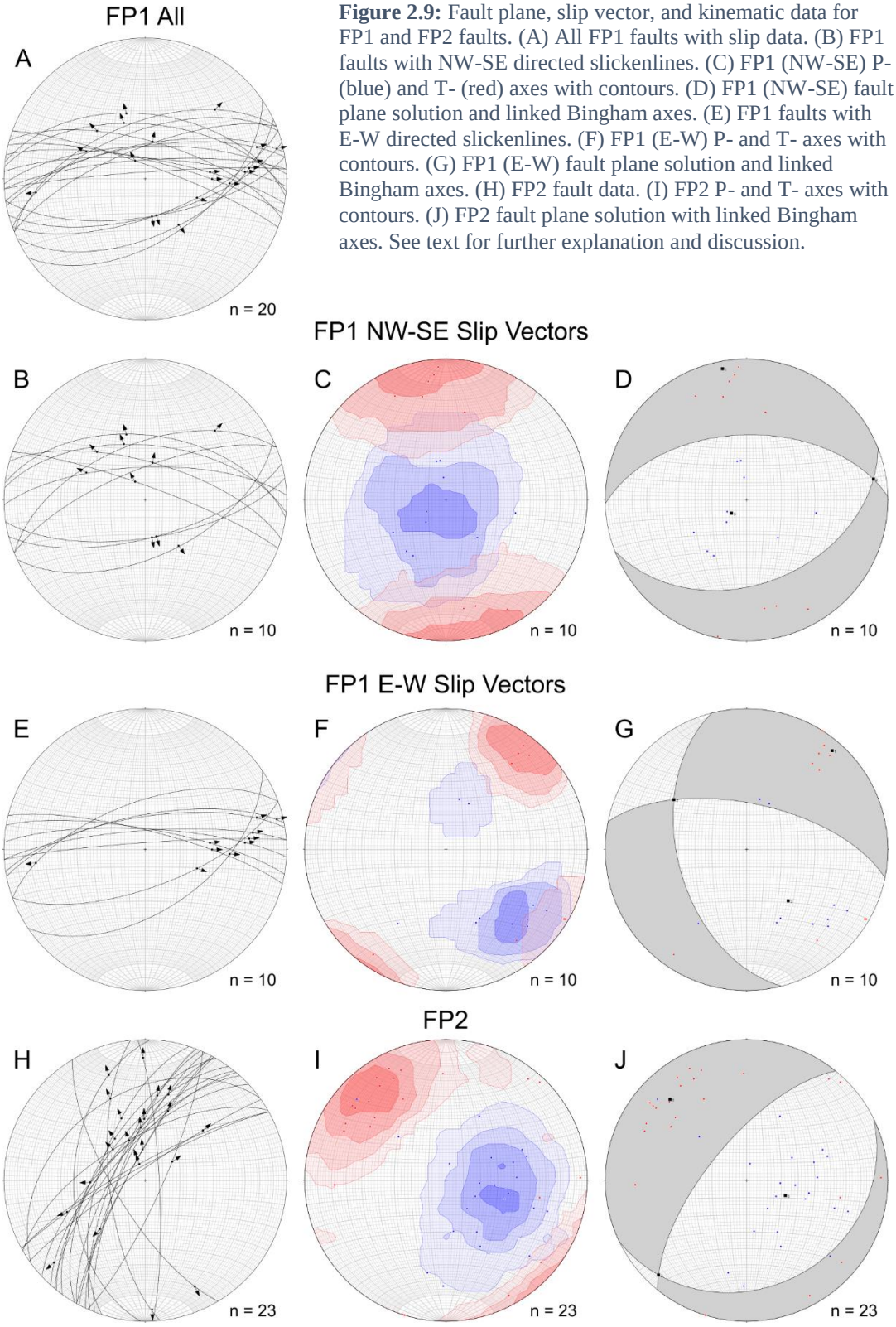

Figure 2.9: Fault plane, slip vector, and kinematic data for FP1 and FP2 faults. (A) All FP1 faults with slip data. (B) FP1 faults with NW-SE directed slickenlines. (C) FP1 (NW-SE) P- (blue) and T- (red) axes with contours. (D) FP1 (NW-SE) fault plane solution and linked Bingham axes. (E) FP1 faults with E-W directed slickenlines. (F) FP1 (E-W) P- and T- axes with contours. (G) FP1 (E-W) fault plane solution and linked Bingham axes. (H) FP2 fault data. (I) FP2 P- and T- axes with contours. (J) FP2 fault plane solution with linked Bingham axes. See text for further explanation and discussion.

Kinematic data for FP2 faults (Fig. 2.9I) are consistent with NW-SE directed extension. Principle shortening axes trend 110° and plunge 66° on average. Extension axes cluster in the NW quadrant, trending 315° and plunging 22° on average. The linked Bingham fault solution nodal plane strikes 210° and dips 70° NW (Fig. 2.9J). The fault plane solution diagram suggests top to the NW normal motion with a minor dextral component.

2.3.4 Interpretation of Fault Data

Fault slip and kinematic data combined with field observations, geologic mapping, and cross section analysis, illustrate the complexity of the deformation history in the LPM study area. Slickenline data from FP1 faults indicate a history of dip slip normal and right lateral strike slip motion. In contrast, the majority of mapped FP1 faults have apparent left lateral offset. This discrepancy is difficult to reconcile unless normal sense motion occurred late or sense of slip on fault planes has been misinterpreted and the faults are actually left lateral reverse faults. Regardless, motion on FP1 faults has contributed to two distinct strain fields, one of N-S extension and one of E-W directed strike slip motion.

The relative timing of normal vs strike-slip motion on FP1 faults is difficult to interpret. Along strike coarsening of Tls1 to the north and the buttress unconformity/south dipping normal fault discussed in section 2.2.2 suggest up to 300 m of N-S directed extension occurred in the earliest stages of deformation. Strike-slip motion on FP1 faults must have occurred later, likely during motion on the LPF. Problematically, FP1 faults with NW-SE directed slickenlines are observed in all parts of the Miocene section,

meaning some dip slip motion (N-S extension) must have occurred later in the evolution of the area as well. NW-SE directed FP1 slickenlines are roughly parallel with FP2 slickenlines suggesting the two populations may have been active at the same time, with FP1 faults reactivated during formation of FP2 faults.

The similar orientation of FP1 faults and the CWF suggests the two are related and may share a similar slip history. Hileman et al. (1990) interpret the CWF as a transform structure dominated by strike-slip motion despite their inference of ~1 km normal sense top to the north offset based on offset basement thrust faults. The inferred trace of the CWF in the LPM study area has an apparent left lateral offset of ~400 m. These observations suggest the CWF has a complex history of north directed normal motion followed by strike-slip or oblique motion similar to FP1 faults.

FP2 fault data indicates dominantly NW directed extension, roughly parallel to the extension direction of the LPF. FP2 faults can be interpreted as antithetic structures formed in response to motion on the LPF. The steep dip of FP2 faults suggests they may have rotated with the LPM block. When FP2 data is rotated to restore bedding to horizontal, fault planes dip ~60° on average, slickenlines trend 310° on average, and principle shortening axes become near vertical instead of inclined to the east, consistent with Andersonian mechanics in a NW-SE oriented extensional stress regime. Motion along FP2 faults was likely synchronous with motion on the LPF.

Overall fault slip and kinematic data suggests a complex history of N-S directed extension, E-W directed strike-slip motion, and NW-SE directed extension with reactivation of older faults. Fault populations are not kinematically compatible with a

single phase of E-W directed extension. The interpreted history favored here is one of minor N-S extension followed by synchronous NW-SE directed extension and strike-slip motion.

2.3.5 Regional Tectonic Scenarios for Faulting

East-west striking FP1 faults have similar sense of displacement and are concentrated near the CWF, suggesting the small-scale faults can help inform the tectonic evolution of the CWF. Several tectonic scenarios may help explain FP1 faults and their multiple sets of slickenlines as well as the CWF. It is possible the fault system represents:

1. E-W striking normal faults associated with an early stage of N-S extension reactivated as strike-slip and dip slip faults during motion on the LPF.
2. A right lateral transform fault system associated with a left step in the LPF.
3. A left lateral transform system associated with a right step in the LPF and/or differential extension between the LPM block and the OW block to the south.

The first scenario is considered the most likely based on interpretation of fault data presented above. The other two scenarios are supported by the relationship between the CWF and LPF (the LPF terminates abruptly against the CWF) but do not explain why the CWF continues for ~8 km NW of the LPF or why dip slip slickenlines are preserved on E-W striking faults.

2.4 Stratigraphic and structural summary of LPM area in the context of the CREC

2.4.1 Overview

Geologic mapping and analysis of fault data from the LPM area has important implications for the evolution of the CREC margin and breakaway zone. The Little Piute Fault has been interpreted as the breakaway zone of the CREC detachment fault, representing the western boundary of the CREC at the latitude of the LPM. This interpretation is reasonable for the exposed length of the LPF as the fault appears to be the westernmost major structure in the area which places a thick Miocene sedimentary and volcanic succession against crystalline basement. This study clarifies key points and reveals greater complexity regarding the evolution of the LPM area.

2.4.2 Stratigraphic Summary

The lowest portion of the Miocene section (Tls) accumulated in a roughly E-W trending basin. Basin formation may have resulted from an early stage of N-S extension, associated with pre-19 Ma northeast directed extension in the southern CREC (e.g. Faulds et al., 2001; Gans et al., 2018). The volcanic section (Tmv) in the LPM records the local eruption of a diverse suite of basaltic to andesitic lavas which constructed a broad volcanic edifice coincident with the early depositional center. The 18.78 Ma Peach Spring Tuff arrived after the cessation of local volcanism, blanketing the entire LPM block and covering local topography. The upper sedimentary section (Tus) is the only accumulation of Miocene rocks which records sedimentation synchronous with motion on the Little Piute Fault. Approximately 2 km of coarse alluvial fan deposits accumulated in the hanging wall of a growth fault basin after ~17.8 Ma.

2.4.3 Structural Summary

Deformation in the LPM study area likely occurred in at least two phases. Fault kinematic data combined with field observations and mapping show the strain field evolved from N-S to NW-SE directed extension with a component of strike slip motion along the southern edge of the LPM block. Map scale and mesoscopic faults appear to be related to motion on the Little Piute and Carson Wash faults. East-west striking FP1 faults have a history of both north directed normal motion and east-west directed strike slip motion, similar to the interpreted history of the CWF. It is unclear whether strike slip motion on the CWF and FP1 faults accommodated differential extension between blocks or a step-over in the LPF. It does however seem likely the CWF formed as a normal fault and reactivated as a strike slip fault during motion on the LPF. FP2 faults are dominantly NW directed normal faults, antithetic to the LPF. These faults likely formed as subsidiary structures during motion on the LPF.

2.4.4 Relation to CREC Breakaway Models

Observations in the LPM area point to several key conclusions regarding the evolution of the CREC margin. There is no evidence for significant E-W or NE-SW directed extension in the study area prior to ~17.8 Ma. This implies the CREC breakaway at the latitude of the LPM area is entirely younger than the breakaway to the south in the vicinity of the Mopah Range (active before 19 Ma), meaning the faults must be separate structures despite being commonly drawn as continuous. Tilting in the footwall (Piute Mountain block, see section 3) is similar to tilting in the hanging wall of the postulated breakaway fault (LPF), implying the fault has rotated roughly 20° westward and had an

original dip of ~60°. Thus, there is no evidence the LPF differs fundamentally from a typical high angle normal fault, and it is possible the LPF is part of a series of high angle normal faults which bound increasingly tilted blocks to the east (e.g. Gans and Gentry, 2016). There is also no direct evidence that the LPF flattens abruptly at depth or that it contributed to slip on a major detachment fault exposed in the central CREC to the east (e.g. Spencer, 1984), but neither is there evidence that argues against this interpretation. Lastly, tilting and fault data indicate the extension direction in the LPM area is NW-SE, orthogonal to the direction generally observed in the central part of the corridor at this latitude.

3. Geology of the Northwest Piute Mountains Study Area

3.1 Area Overview

The northwest Piute Mountains (NWPM) study area is located approximately 10 km west of the inferred trace of the CREC breakaway at a latitude of ~34.76° N (see Fig. 1.5). The study area contains Miocene sedimentary and volcanic rocks exposed over an area of ~8.5 km^2 which preserve populations of NE-SW striking normal faults and E-W striking strike-slip faults. The entire Piute Mountain crustal block is tilted ~20° NW, sits in the hanging wall of an inferred SE dipping normal fault obscured by alluvium in the Fenner Valley to the west (see Fig. 1.6; Foster et al., 1991), and in the footwall of the LPF described in the previous section.

3.2 Miocene Stratigraphy

3.2.1 Overview

The exposed Miocene section in the NWPM area ranges from ~50-250 m thick and consists of coarse clastic sedimentary rocks and Peach Spring Tuff. The PST serves as a key temporal and lithologic marker across the field area, dividing the otherwise sedimentary sequence. The section is deposited nonconformably on pЄx and Pz metamorphic basement and displays lateral facies variation over distances of <500 m. Stratigraphy described here and used during geologic mapping is significantly more detailed than reported by previous workers (Hileman et al., 1990; Foster et al., 1991).

3.2.2 Description of Map Units

The base of the Miocene section throughout most of the study area is a monolithologic conglomerate composed of hypabyssal dacite clasts ranging from pebbles

to cobbles up to 10 cm. Clasts are angular and supported in a sandy matrix. This unit (Tdc) rests directly on pЄx basement. Unit thickness varies from nearly 50 m in the western field area to 20 m or less in the east. Tdc is not exposed in the northeast portion of the mapping area, apparently never deposited. Foster et al. (1991) published a K-Ar date of 19.4 Ma for a dacite boulder from this unit.

The most areally extensive sedimentary unit is a coarse polymict volcanic boulder conglomerate. This unit (Tbc, Fig. 3.1B) consists of dominantly matrix supported cobbles and boulders up to 1.5 m in diameter. Clast composition ranges from basalt to andesite, with phenocryst abundance less than 15%. Tbc is deposited directly on basement rocks in the northeast, and conformably on Tdc in the east. Tbc is not exposed in the western half of the map area. Tbc ranges in thickness from approximately 10 m to 45 m.

Directly overlying Tdc in the western half of Plate 2 is a coarse sandstone with minor conglomerate (Tss, see Fig. 3.2) composed of ~80% quartz, ~15% feldspar, and ~5% mafic minerals. Average grain size is 2 mm with subordinate pebbles up to 5 mm. The coarse fraction is dominated by marble and gneiss with rare silicic volcanic detritus suggesting either a change in sediment source region or complete removal of Tdc clast source material. Tss has a maximum thickness of 40 m in the west and thins eastward to <10 m.

The oldest primary volcanic deposits directly overlie Tss. In the south, a ~2 m thick ash and lapilli fallout tuff crops out below the base of the Peach Spring Tuff. It appears to represent a small precursor eruption prior to eruption of the Peach Spring Tuff. An additional ~50 cm of reworked tuff is present in the southern area. The tuff is buff

white with consistent fine grain size and minimal lithic fragments. This tuff appears to have been deposited in a shallow lacustrine environment reworking and consolidating the fine material and reducing its areal extent.

The Peach Spring Tuff is the thickest and most extensive Miocene volcanic rock in the NWPM area. The tuff exhibits all the traits typical of ignimbrites including a massive unsorted fragmental character and characteristic zonation in: welding, crystal abundance, glass preservation, and vapor-phase alteration. The PST in the NWPM area ranges from ~60–130 m thick, including some of the thickest identified sections in the CREC region. In this report, the tuff is divided into six members to provide additional detail during geologic mapping.

The lowest member (Tpul, Fig. 3.1C) consists of rarely preserved basal surge deposits and the overlying unwelded portion of the ignimbrite sheet. Tpul is white to tan unconsolidated ash and lapilli-sized pumice and lithics and is typically covered by more resistant debris from the overlying resistant part of the tuff. Tpul averages 8–12 m thick. It is overlain by the lower vitrophyre (Tpv), a black to grey moderately welded layer approximately 3–5 m thick. Tpv is recessive and poorly exposed in the field area, forming slopes often covered by overlying debris. The third member (Tpd, Fig. 3.1D) is densely welded and devitrified with a microcrystalline groundmass. Tpd is the most resistant and best exposed member, often forming cliffs or steep ridges. Cooling joints are well-preserved and vapor-phase alteration becomes prevalent in this member. Average unit thickness is approximately 15 m but can range up to 25 m. The fourth member (Tpi) is the poorly exposed middle portion of the tuff, characterized by pervasive vapor-phase

alteration and a devitrified groundmass. Dense welding, fiamme, and lithophysal cavities are typical of Tpi and lithic fragments are increasingly rare up-section. Tpi is the thickest member of the PST ranging from ~35–60 meters. The fifth member (Tpdu) is similar to Tpd. The unit exhibits a devitrified groundmass but little vapor-phase alteration and forms erosion resistant cliffs which define topography. The uppermost Peach Spring Tuff member (Tpuu) is unwelded with a vitric groundmass and abundant crystals (up to 20%) but little to no lithic or pumice fragment preservation. It is poorly exposed and sometimes not present at all due to erosion and reworking following deposition. Thickness of the upper member is poorly constrained but does not exceed 15 m.

Minor poorly exposed sections of coarse siliciclastic sedimentary rocks (Tcs) locally overlie the PST and exhibit tilting comparable to the tuff and lower rock units. Deposits are primarily coarse conglomerate and interbedded sandstone with ~40% Peach Spring Tuff and ~60% basement clasts, hypabyssal dike rock, and volcanic boulders. Quaternary alluvium in the Piute Mountains is composed of coarse angular to rounded cobble conglomerates and coarse gravel beds. Alluvial deposits are flat-lying and undeformed.

3.2.2 Interpreted Stratigraphic History

The Miocene section in the NWPM study area preserves a history of coarse clastic sedimentation and distal volcanism. There is no obvious structural control on sedimentation and it seems more likely sediments accumulated in a broad paleovalley along the flank of the Piute Mountains.

Pre-PST sediments contain a mix of Miocene volcanic and older plutonic/metamorphic basement clasts in a mixed sand and gravel matrix. The monolithologic, angular clasts of Tdc suggests hypabyssal intrusions occurred nearby, and the quartz sand matrix suggests dikes intruded plutonic or metamorphic basement. The presence of large basaltic boulders (>2 m diameter) and coarse angular nature of Tbc suggests very short transport distance and implies primary volcanic rocks were present near the study area in the Miocene. The pre-PST section ranges from <20 m to >70 m over lateral distances of <1 km indicating sedimentation was locally controlled from the beginning of deposition in the study area.

The basal unconformity is tilted 20°–30° westward similar to the rest of the section. The map distribution of Tbc and Tss, both of which overlie Tdc, suggests sediments are for the most part locally derived and were deposited across an area of low topographic relief. Tbc accumulations are thickest and coarsest adjacent to basement rock and thin dramatically to the west where sandstone and gravel conglomerate are more common.

The stratigraphy and map pattern of sediments in the NWPM area suggests a history of deposition in a paleovalley. The PST then flowed into the same paleovalley blanketing the entire Miocene section. Minor post-PST sedimentation finished filling the valley prior to the onset of significant deformation in the study area.

Figure 3.1: Field photos of select rock units described in text.
A-Coarse sandstone beds within boulder conglomerate (Tbc).
B-Boulder conglomerate (Tbc).
C-Unwelded base of PST (Tpul).
D-Welded, devitrified interior of PST (Tpd).
E-Tbc and lower PST stratigraphy.

3.3 Structural geology

3.3.1 Overview

Miocene rocks in the Piute Mountains are typically tilted 20-30°, mostly dipping to the northwest. Orientation data for the Peach Spring Tuff is measured using the compaction foliation defined by flattened pumice fragments (fiamme, see Fig. 3.1D). Sedimentary bedding is measured for all other units (Fig. 3.2B). Although major faults are rarely exposed, stratigraphy is offset and repeated across several structural blocks bound by steeply dipping normal faults (see Plate 2B). A broad syncline is present in the west map area. Strata in each limb of the syncline dip approximately 30° and define an open fold axis which trends 009° and plunges 12.5° to the north (Fig. 3.2D). The fold axis orientation is within 20° of the average normal fault orientation in the area suggesting folding could be associated with motion along major normal faults on both sides of the syncline. The entire Miocene section is folded and faulted to the same degree indicating deformation completely postdates deposition.

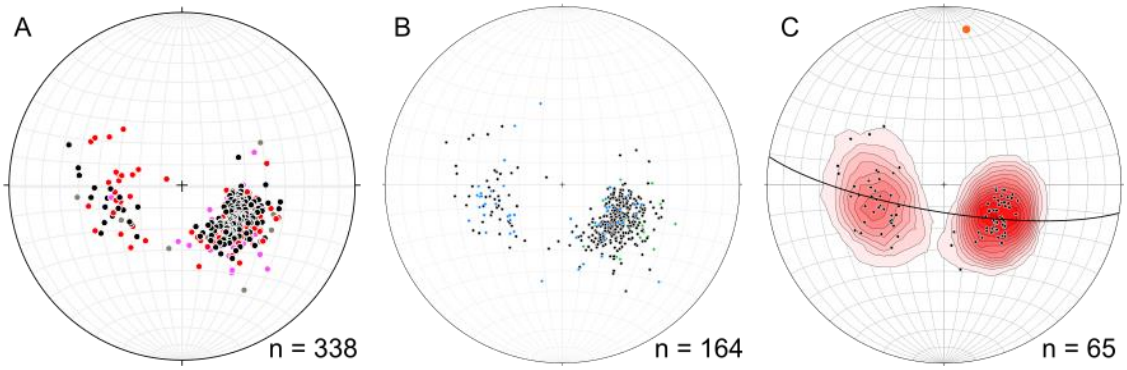

Figure 3.2: Equal area lower hemisphere stereographic projections of bedding and compaction foliation data.
A-Poles to Peach Spring Tuff compaction foliation (black=Tpd, red=Tpi, pink=Tpu, grey=Tpv).
B-Poles to bedding/compaction foliation for all Miocene rocks (black=Tp, blue=Tdc, green=Tbc/Tss).
C-PST/bedding contour and cylindrical best fit for data near syncline (fold axis=009°,12.5°).

3.3.2 Fault Data

Brittle faults are abundant throughout the NWPM study area, but are poorly preserved. Of 160 faults measured in the study area, 143 come from the PST. Only 15 faults preserve measurable slickenlines, all of which are in the PST. Faults are found as discrete planes with cataclasite and as brecciated zones up to ~15 cm wide (Fig. 3.4). Slickenlines, Riedel shears, and observed offsets indicate the presence of dip-slip normal and right lateral strike slip faults. Offsets across observed faults range from <20 cm to >100 meters. The largest faults have an apparent offset of 150-250 m. Mesoscopic planes strike in all quadrants and have a wide range of dips (~20°–90°) but are concentrated into two populations: NE-SW striking dip slip normal faults and E-W striking right lateral faults (Fig. 3.3). Map scale faults (>10 m offset) consist exclusively of NE-SW striking normal faults.

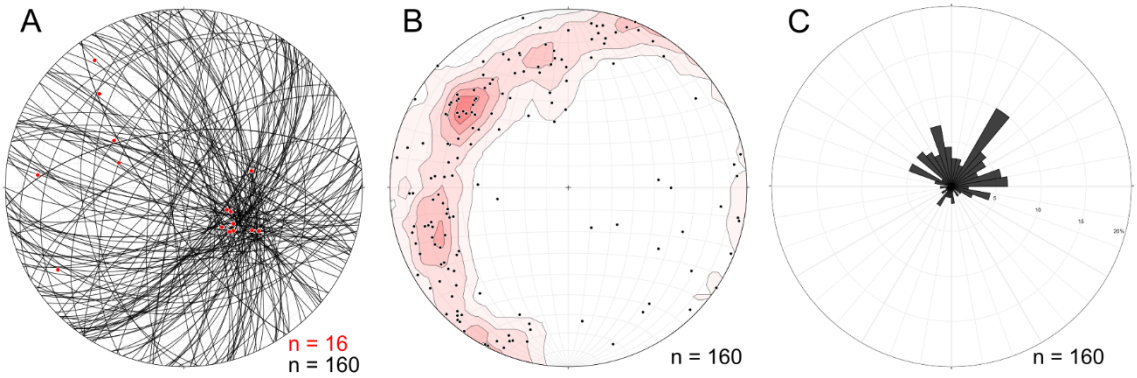

Figure 3.3: (A) All fault planes (black) and slickenlines (red).
(B) Poles to all faults with contour.
(C) Rose diagram of all fault planes by strike (unidirectional, bin size = 10%)

Map scale normal faults in the study area strike between 020° and 040° and dip from 45° to 65° SE and NW. Slickenlines preserved on these faults are almost entirely dip slip (average rake = 86°) trending NW-SE (Fig. 3.4A). Kinematic data from normal faults (Fig. 3.4B) shows that principle extension axes (T-axes) are oriented parallel to slip direction (average = 117°, 10°) and principle compression axes are near vertical (average = 288.6°, 79.7°). Kinematic axes are tightly clustered as expected for a uniform data set. The fault plane solution from Bingham axes yields nodal planes oriented 025°, 55° and 205°, 25°.

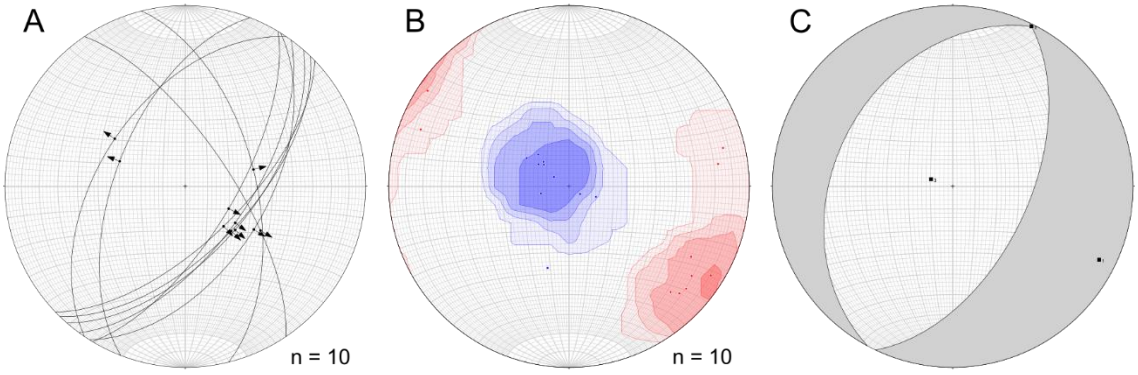

Figure 3.4: (A) Normal fault planes with slip vectors.
(B) P- (blue) and T- (red) axes for normal fault with contours.
(C) Fault plane solution with linked Bingham axes.

East-west striking faults have subvertical dips and strike slip displacement. These faults are small offset (<3 m) and do not appear on the geologic map. The faults rarely preserve slickenlines but have mostly right lateral offset with a possible oblique component. East-west striking faults clearly cut and offset NE-SW striking faults in at least two locations indicating strike slip faulting postdates normal faulting. Kinematic data from strike-slip faults is incoherent due to a lack of slip data.

Figure 3.5: Field photos of faults
(A) through (D) – Typical fault plane exposures in the study area.
(E) – Major fault trace separating Pzm and Tpd/Tbc showing repeated section of Tp.

3.3.3 Extensional Folding

The west limb of the syncline exposed in the westernmost map area contains the only east dipping rocks observed in the NWPM. The reason for folding instead of uniform tilting in this area is enigmatic. Two observations may help explain the presence of the syncline. Folded Miocene rocks are located between exposures of relatively competent and isotropic pre-Miocene basement. and the eastern margin a depositional contact and the western margin a major east-dipping fault contact.

It seems most likely that the syncline formed due to drag on the fault which bounds the section. Competent basement on either side of the fold may have enhanced drag on the fault and prevented the development of additional normal faults observed elsewhere in the map area.

3.3.4 Relationship Between Folding and Faulting

The relationship between and relative timing of normal faulting and folding/rotation of strata is unclear. Faults currently dip ~60°, have bedding to fault cutoff angles ~90°, and dip away from the fold axis in both limbs of the syncline. Unfolding stratigraphy and faults restores normal faults to subvertical (Fig. 3.6). These observations raise the question of whether faulting in the NWPM area occurred before, during, or after rotation of Miocene strata. It is possible the faults initiated as subvertical extension fractures and reactivated as normal faults during or after block rotation (Fig. 3.7A). It is also possible the faults formed as typical ~60° normal faults during or after block rotation (Fig. 3.7B).

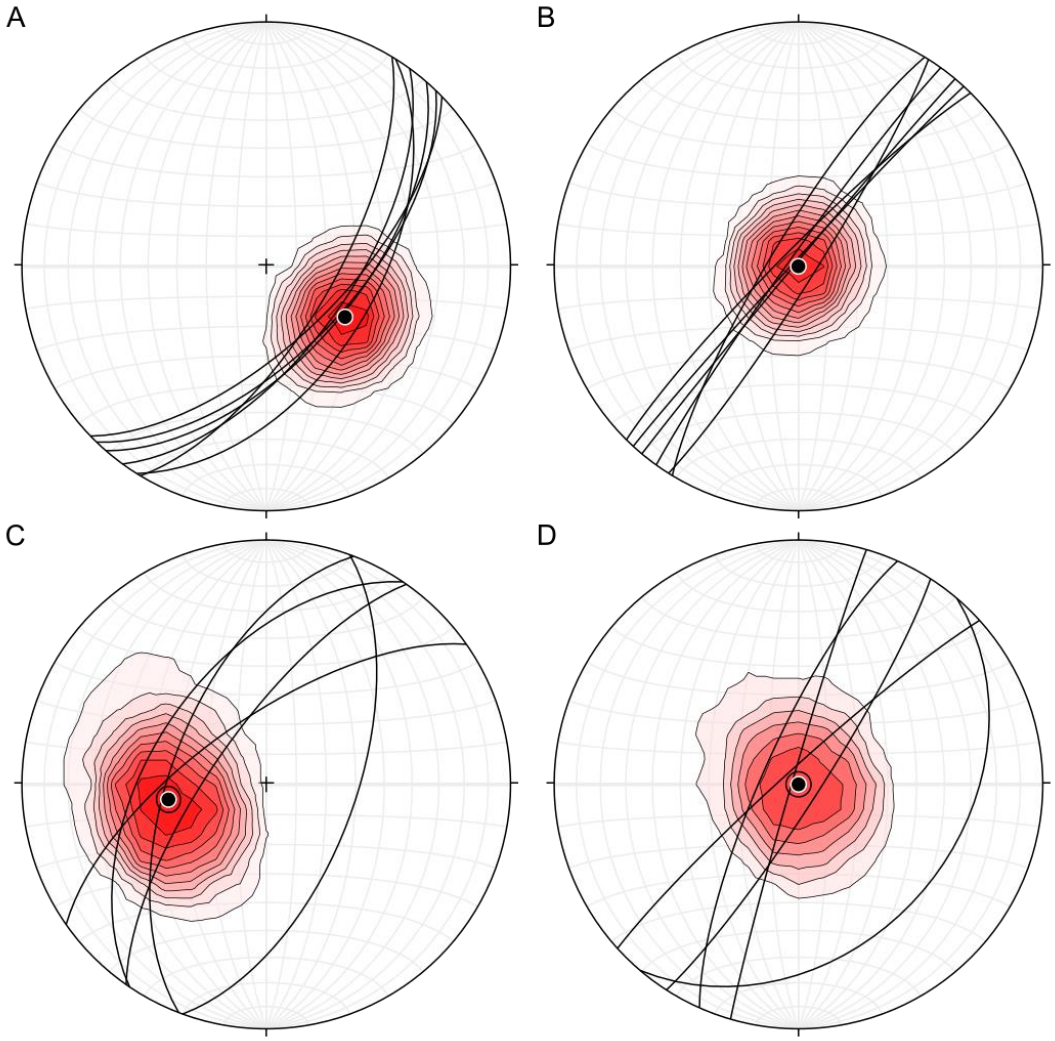

Figure 3.6: Equal area lower hemisphere stereographic projections showing rotation of fault data.
A-Normal faults and contoured poles to bedding with mean vector (123°,59°) – east of syncline axis
B-Faults and bedding contour restored to bedding horizontal – east of syncline axis
C-Normal faults and contoured poles to bedding with mean vector – west of syncline axis
D-Faults and bedding contour restored to bedding horizontal – west of syncline axis

Observations in the study area cannot establish which of these scenarios is more likely, although rocks outside of the study area to the west are tilted westward implying folding and eastward tilting are local phenomena. Foster et al. (1991) showed that the entire Piute Mountain block is tilted ~20° westward, also suggesting folding and west directed faulting are localized in the study area. These broader observations suggest faulting likely occurred during or after folding and 90° cutoff angles are coincidental rather than indicative of a change in deformation style.

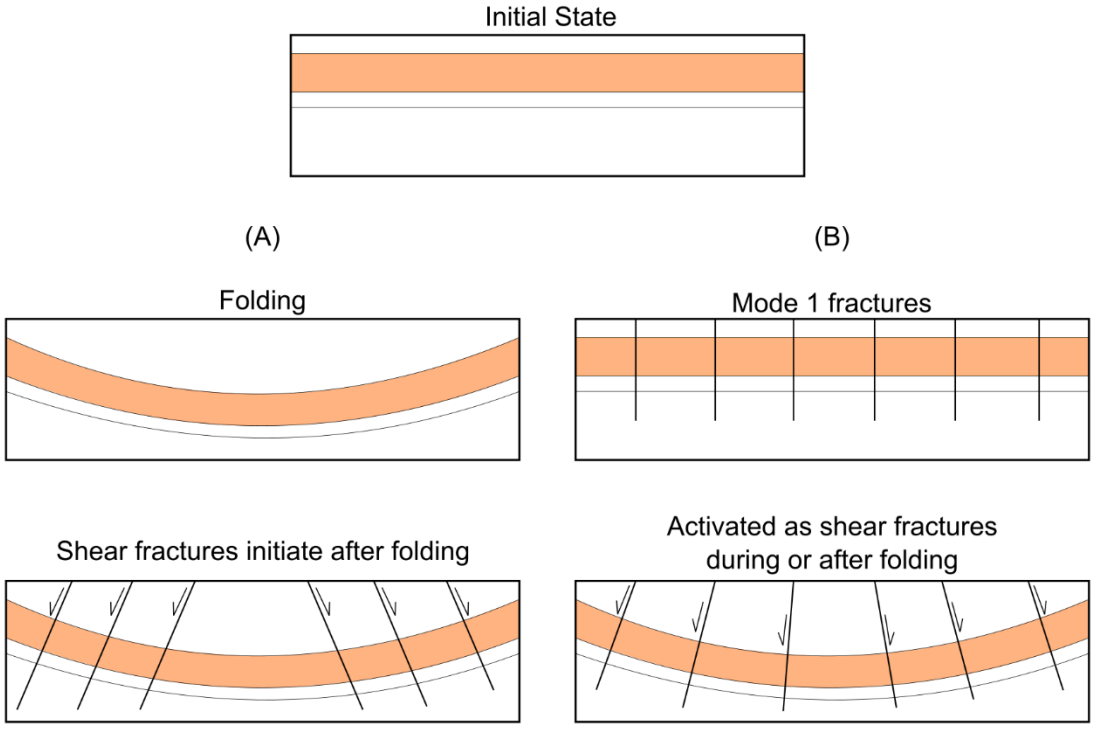

Figure 3.7: Schematic illustration of possible normal fault formation scenarios leading to 90° cutoff angle.
(A) Faults initiate as ~60° shear fractures.
(B) Faults initiate as vertical extension fractures and reactivate as shear fractures during folding.

3.3.4 Magnitude of Extension

Extension magnitude in the NWPM area is an order of magnitude lower than in ranges in the CREC to the east. Results from this study are in agreement with Hileman et al. (1990) who reported an extension estimate of 12–35% (stretching factor 1.12–1.35). Extension estimates are calculated using the geometric relationship between fault dip and percent extension shown (see Thompson, 1960; Wernicke and Burchfiel, 1982) and palinspastic reconstruction of cross sections (Fig. 3.8). Total extension calculated using fault and bedding geometry is 15% (stretching factor of 1.15). Extension estimated from palinspastic reconstruction (Fig. 3.8) is 7.5% with a horizontal stretch factor of 1.075. Extension magnitude estimates depend on fault geometry and reconstruction location but total horizontal extension is approximately 200 m across the area. However, estimates of the amount of extension from Figure 11 are underestimated because the cross section does not include the major east dipping normal fault which bounds the section. Including a fault with an estimated horizontal displacement of 100 m increases the stretching factor to approximately 1.15.

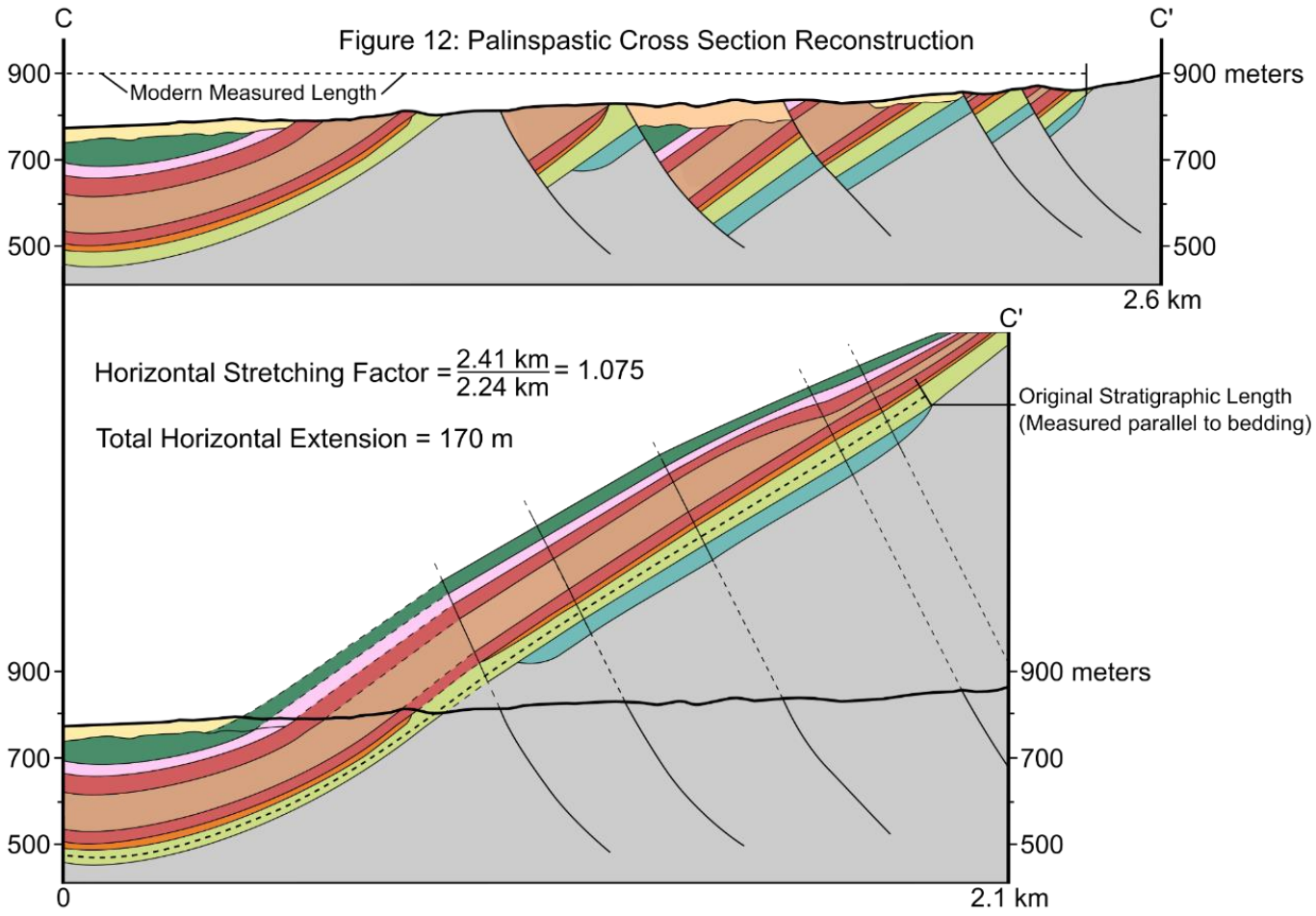

Figure 3.8: Palinspastic reconstruction of cross section line C-C’ from Plate 2. Restored offset across faults is used to calculate total extension due to normal faulting.

3.4 Summary of NWPM Area

3.4.1 Stratigraphic Summary

Sedimentation in the NWPM study area occurred sometime between ~19.4 Ma and ~18.8 Ma. Locally derived coarse clastic sediments shed from the Piute Mountain block into isolated north-south trending topographic lows along the western flank of the range and deposited sections ranging from 20–80 m thick. Thick accumulations (>100 m) of the Peach Spring Tuff then arrived, filling much of the remaining depositional centers. The top of the PST eroded and minor sedimentation continued in the western map area, depositing ~20 m of post-PST conglomerate and sandstone. The sedimentation history of the NWPM is not clearly related to any active deformation in the study area and is probably related mostly to uplift of the Piute Mountain block as a whole.

3.4.2 Structural Summary

Deformation in the NWPM study area initiated after emplacement of the PST (~18.8 Ma) and persisted for an uncertain amount of time. Top to the southeast directed normal faulting with minor antithetic northwest directed normal faulting dominated the area initially. Normal faults have a cumulative offset of ~1 km and cumulative horizontal extension of ~300 m across the study area (extension factor = 1.15). Minor east-west striking right lateral faults formed subsequent to the majority of normal faulting and have offsets <10 m. The broad syncline in the western study area is likely an extensional feature formed as a result of drag on the major east dipping normal fault which bounds the west edge of the Miocene section. It is possible normal faults in the study area initiated as subvertical extension fractures and reactivated as shear fractures during tilting/folding,

although there is no definitive evidence. The entire Piute Mountain block is tilted 20° westward due to motion on the major normal fault inferred to lie under the Fenner Valley west of the study area. Westward tilting of the Piute Mountain block as a whole ceased by ~16.6 Ma although local tilting occurred as late as ~10 Ma (see Miller et al., 1998).

3.4.3 Relation to CREC Breakaway

The deformation history in the NWPM study area has implications for the history of the CREC margin. The study area lies in the footwall of the CREC detachment approximately 10 km west of the inferred trace of the breakaway, yet there is abundant evidence for extension in the study area between 18.8 Ma and 16.6 Ma. Normal faulting in the NWPM area is roughly contemporaneous with deformation in the Little Piute Mountains and the Sacramento Mountains to the east. The dominant extension direction (SE) observed in the NWPM area is perpendicular to the extension direction observed in the central CREC (NE). Although extension magnitude is less in the NWPM than in the central CREC, Miocene extensional deformation clearly persisted well beyond the interpreted CREC breakaway. A major east dipping normal fault must be present west of the CREC breakaway to account for block rotation of the NWPM. Other than preservation, it is difficult to see any fundamental difference between the Fenner Valley Fault and the Little Piute Fault/CREC breakaway fault.

4. Geology of the Piute Range Study Area

4.1 Area Overview

The Piute Range (PR) is an approximately 30 km long, 5 km wide mountain range located 50 km north of the OWP area and 40 km west of Laughlin, NV (Fig. 4.1). The range is comprised of Miocene volcanic and sedimentary rocks deposited nonconformably on Cretaceous and Precambrian basement. The southernmost portion of the range is pervasively deformed by N-S striking brittle normal faults which offset Miocene stratigraphy and underlying basement. The E-W trending Piute Canyon bisects the range providing exceptional exposure of stratigraphy, fault planes, and slip direction indicators. The entire southern Piute Range crustal block—including crystalline basement—is tilted 20° eastward, consistent with block rotation due to west-directed normal faulting.

Previous workers (e.g. Spencer, 1985; Howard and John, 1987) have placed the east directed CREC breakaway under alluvium east of the Piute Range (see Fig. 1.2) and assumed the area to the west (the PR block) is unextended. In the model of Spencer (1985) the Newberry Mountains (~30 km east of PR) are the domal uplift in the footwall of the CREC detachment fault and the Piute Wash area contains the synformal upper plate. Spencer (1985) also proposed the breakaway is exposed in the Piute Wash Hills ~5 km east of the Piute Range front.

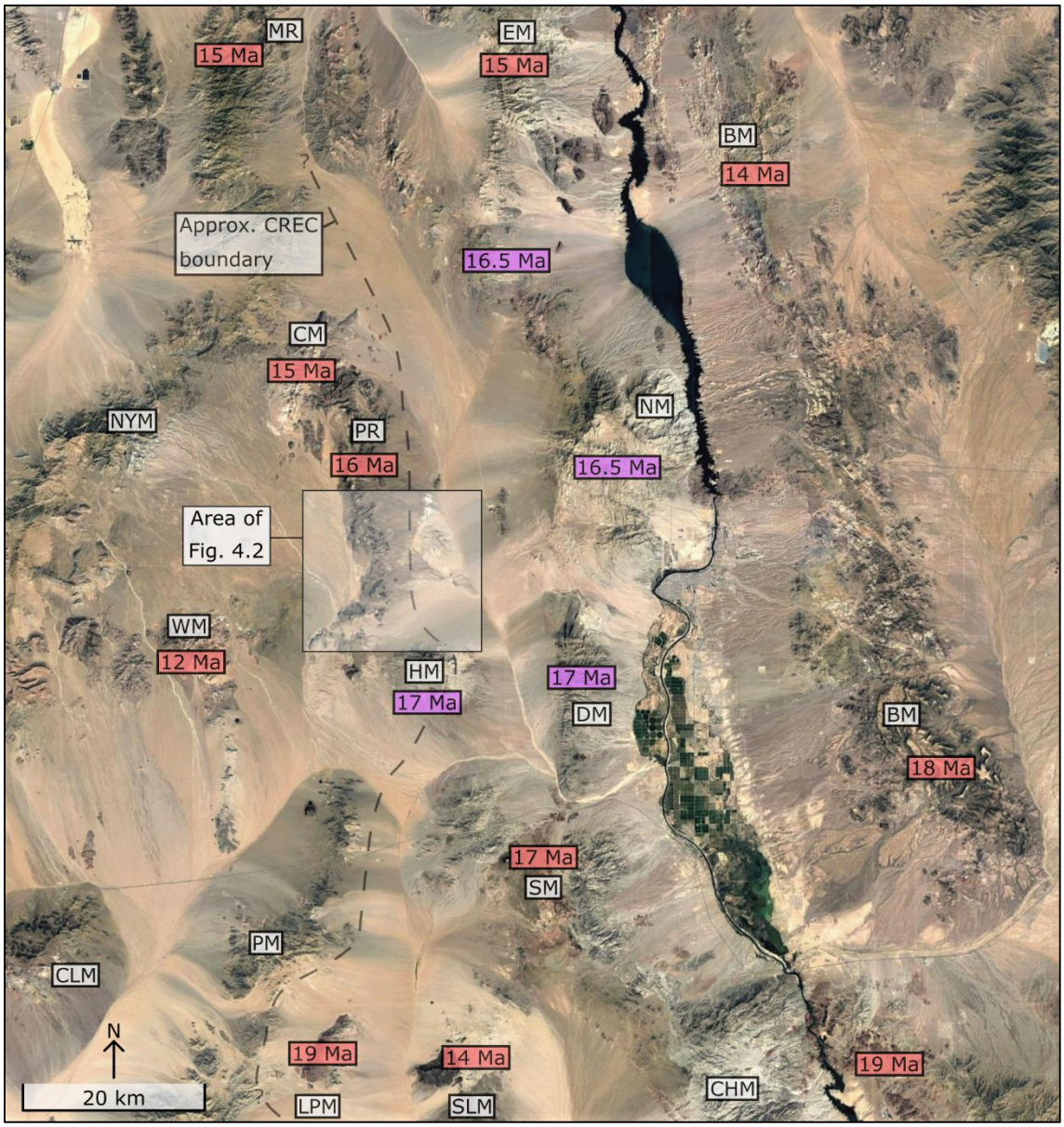

Figure 4.1: Satellite overview map of central CREC and Piute Range area. Dashed line marks approximate western limit of CREC, as drawn by previous workers. Red boxes show approximate age of volcanism in individual areas. Purple boxes show approximate ages of magmatism and pluton/dike emplacement in ranges with deeper structural exposure. White boxes label mountain ranges: CLM-Clipper Mountains, LPM-Little Piute Mountains, SLM-Stepladder Mountains, CHM-Chemehuevi Mountains, PM-Piute Mountains, SM-Sacramento Mountains, BM-Black Mountains, DM-Dead Mountains, HM-Homer Mountain, WM-Woods Mountains, NYM-New York Mountains, PR-Piute Range, NM-Newberry Mountains, CM-Castle Mountains, MR-McCullough Range, EM-El Dorado Mountains.

Volcanism in the central CREC and Eastern Mojave Desert occurred between 18 Ma and 10 Ma (see Fig. 4.1). Although the age of magmatism in areas around the Piute

Range has been constrained by previous workers (e.g. Musselwhite et al., 1989; Miller et al., 1998; Gans and Bohrson, 1998; Walker et al., 2007), the age of volcanism in the PR itself is virtually unknown. A single sample from the northern PR yields a K-Ar age of 15.8 Ma (Okaya, unpublished). There are no other reported ages in the Piute Range but based on the northward propagation of magmatism through the CREC and the age of

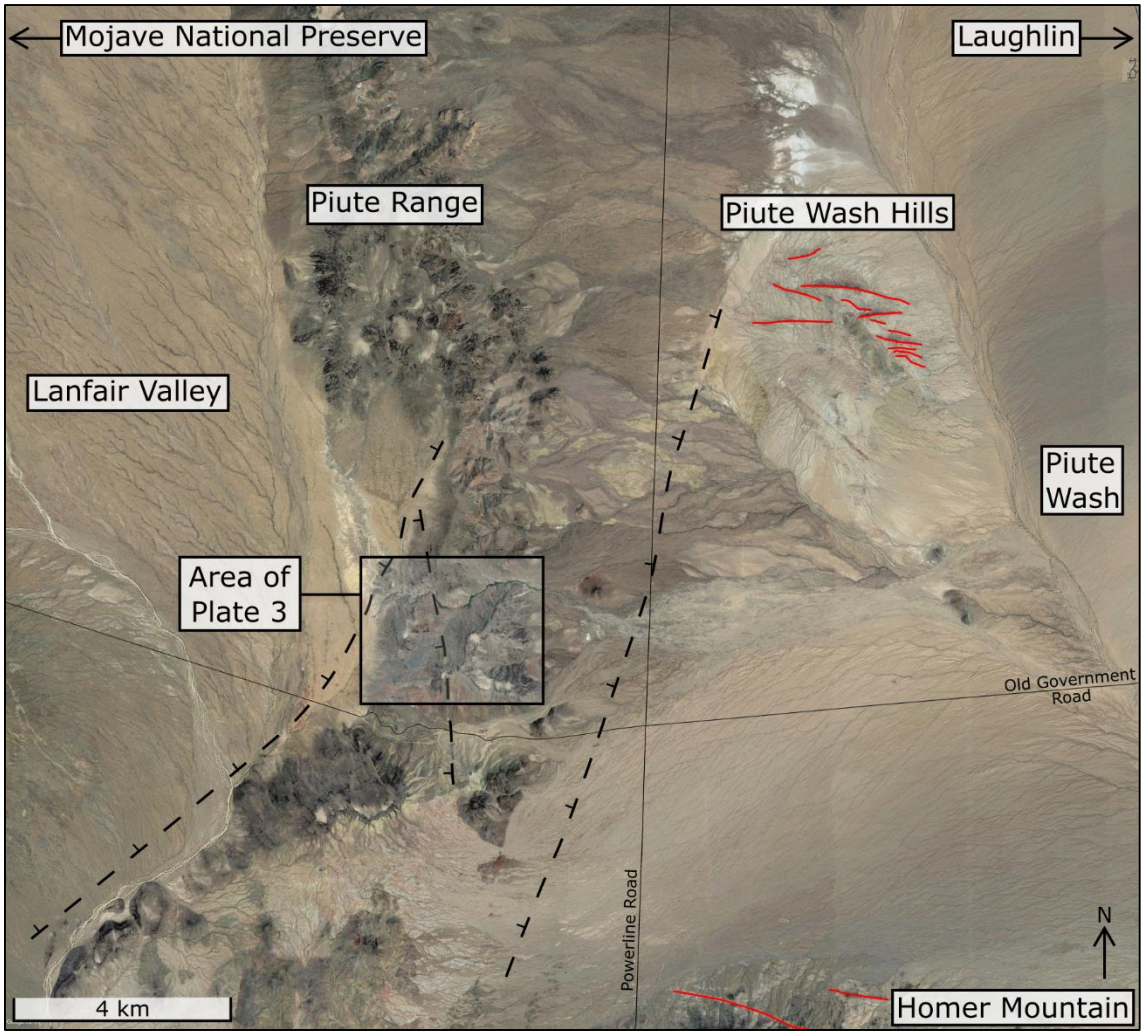

Figure 4.2: Satellite overview map of the Piute Range area showing area of Plate 3 geologic mapping, inferred major west directed normal faults (black dashed lines), and probable Miocene dikes (red lines).

surrounding volcanic and intrusive rocks it seems likely that volcanism in the southern PR occurred between ~17 Ma and ~15 Ma.

New geologic mapping and structural data combined with an improved understanding of Miocene stratigraphy allows the structural and volcanic evolution of the Piute Range area and its relationship to the CREC margin to be interpreted in greater detail than accomplished by previous workers.

4.2 Miocene stratigraphy

4.2.1 Overview

Miocene units exposed in Piute Range study area consist predominantly of mafic to intermediate volcanic rocks with subordinate intervals of volcaniclastic sediments. Rocks dip moderately (15°-20°) to the east but are offset by west dipping normal faults causing the section to repeat several times across the study area. Exposure is generally poor. Resistant mafic lavas form armored ridges and dip slopes and shed talus onto hill slopes, commonly obscuring stratigraphy between resistant units. Rubble and colluvium blanket areas up to 750 m across and sparse outcrops are generally difficult to correlate. The exception is Piute Canyon, a roughly 1 km long east-west incision in the range which cuts perpendicular to strike of rocks and faults (see Fig. 4.4). Rocks are well exposed throughout the canyon and fault plane preservation is exceptional making the area (located in the NW portion of Plate 3) the most fruitful source of stratigraphic and structural information.

Previous mapping in the Piute Range by Nielson et al. (1987) treated the entire Miocene section as undivided Miocene volcanics. This study presents the first effort to subdivide Miocene rocks in and around Piute Canyon. The section is divided on the basis of rock type, composition of lavas, and stratigraphic position. Individual lava flows are

discontinuous and difficult to map; thus map units generally contain 5 or more distinct lava flows and are grouped as sequences of similar composition. Individual flows range from <2 m to >10 m thick and map units range from ~20 m to >100 m thick. At the latitude of Piute Canyon, the complete Miocene section is estimated to be 1.2 km thick.

The Piute Range study site contains a mix of lava flows, near vent facies rocks (i.e. cinder cone remnants), and intrusive feeder dikes, all indicating the area was an active volcanic center with some associated sedimentation in the Miocene.

4.2.2 Stratigraphic Description

The base of the Miocene section (Tvc1) consists of 20–150 m of volcaniclastic sediments ranging from gravel to cobble conglomerate. Sediments are dominated by angular mafic volcanic clasts in a coarse sand matrix with up to 50% clasts in coarse beds (Fig. 4.3D). The abundance of angular volcanic fragments suggests clasts were sourced from nearby eruptive deposits and deposited in an area that had not yet experienced any volcanism.

A series of andesite lava flows (Ta1) overlie basal sediments and form a package ~80 m thick. These lavas contain roughly 7-15% phenocrysts of plagioclase, clinopyroxene, and orthopyroxene with trace olivine in a holocrystalline groundmass of plagioclase and clinopyroxene. Phenocrysts are blocky and form crystal clots up to 5 mm across (Fig. 4.4A). Exposures of lower andesite are entirely lava flows and do not contain any features indicative of an eruptive center. A sequence of erosion resistant olivine basalt lava flows (Tb1) overlies Ta1 and forms the highest ridges in the study area. Lower basalts contain 8–13% phenocrysts of olivine and plagioclase in a diabasic groundmass

(Fig. 4.4C) of clinopyroxene and plagioclase. Crystals cover a continuous spectrum of sizes from <100 µm to ~500 µm and form crystal clots up to ~3 mm across (Fig. 4.4B). Tb1 basalts consist entirely of lava flows and likely flowed in from an eruptive center outside of the study area.

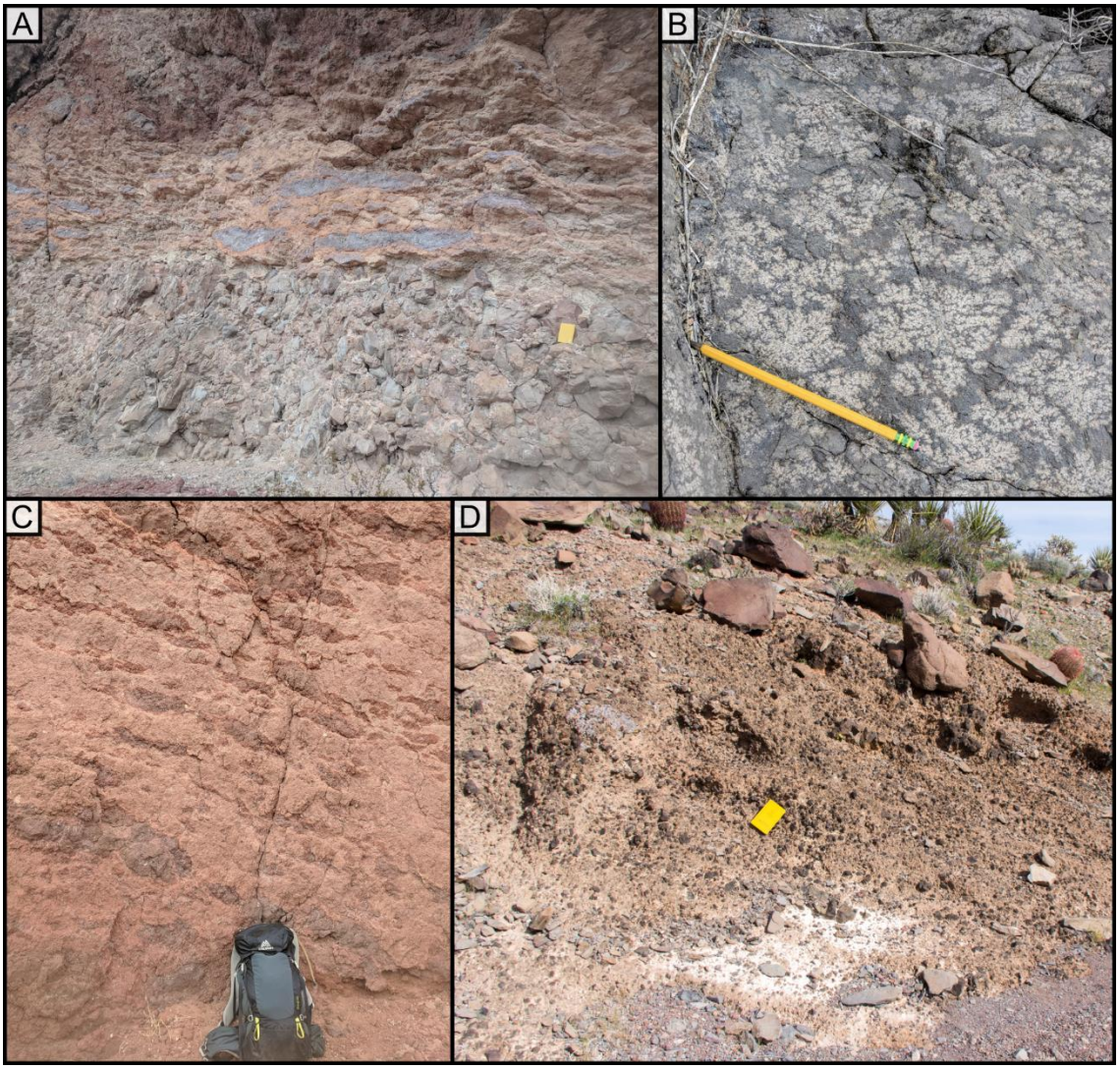

Figure 4.3: Field photos showing select map units in Piute Range study area.
(A) Andesite breccia flow (Ta2) overlain by andesite cinder eruptive deposits (Tav).
(B) Spherulitic texture in middle andesite (Ta2).
(C) Andesite cinder eruptive deposits (Tav).
(D) Volcaniclastic conglomerate from base of section, dominated by cobble size angular basalt (Tvc1).

The lower basalt section is overlain by a mix of andesitic lava flows and breccias (Ta2) with interbedded vent facies rocks (Tav). Ta2 lavas contain 8–13% phenocrysts of plagioclase and clinopyroxene up to 2 mm with trace olivine and orthopyroxene. The groundmass ranges from 50–100% crystalline with spherulites preserved in upper flows (Fig. 4.3B). Individual flows range from <3 m to >10 m thick extend up to ~1 km laterally. Vent facies rocks are generally exposed in layers approximately 5–10 m thick. Tav exposures contain lapilli to bomb size scoria, agglutinate, and cinder cone remnants (Fig. 4.3A+C) that are clearly derived from very close to the original vent location. Although original vent geometry cannot be reconstructed due to subsequent faulting and erosion, it seems likely the vent was centered in Piute Canyon. The entire middle andesite section including interbedded vent rocks is roughly 130 m thick. The middle andesite is also the uppermost portion of the Miocene section exposed in Piute Canyon making stratigraphic relationships above Ta2 relatively uncertain. Ta2 and Tav rocks are the best evidence for a major volcanic center in the study area.

Middle andesite rocks are overlain by a mix of upper volcaniclastic sediments (Tvc2), dacitic lavas (Td), and basaltic lavas (Tb2). Upper volcaniclastic rocks overlie Ta2 and are found interbedded with lavas of Td and Tb2. Sediments consist mostly of pebble to cobble conglomerate with minor interbedded sandstone and include clast supported and matrix supported horizons. Clasts are locally derived and dominated by dacite lavas (~30%), oxidized pumice (~30%) and plutonic basement (~20%). Basaltic and andesitic clasts are less frequent (~20%) and appear to be derived from underlying volcanic units. Oxidized pumice clasts are unique to Tvc2 in the study area and are

presumably sourced from a silicic volcanic center somewhere north of the study area. Clasts are mostly subrounded, range from pebble to cobble size, and sit in a coarse sand to gravel matrix. Tvc2 sediments are buttressed against and interbedded with volcanic rocks in the upper third of the Miocene section suggesting they represent a period of coarse sedimentation along the flanks of the southern PR volcanic center after eruption of Ta2 and during eruption of Td and Tb2.

Dacite lavas are restricted to the north-central study area but are abundant in the central and northern Piute Range (Miller et al., 1991) and contain roughly 20% phenocrysts of plagioclase, clinopyroxene, and characteristic hornblende in a glassy groundmass. Hornblende is tabular and elongate, up to 5 mm long, and commonly found in crystal clots. Plagioclase and clinopyroxene are generally <2 mm across, equant, and evenly distributed throughout the rock. Td lavas have a platy texture, weather to a distinctive brown, and form cliffs up to 10 m. Individual flows in dacite lavas cannot be evaluated but the unit as a whole is roughly 100 m thick. It is unclear whether dacitic rocks in the map area are entirely lava flows or partly intrusive domes.

Upper basalts (Tb2) are similar in composition to lower basalts but contain fewer phenocrysts (~5%) and form broad sheets which weather into dip slopes up to 1.5 km wide. The complete unit is ~200 m thick and contains numerous individual lava flows ranging from 2–10 m thick. Flows have rubbly, vesicular bases and tops and massive glassy interiors. Tb2 lavas overlie all other exposed rocks in the study area and cap the Miocene section in the southern Piute Range.

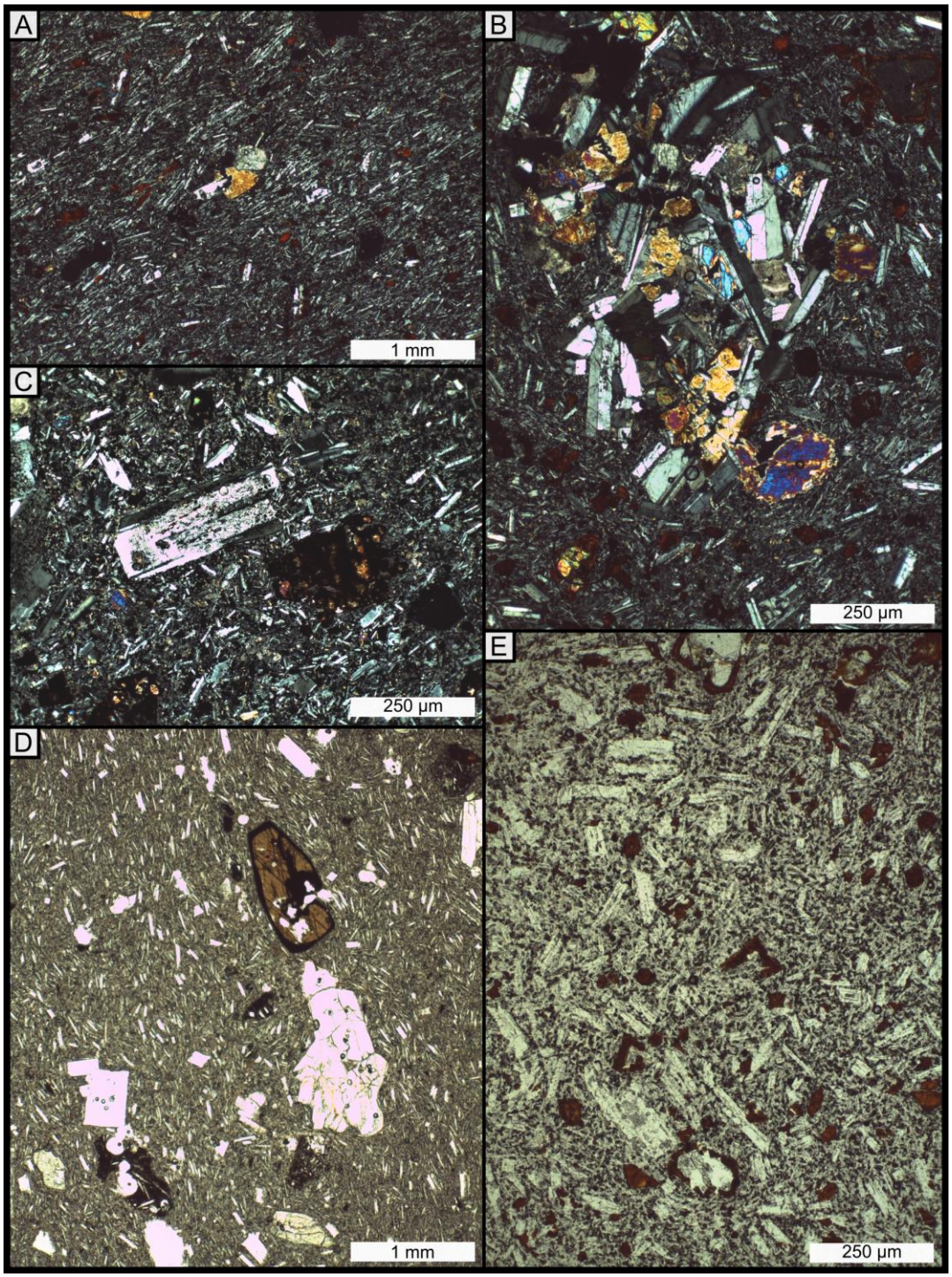

Figure 4.4: Photomicrographs from thin sections of PR area volcanic rocks.
(A) Andesite breccia flow overlain by andesite cinder eruptive deposits.
(B) Spherulitic texture in middle andesite.
(C) Basaltic cinder eruptive deposits.
(D) Volcaniclastic conglomerate from base of section, dominated by cobble size angular basalt.

Quaternary to Tertiary postvolcanic sediments in the study area include old alluvial deposits (QToal), fine grain lacustrine deposits (QTl), a caliche horizon (Qca), and young alluvial (Qal) and colluvial (Qc) deposits. Old alluvium is incised and eroded by active stream channels and is faulted against Miocene rocks at the west end of Piute Canyon (see Sec. 4.3.3). QToal near the fault dips up to ~20° westward. Approximately 100 m of flat lying, well stratified, lacustrine clay/mud deposits are exposed northwest of the canyon in its headwaters. QTl deposits suggest a lake was present along the west flank of the PR block during and after faulting. A horizon of caliche and young alluvium overlies QTl deposits and caps the Quaternary section. Quaternary alluvium is also found in active drainages throughout the map area. Colluvium (Qc) covers hillsides throughout the study area and is composed of volcanic talus derived from Miocene rocks.

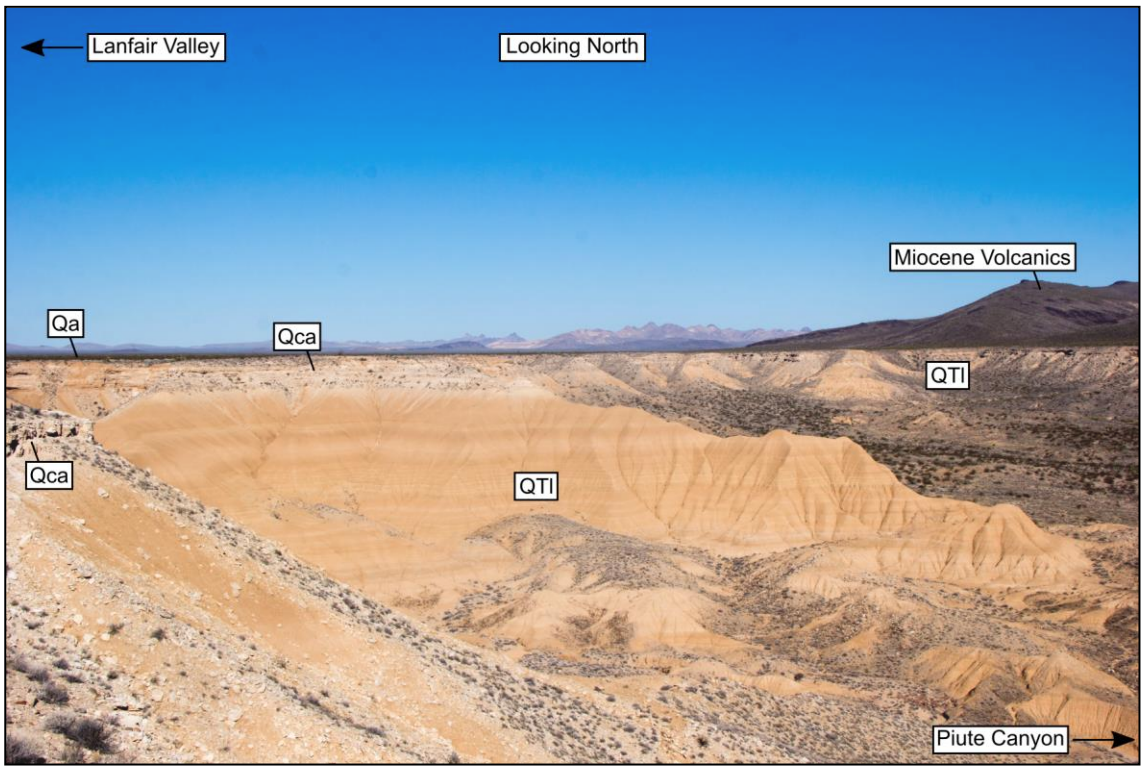

Figure 4.5: Field photo showing exposure of Quaternary/upper Tertiary sediments along west flank of Piute Range. See text for explanation of symbols.

4.2.3 Interpreted Stratigraphic History

The Piute Range study area contains a complex and incomplete record of Miocene volcanism and sedimentation. Despite uncertainty regarding the source of most volcanic rocks and their relative eruptive order, the map distribution and general stratigraphy of units permits a basic interpretation of the Miocene history.

Coarse clastic sedimentation began in the southwestern map area, depositing volcaniclastic conglomerate/breccia directly on Precambrian and Cretaceous basement. Volcanic clasts likely derived from an active eruptive center south of the study area. Andesite and basalt lava flows from this southern vent were then emplaced in the study area with interbedded sedimentary deposits. Eruptive activity then shifted north to the Piute Canyon area depositing Tav and Ta2 across the study area. Dacitic volcanic activity followed in and north of the map area with localized sedimentation in the eastern study area along the flanks of the volcanic center. Basaltic lavas cap the volcanic section and mark the end of local volcanism.

After eruption/deposition of the Miocene section, a period of intense normal faulting affected the entire study area. The major normal fault which forms the western boundary of the Miocene section created a closed hanging wall basin which filled with Miocene to Quaternary alluvial and lacustrine deposits. Subsequent erosion formed the Piute Canyon drainage, bisecting the range and exposing the Miocene and Quaternary sections.

4.3 Structural geology

4.3.1 Overview

The Miocene section and underlying basement in the southern Piute Range are tilted eastward and pervasively deformed by north-south striking, west dipping normal faults. Exposed fault planes are generally small displacement (<10 m) although offsets of greater than 100 m are inferred on a few large faults from mapping. Individual fault planes are typically exposed as 0.5–3 cm wide zones of cataclasite (Fig. 4.6) and sometimes form larger fault breccia zones (up to ~30 cm) with multiple internal fault planes preserved. Slickenlines, Riedel shears, and mullions are well preserved on some fault planes in Piute Canyon, allowing for kinematic analysis of fault slip data.

4.3.2 Orientation of Rock Units

Miocene rocks throughout the Piute Range study area are uniformly tilted 20° eastward (Fig. 4.8A) forming a set of tilted blocks. Where exposed, the basal unconformity also dips 20° to the east. The orientation of rock units is reliably determined from bedding in sedimentary intervals, flow banding/margins in volcanic units, and overall map trace of individual units.

Eastward tilting in the Piute Range study area contrasts with westward tilts observed in other parts of the PR and neighboring ranges. Rocks in the southernmost Piute Range and at Homer Mountain are tilted as much as 60° to the west (Spencer, 1985; Gans et al., 2018). In the central and northern Piute Range rocks dip gently (<10°) west and are minimally faulted (Nielsen et al., 1987). To the east of the PR study area, the Newberry Mountain block and associated detachment fault appear to have rotated at least

45° westward (Spencer, 1985; Walker et al., 2007). Thus, eastward dips and west directed normal faults in the Piute Range study area are anomalous.

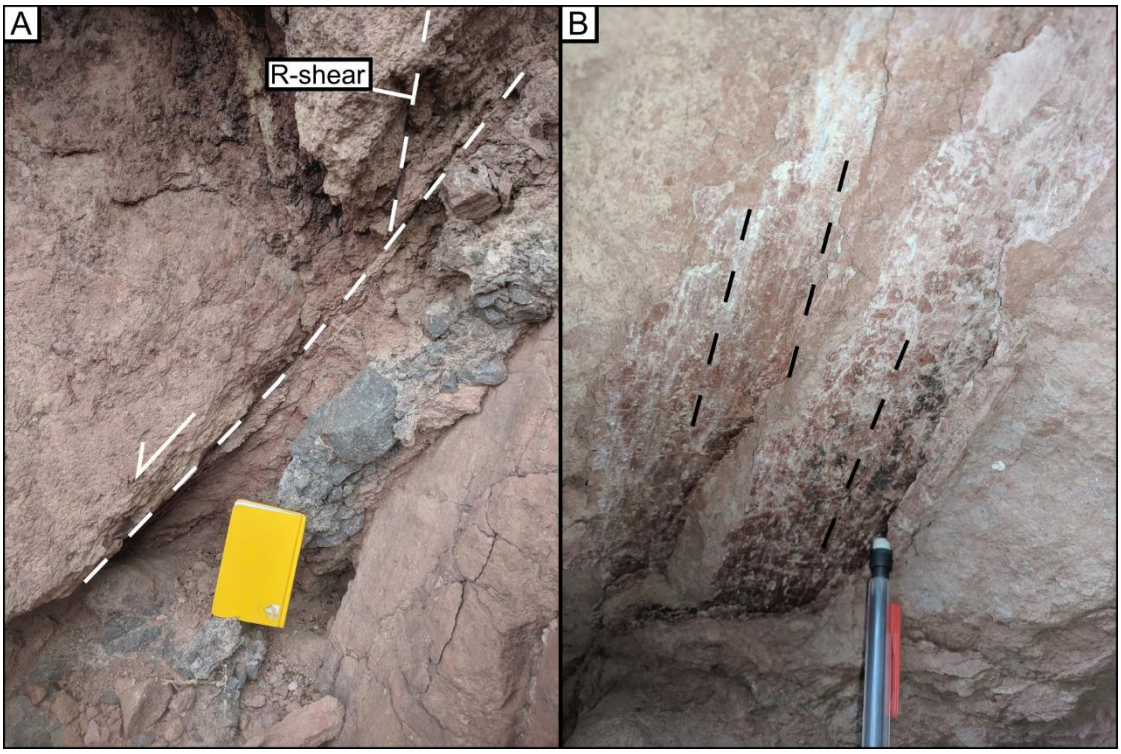

Figure 4.6: Field photos of fault plane preserved in Piute Canyon.
(A) Along strike view of fault zone with discrete plane and R-shear plane labeled (white lines).
(B) View of fault slip surface with slickenlines (black lines) and mullions.

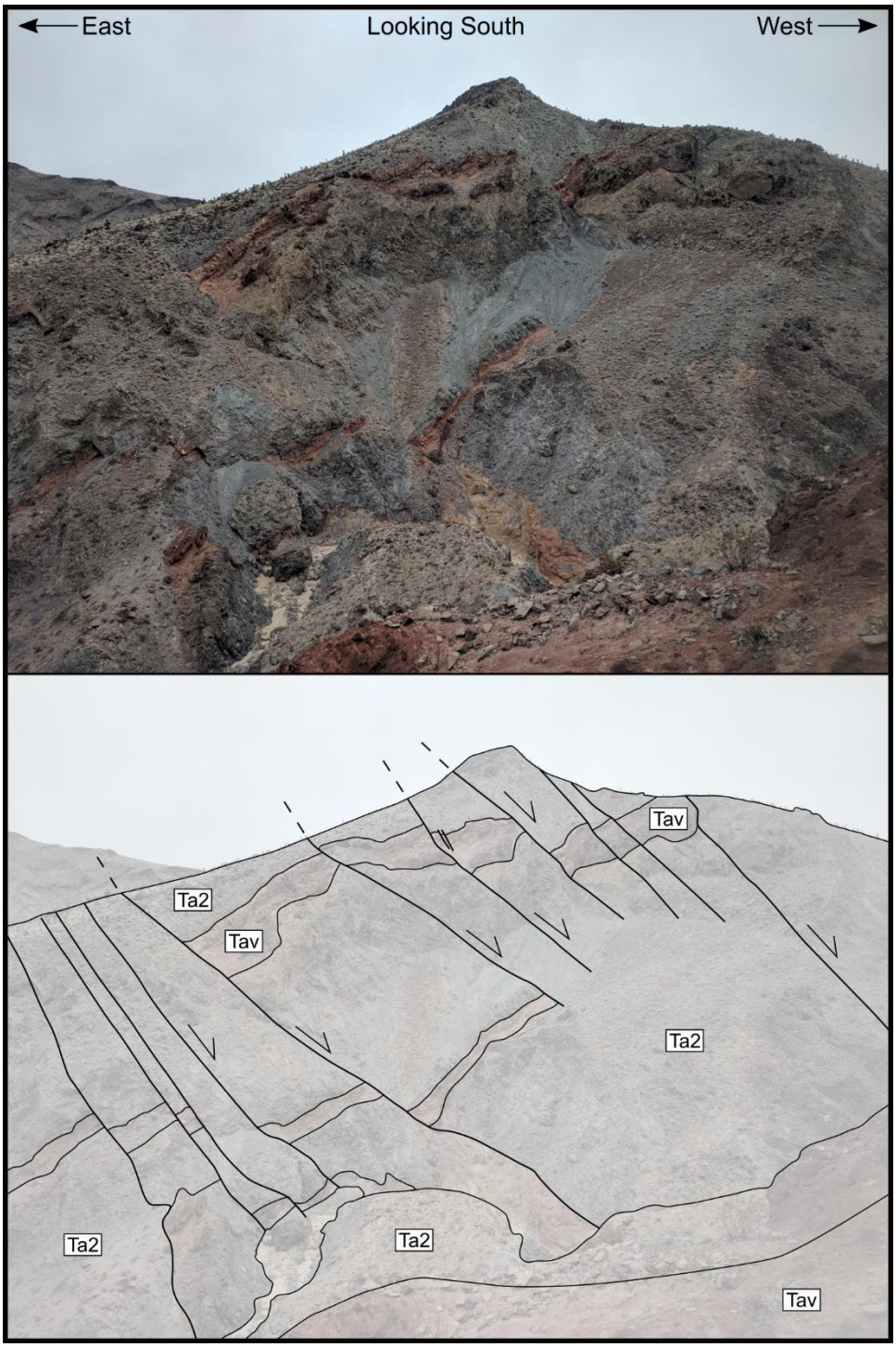

Figure 4.7: Annotated field photo of south wall of Piute Canyon showing exceptional exposure of stratigraphy and faults. Note obvious and uniform east dip of rocks and close spacing of faults.

4.3.3 Fault and Kinematic Data

The majority (64/81) of exposed faults strike between 150° and 200° and dip between 40° and 60° westward (Fig 4.8B+C). Riedel shears and mapped offsets indicate faults are normal or oblique-normal. Slickenlines preserved on 14 fault planes show a range of slip directions. The dominant fault motion direction is west-southwest (230°–270°), near dip-slip (average rake = 83°). An additional small population (n = 3) of slip vectors trend north with rake less than 10°, indicating a component of probable right-lateral slip on some faults. Both sets of slickenlines are preserved on a single fault plane, with the north trending set clearly younger than the west trending set, suggesting strike slip motion occurred after normal faulting.

Faults are distributed throughout the study area but are best exposed in Piute Canyon biasing their map distribution. Small displacement faults are not shown on Plate 3 but are by far the most commonly measured within the canyon and provide the majority of kinematic data. Measurable planes are preserved for 14 map scale faults in Piute Canyon and only 5 map scale faults in the remainder of the study area. Major faults (offset > 80 m) are rare (~6 faults total) and spaced approximately evenly across the study area. Structural blocks bounded by these faults are 250–450 m wide. Minor faults are generally closely spaced (from <1 m to ~10 m).

Cross cutting relationships between faults are rare. The majority of faults are subparallel and bound coherent structural blocks without other faults cutting through them. Two major faults which strike ~170° cut smaller faults which strike due south suggesting faults may have formed in two distinct generations. One of these faults (at the

east end of Piute Canyon) also preserves north trending strike slip slickenlines which indicate strike slip motion occurred after normal faulting.

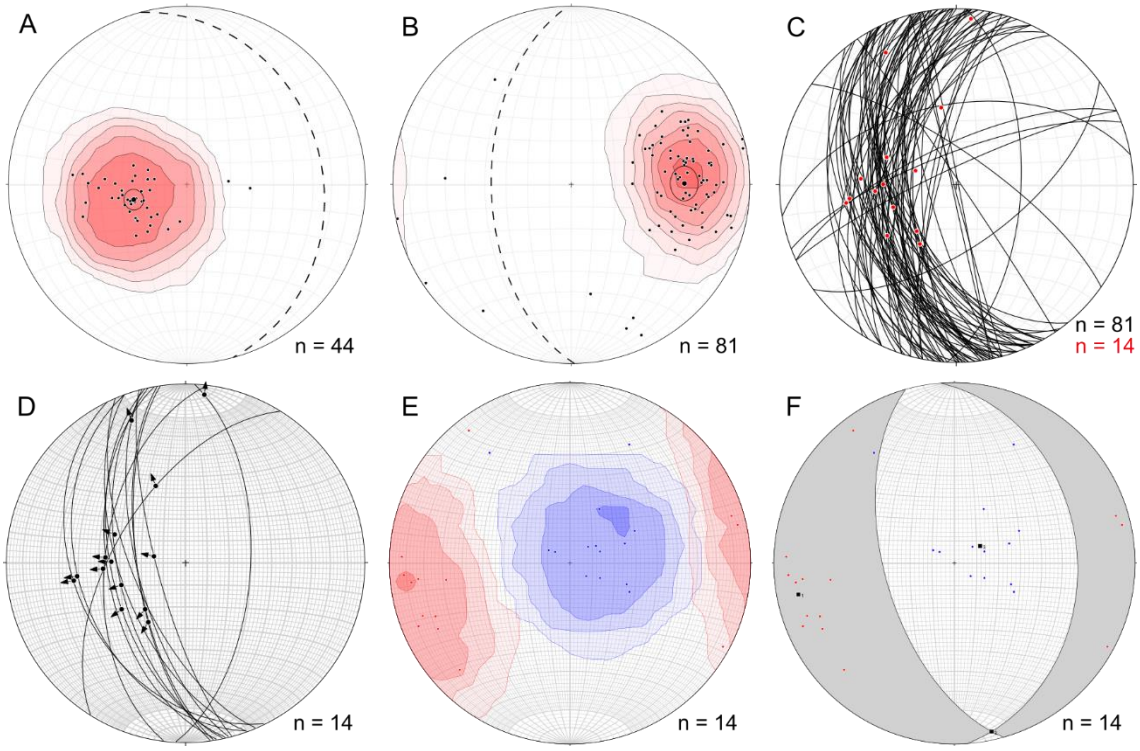

Figure 4.8: Structural data from Piute Range study area on equal area lower hemisphere stereonet projections.
(A) Poles to bedding/flow margin measurements with contour, mean vector (255°, 65°), and mean plane (dashed; 345°, 25°).
(B) Poles to all fault plane measurements with contour, mean vector (089°, 37°), and mean plane (dashed; 179°, 53°).
(C) All fault planes (black) with slip vector measurements (red).
(D) Fault planes with measured slip vectors.
(E) Contoured P- and T- axes for faults with slip data.
(F) Fault plane solution with linked Bingham axes
(nodal plane = 165°, 58°; A1 = 259°, 13°; A3 = 056°, 76°).

The average fault to bedding cutoff angle is 84° (Fig. 4.8) suggesting faults in the Piute Range may have initiated as subvertical mode 1 extension fractures and activated as shear fractures during subsequent eastward tilting of the block. Alternatively, west dipping normal faults may have initiated at angles closer to 60° after the crustal block had

already experienced ~20° eastward tilting. The homoclinal nature of the section makes it difficult to determine which of these scenarios is more likely, although the presence of younger strike slip faults oriented ~170° suggests faults may have formed in two distinct populations with similar orientations.

Kinematic data calculated from fault slip data is shown in Figure 4.8E and 4.8F. Incremental shortening axes (P-axes) cluster near east-west and horizontal (average = 259°, 13°). Incremental extension axes (T-axes) cluster near vertical (average = 056°, 76°). Three data points corresponding to strike-slip faults appear as outliers and suggest strike-slip faulting occurred under different stress conditions. The fault plane solution from linked Bingham axes (Fig. 4.8F) shows an average fault plane based on kinematic data. The average nodal plane strikes 165° and dips 58° to the west with a nearly dip slip normal sense of motion, indicating the average extension direction in the PR area is ~255°.

4.3.4 Western range bounding fault

The westernmost exposed fault in Piute Canyon places coarse alluvial conglomerate against basaltic lavas (Fig. 4.5A). The fault is exceptionally exposed with several distinct slip surfaces which strike 185° and dip 54° to the west. Slickenlines (T:259°, P:52°), cataclasite, and fault gouge are preserved in the fault zone and Riedel shears clearly indicate normal sense displacement. Alluvial deposits coarsen dramatically toward the fault (clasts > 60 cm) and display clast imbrications indicative of west directed transport, suggesting the fault was active during deposition and debris was shedding from the central Piute Range westward over the fault escarpment. Bedding in old alluvial

deposits dips west and steepens significantly toward the fault from 7° about 100 m west of the fault to 20° adjacent to the fault (Fig. 4.5B), likely either a result of drag folding due to motion on the fault, or original dips on the proximal portion of the ancestral alluvial fan. The fault is interpreted as an ancient range bounding fault which continued to slip during and after deposition of the undated (post volcanic) alluvium and lake beds. Nearly flat dips in the rest of QToal suggest the unit is either less deformed than the main Piute Range block, or younger than the majority of the faulting within the Piute Canyon area.

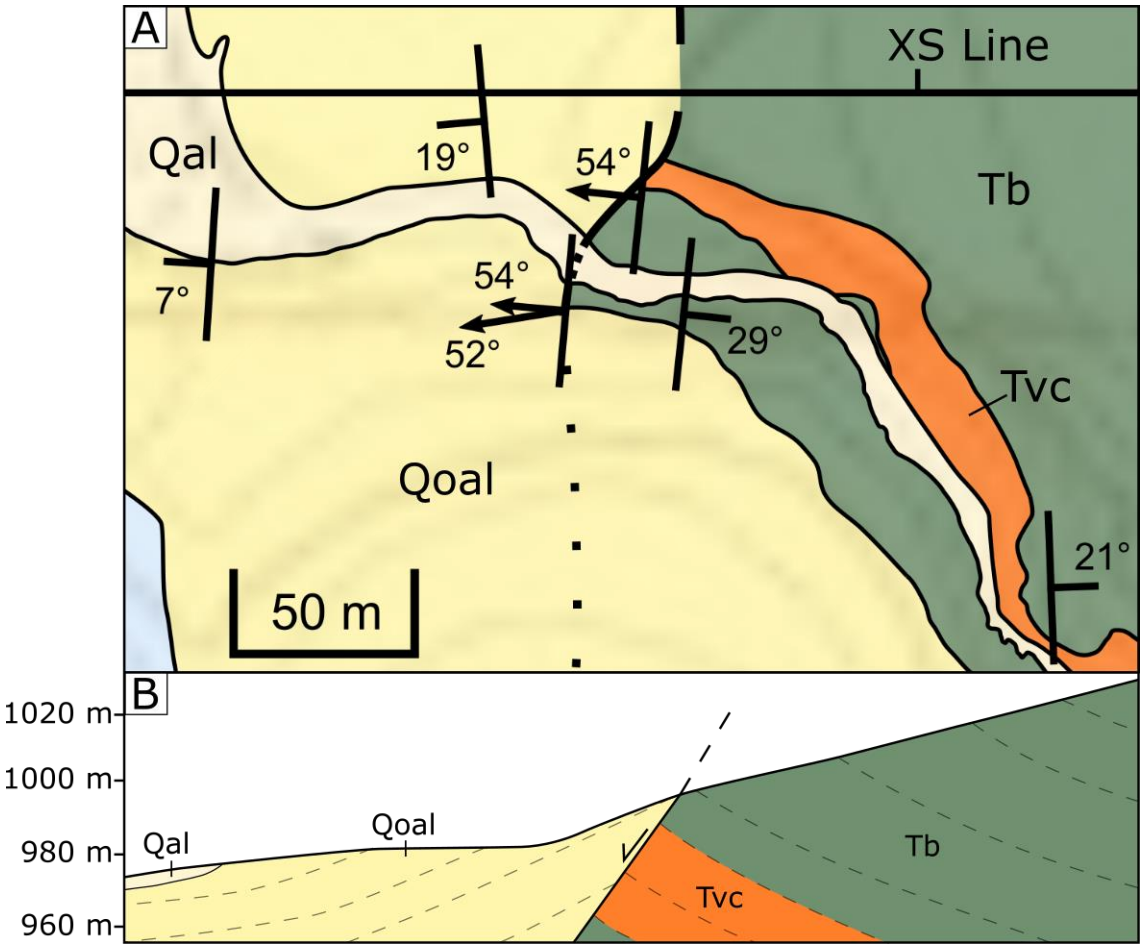

Figure 4.9: (A) Map view of western range front fault exposures and surrounding rock units. (B) Schematic cross section of range front fault area showing minor drag folds and change in dip direction across fault.

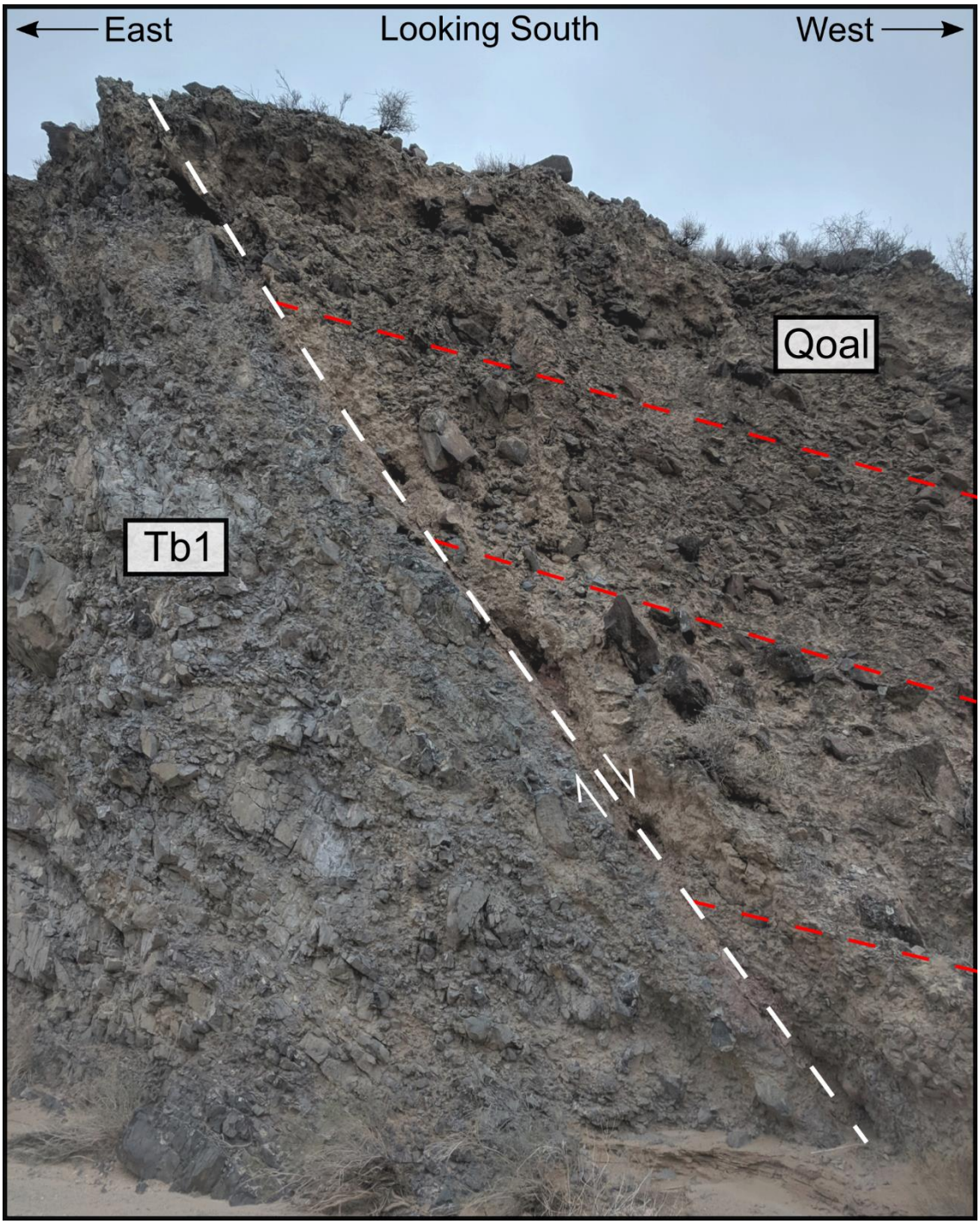

Figure 4.10: Field photo of range front fault which bounds Miocene section in westernmost Piute Canyon. Fault dips 54° west and preserves near dip slip slickenlines. Footwall of Qoal dips moderately westward, likely as a result of drag folding due to motion on the fault. See text for further discussion.

4.3.5 Interpreted Structural History

Structural data and mapping show that Miocene deformation in the Piute Range is dominated by west directed normal faulting. No evidence has been found for normal faulting prior to or during volcanism, suggesting the majority of faulting occurred after eruption and deposition of Miocene rocks. The near vertical average cutoff angle in the study area indicates faults had initially steep dips (70–90°) and rotated to their present orientation. The cutoff angle and average dip of bedding also imply a modest 15–20% total extension across the study area. The abundance of subparallel, planar, west dipping normal faults cutting homoclinally east dipping strata suggests the current orientation of faults and bedding is a consequence of simple domino style block rotation (e.g. Proffett, 1977). A minor episode of later strike slip faulting likely followed extension. Several major normal faults (displacement > 100 m) are found throughout the study area including the ancestral range front fault which bounds the Piute Range on its west side. This fault places Miocene to Quaternary rocks against Miocene volcanics and likely formed a closed hanging wall basin where lake beds were deposited. An additional major west directed normal fault is inferred to lie just to the east of the Piute Range to account for uniform tilting of the entire PR block.

4.4 Summary of Geology of Piute Range

The Piute Range study area contains a record of Miocene volcanism, sedimentation, and deformation. Sediment deposited in the study area is clearly locally derived from volcanic centers in and around the study area. Volcanism likely occurred throughout the study area, especially in Piute Canyon where vent facies rocks are

preserved. Quaternary alluvial and lacustrine deposits then accumulated in a closed basin along the west flank of the range.

Following eruption and deposition of the Miocene section, moderate magnitude west directed brittle normal faulting occurred throughout the study area. Minor late stage strike slip faulting also occurred. Activity on the western range front fault appears to have persisted into the Quaternary, offsetting and drag folding alluvial deposits which dip opposite to the main Piute Range block. Additional unexposed west-dipping normal faults must be present along the eastern flank of the range to account for uniform eastward tilting of the PR block. West directed normal faulting and associated eastward tilting define a change in tilt block polarity relative to the surrounding area (Homer Mountain, southern Piute Range, Newberry Mountains).

5. Discussion

5.1 OWPM Area and the CREC

5.1.1 Structural Geometry

The deformation history of study sites in the Old Woman-Piute Mountain area (LPM and NWPM) has important implications for the evolution of the margin of the CREC and proposed breakaway models. Several key points emphasize the complexity of the margin at this latitude:

1. North-south directed extension precedes east-west directed extension in the LPM area.
2. NW-SE directed strike slip faulting accommodates either differential extension between LPM block and OWM block or a step over in LPF. Minor strike slip faulting also affected the NWPM area.
3. The OWPM block is rotated 20° NW suggesting east directed normal faulting persists up to 20 km west of the interpreted CREC breakaway, with a major fault present beneath alluvium in Fenner Valley.
4. Based on rotation of the PM block, the LPF likely formed as a high angle normal fault (dip > 55°) and rotated to its present orientation.

Based on these observations, the western margin of the CREC does not exist as a singular, discrete normal fault in the OWPM area, separating highly extended from unextended upper crust. Deformation along the western margin of the CREC at this latitude is dominated by diffuse high angle normal faulting and tilting with no obvious sign that there is one master LANF that surfaces as a breakaway.

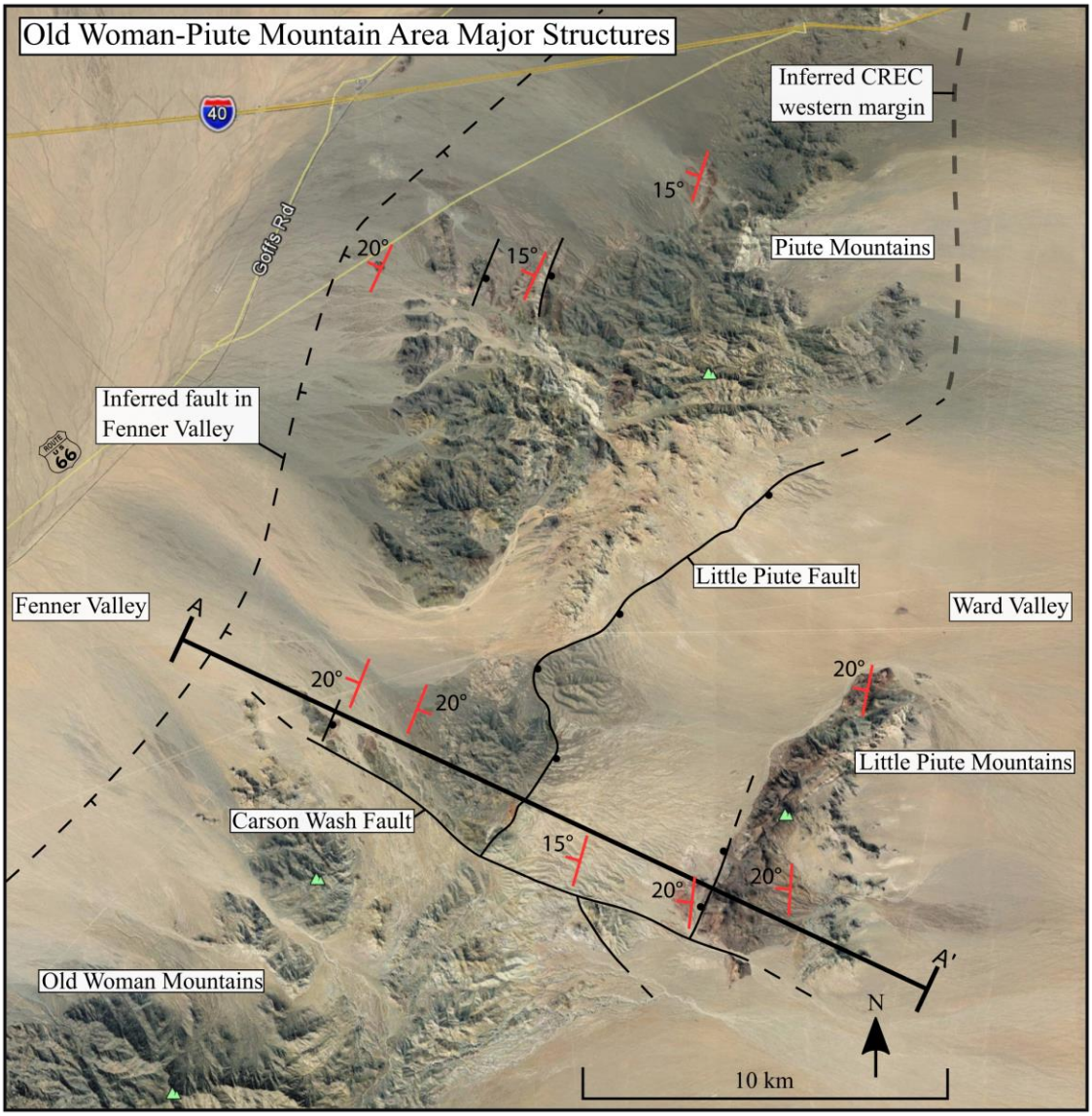

Figure 5.1: Satellite image showing major faults and average orientation of rock units in OWPM area. Cross section A-A' shown in Fig. 5.2.

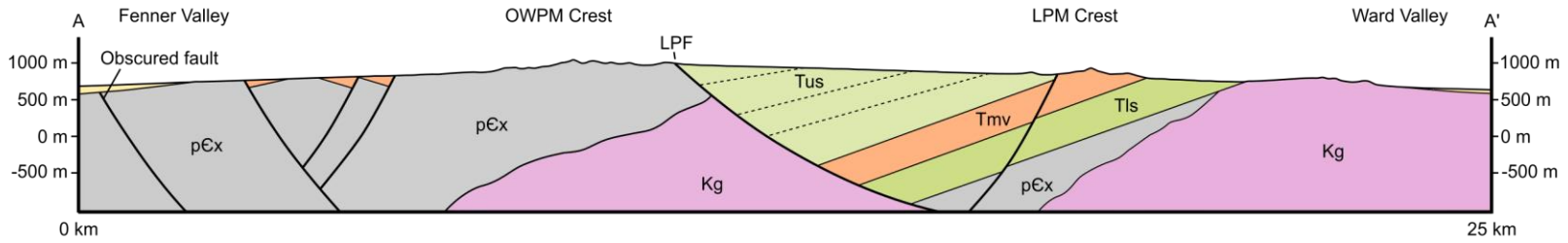

Figure 5.2: Cross section A-A' (from Fig. 5.1) across OWPM area from Fenner Valley to Ward Valley showing major normal faults and inferred basement relationships.

5.1.2 Extension Direction in OWPM vs CREC

The dominant extension direction observed in the OWPM area is NW-SE (~110°). Southeast directed extension differs markedly from documented extension directions in the southern and central CREC (Fig. 5.3). Based on detachment fault slickenline lineations, the dominant extension direction in the central MCC belt is northeast (~045°), nearly perpendicular to extension in the OWPM area. If the LPF is the breakaway for the regional detachment fault in the Chemehuevi and/or Sacramento Mountains, the extension direction should be roughly parallel. This discrepancy in extension direction suggests faulting in the OWPM area is distinct and not inherently related to detachment fault motion to the east.

5.1.3 Extension Timing in OWPM vs CREC

Northwest-southeast directed extension in the OWPM area likely occurred between approximately 17.7 Ma and 16.6 Ma. This ~1 Ma period of deformation is similar in duration to extension episodes in other parts of the CREC, but differs in exact timing. As outlined in the introduction (Sec. 1.2.4), hanging wall blocks in a regional detachment should grow progressively younger down dip toward the exposed MCC. Current available data on the timing of detachment fault motion (Fig. 5.3) suggests widespread extension in the central CREC occurred prior to and coeval with motion on the LPF. If detachment faults to the east and south were active at the same time as the (high angle) LPF, it is geometrically impossible for the LPF and detachment fault to be the same structure. The inferred presence of an additional coeval major normal fault in Fenner Valley also suggests extension was distributed broadly across the CREC region.

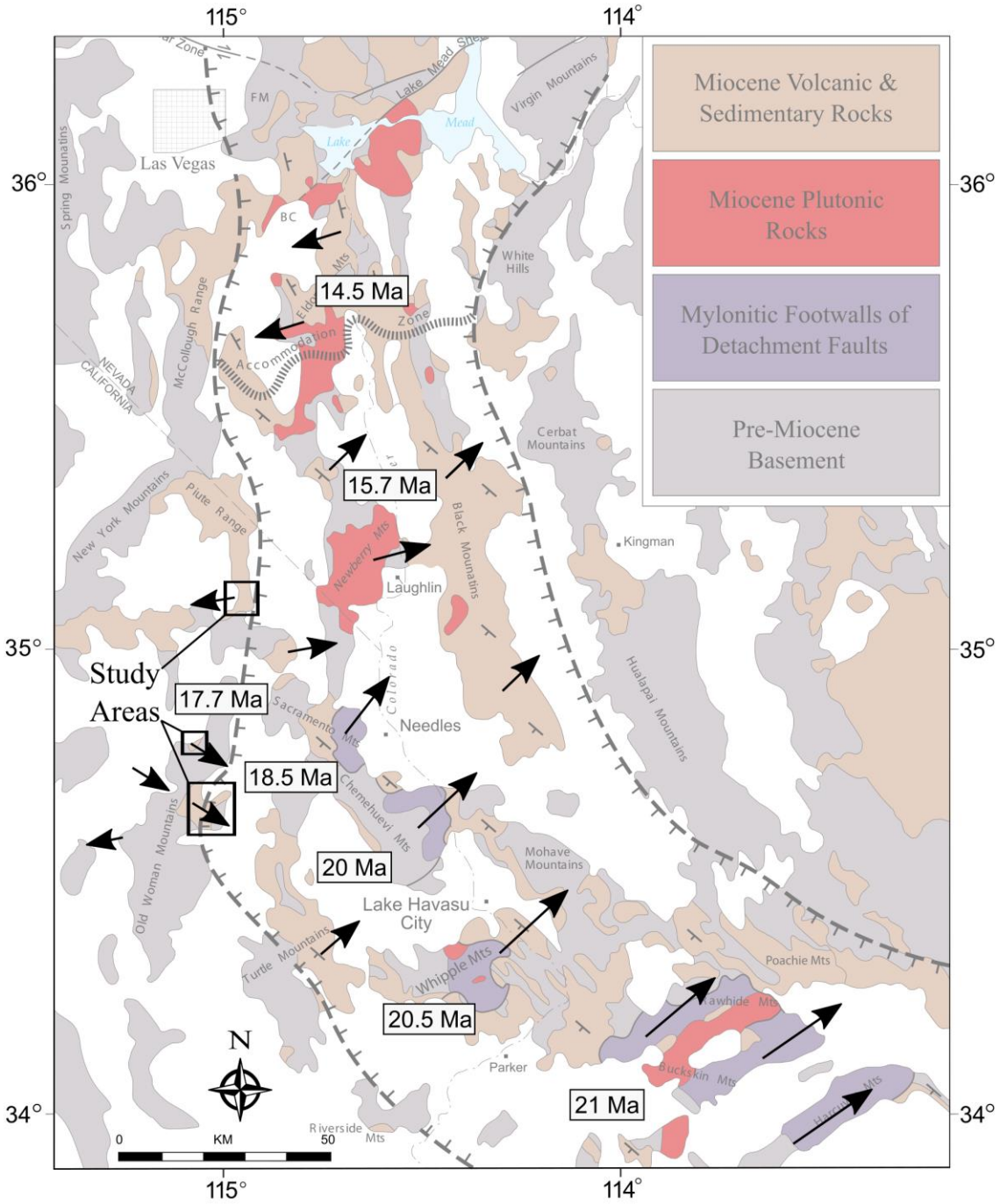

Figure 5.3: Simplified geologic map of CREC region with dominant extension directions (arrows, length = relative magnitude) and approximate age of onset of extension for individual ranges.

5.2 Piute Range and the CREC

5.2.1 Structural Geometry

The relationship between deformation in the Piute Range study area and surrounding ranges is enigmatic. Normal faulting in the PR study area is uniformly west directed, opposite the polarity of faulting in areas north, south, and east of the study site (Fig. 5.4). There is strong evidence for large west-southwest dipping normal faults on both sides of the Piute Range block at the latitude of Piute Canyon, but to the south at Homer Mountain normal faults clearly dip east. West directed normal faulting is the dominant mode of extension in the El Dorado and northern Black Mountains (~65 km north of PR study area), but is not commonly observed south of the northern CREC accommodation zone. It is clear from mapping that some kind of tilt domain transition or accommodation zone must be present in the area between Piute Canyon and Homer Mountain (Fig. 5.4). The exact nature and geometry of this transition is unclear and the subject of future study, however several hypotheses may help account for anomalous fault polarity in the Piute Range study area:

1. West directed faulting occurred significantly later than in surrounding areas, under different stress conditions and subsequent to detachment faulting in the ranges to the east.
2. West directed faulting occurred as a localized phenomenon associated with heterogeneities in the crystalline basement.
3. West directed faulting occurred as a localized phenomenon associated with active local volcanism.

The first scenario is supported by the presence of presumed latest Miocene to Quaternary alluvial and lacustrine deposits in the hanging wall of the western range front fault (see Sec. 4.3.4). Drag folding of possibly post-Miocene rocks implies some west directed faulting persisted beyond the early Miocene when the majority of deformation was occurring in the CREC.

The second scenario is hypothesized because the Miocene section in the PR is deposited roughly along the contact between Precambrian metamorphic and Mesozoic plutonic basement. It is possible a difference in rock strength between the unmetamorphosed Mesozoic pluton and highly metamorphosed, foliated Precambrian rock helped localize west dipping faults along the western margin of the pluton. After initiation of west directed faulting, domino style block rotation and establishment of a dominant fault polarity likely drove further west directed normal faulting.

The third scenario is hypothesized due to the high cutoff angle of faults in the study area. It is likely extension through dilation and dike emplacement was occurring during volcanism in the southern PR. Mode 1 vertical extension fractures were likely also forming (at high angles to untilted rocks), and some disequilibrium caused eastward tilting of the block which led to activation of vertical fractures as top to the west shear fractures.

Each of these hypotheses may have influenced the structural evolution of the Piute Canyon area but it is difficult to test or further interrogate them with current data. It is clear however, that a tilt domain transition occurs over <10 km in the southernmost Piute Range (Fig. 5.4).

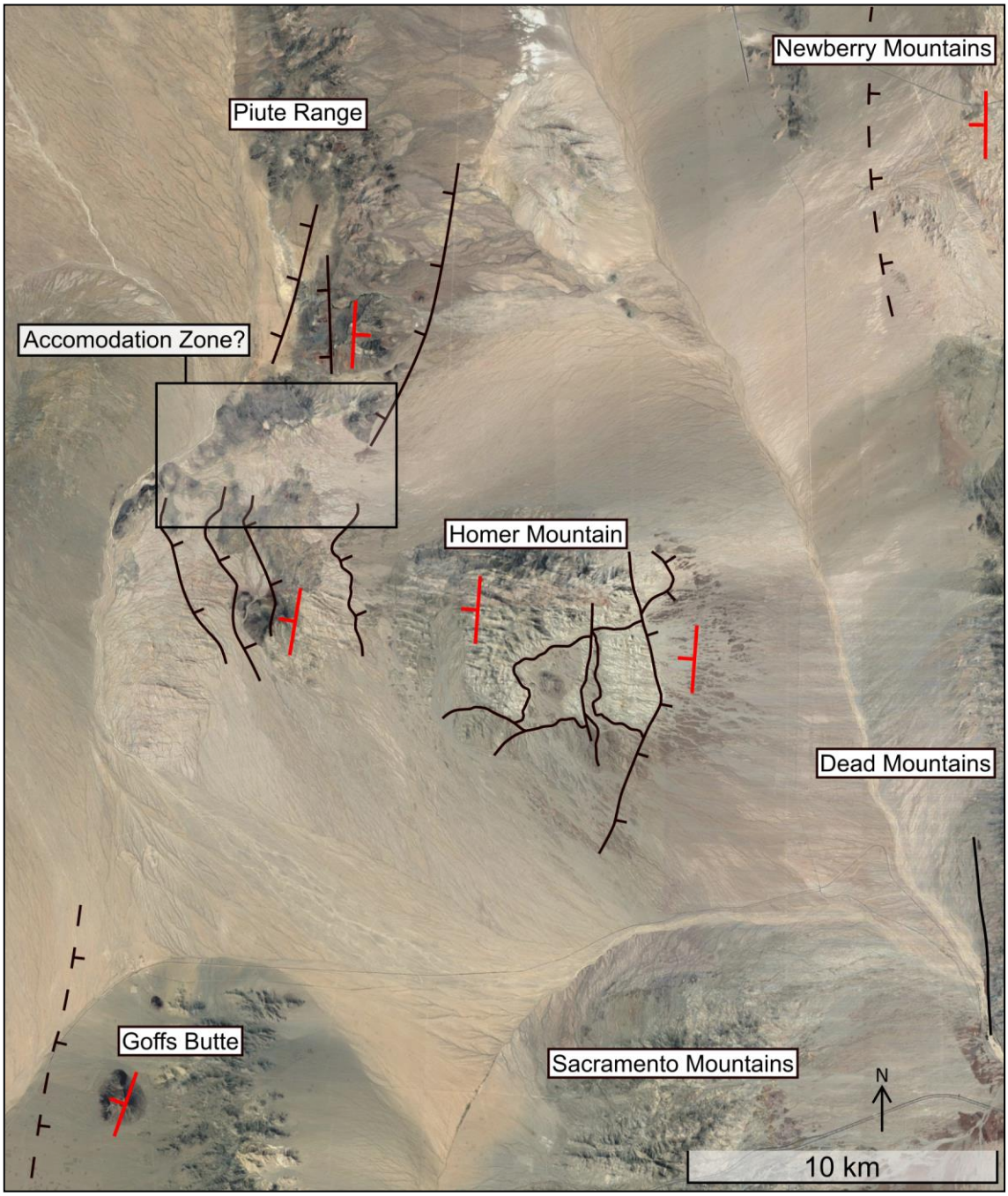

Figure 5.4: Satellite image of southern Piute Range/Homer Mountain area showing location of major known (solid lines) and inferred (dashed lines) normal faults and tilt directions (red strike and dip symbols). Box highlights likely location of accommodation zone between opposing tilt domains in the Piute Canyon area and southernmost Piute Range/Homer Mountain area.

5.2.2 Timing of Deformation

The timing of faulting in the study area is poorly constrained, leading to difficulty in interpreting the relationship between deformation in the Piute Range and in surrounding areas. The homoclinal nature of the section suggests west directed faulting initiated in the PR after ~15.8 Ma (only age from PR volcanics). As discussed in the previous section, west directed faulting involving late Miocene to Quaternary rocks implies deformation continued until that time.

East directed faulting at Homer Mountain to the south likely initiated after ~16.5 Ma (Gans et al., 2018). Relatively young basalts south of the study area at Billie Mountain (14.5 Ma, Spencer, 1985) and Goffs Butte (10.4 Ma, Miller et al., 1998) are tilted ~25° west-northwest implying east directed faulting persisted into the middle Miocene. East directed detachment faulting occurred during a similar time period (roughly 16–14 Ma) in the Newberry and Dead Mountains to the east of the Piute Range.

Based on current timing constraints it is possible east and west directed normal faulting were occurring along strike at the same time only ~10 km apart. If this is the case, there must be an accommodation structure of some kind present to account for the tilt domain transition in the Homer Mountain/southern Piute Range area.

5.2.3 Central CREC Breakaway

The geometry and timing of extension in the Piute Range and along the western margin of the central CREC is broadly incompatible with detachment fault breakaway models. Spencer (1985) proposed the Homer, Sacramento, Dead, and Newberry Mountains all lie in the footwall of a regional detachment fault, with a breakaway trace

generally inferred under alluvium in the Piute Wash Valley. The absence of large sedimentary basins and low angle east directed normal faults, and the presence of abundant high angle normal faults, suggest low angle normal faulting was not the primary mode of extension in the central CREC.

The Newberry-Dead Mountains Detachment currently dips east at a low angle (~15°). The Spirit Mountain pluton in the Newberry Mountains appears to have rotated roughly 45° westward, implying the detachment fault had an original dip of near 60° and that at least one additional major east directed normal fault is present under alluvium west of the Newberry Mountains. If these major faults slipped at low angles their up dip projection would intersect west directed faults in the Piute Range. The LANF models of Spencer (1985) and Howard and John (1987) do not predict coeval antithetic faults to cut the detachment fault breakaway. The presence of an apparent tilt domain transition in the southern PR/Homer Mountain area also suggests greater complexity than implied by simple detachment fault models.

It seems likely that formation of "detachment faults" in the central CREC is actually the result of rotation of a system of high angle normal faults, and that Miocene deformation in the central CREC cannot be described through a simple detachment fault model.

5.3 Summary and Conclusions

5.3.1 Breakaway Models in the CREC

Results of this study generally do not support the existence of a regionally extensive detachment fault throughout the CREC with a single discrete and recognizable

"breakaway" fault where the detachment breached the surface. Extensional deformation along the western margin of the corridor appears to be characterized by a diffuse gradation in high angle normal fault spacing and block rotation that varies in time, magnitude, and direction, and is not clearly bounded by an individual master fault or breakaway. In the OWPM area the extension direction is perpendicular to the dominant extension direction in the central part of the corridor. Although the Little Piute Fault presently dips at a moderate angle, it has likely been tilted together with the Piute Mountain block in its footwall and has no unique characteristics to differentiate it from other high angle faults in the region. More importantly, it must lie in the hanging wall of additional high-angle faults to the west. Extension in the OWPM area initiated after extension in the Whipple and Chemehuevi mountains was well underway making it difficult to see how a regional scale detachment fault associated with those ranges could be exposed in the OWPM area. In the Piute Range area to the north, extension is west directed, opposite the extension direction of neighboring areas in the CREC. Detachment faults to the east and south appear to be rotated high angle normal faults and have no clear up dip exposures.

Overall, the results of this study suggest the structural geometry of the western margin of the CREC is a diffuse gradation in upper crustal extensional strain with highly variable magnitudes and directions of extension and does not conform to a simple detachment fault model.

5.3.2 Evolution of the CREC

Results of this study demonstrate greater complexity in extensional patterns and the overall extensional strain field than previously identified in the Colorado

River/eastern Mojave region. Episodic north-south extension followed by east-west extension in the Little Piute Mountains—similar to deformation patterns in the Homer and Newberry Mountain areas—suggests the presence of an evolving stress field along the margin of the CREC. As large magnitude NE directed extension proceeded in the Whipple and Chemehuevi Mountains the stress field in the OWPM area may have reoriented in response to thinning crust to the southeast, driving N-S and eventually SE directed extension. In the Piute Range west directed normal faults show that the extensional strain field is variable at the same latitude, suggesting local controls may have played a part in fault formation regardless of regional patterns.

The results of this study highlight the complexities of Miocene deformation patterns in just a few small areas along the western boundary of the CREC. The history of extensional faulting, volcanism, and sedimentation illustrated here provides additional evidence for dynamic evolution of the intracontinental rift system and suggests current structural models for intracontinental rifting are insufficient to account for the complexity of deformation in rift zones.

5.3.3 Future Research Opportunities

The results of this research indicate the CREC is still poorly understood in several ways. Improved geochronology in the study areas should vastly improve understanding of the timing of extension and volcanism, especially in the Piute Range. Expanded geologic mapping efforts in the southern Piute Range and Homer Mountain area may help explain the change in dominant tilt direction. Expanded mapping in general in areas distal to the highly extended portions of the corridor will likely reveal further complexity in the

timing and nature of extension and may help answer questions about the variable nature of the stress field along the edges of areas affected by intracontinental rifting as well as the controls on tilt domain transitions and extensional terrane margins in general.

References

RW Allmendinger. Faultkin (version 7.4.1): Ithaca, New York, Department of Geological Sciences, Cornell University, 2015.

RW Allmendinger, RA Marrett, and T Cladouhos. Faultkin. *http://www.geo.cornell.edu/geology/faculty/RWA/RWA. html*, 1992.

Jacques Angelier. Tectonic analysis of fault slip data sets. *Journal of Geophysical Research: Solid Earth*, 89(B7):5835–5848, 1984.

Victoria C. Bennett and Donald J. DePaolo. Proterozoic crustal history of the western united states as determined by neodymium isotopic mapping. *GSA Bulletin*, 99(5):674–685, 1987.

CC Bishop. Geologic map of California, needles sheet, scale 1: 250,000. *California Division of Mines and Geology Regional Geologic Map Series*, 1963.

Gregory Davis and Gordon Lister. Detachment faulting in continental extension; perspectives from the southwestern U.S cordillera. 218:133–159, 01 1988.

James E Faulds and Robert J Varga. The role of accommodation zones and transfer zones in the regional segmentation of extended terranes. *Geological Society of America Special Papers*, 323:1–45, 1998.

James E Faulds, Daniel L Feuerbach, Mark K Reagan, Rodney V Metcalf, Phil Gans, and J Douglas Walker. The Mount Perkins block, northwestern Arizona: An exposed cross section of an evolving, pre-extensional to synextensional magmatic system. *Journal of Geophysical Research: Solid Earth*, 100(B8):15249–15266, 1995.

James E Faulds, Daniel L Feuerbach, Calvin F Miller, and Eugene I Smith. Cenozoic evolution of the northern Colorado River extensional corridor, southern Nevada and northwest Arizona. 2001.

Charles A. Ferguson, William C. McIntosh, and Calvin F. Miller. Silver creek caldera: the tectonically dismembered source of the peach spring tuff. *Geology*, 41 (1):3, 2013. doi: 10.1130/G33551.1.

David A Foster and Barbara E John. Quantifying tectonic exhumation in an extensional orogen with thermochronology: examples from the southern basin and range province. *Geological Society, London, Special Publications*, 154(1):343–364, 1999

David A Foster, T Mark Harrison, Calvin F Miller, and Keith A Howard. The 40ar/39ar thermochronology of the eastern Mojave Desert, California, and adjacent western Arizona with implications for the evolution of metamorphic core complexes. *Journal of Geophysical Research: Solid Earth*, 95(B12):20005–20024, 1991.

PB Gans and WA Bohrson. Suppression of volcanism during rapid extension in the basin and range province, united states. *Science*, 279(5347):66–68, 1998.

PB Gans, EL Miller, Jill McCarthy, and ML Ouldcott. Tertiary extensional faulting and evolving ductile-brittle transition zones in the northern snake range and vicinity: New insights from seismic data. *Geology*, 13(3):189–193, 1985.

Phillip B Gans and Beau J Gentry. Dike emplacement, footwall rotation, and the transition from magmatic to tectonic extension in the Whipple Mountains metamorphic core complex, southeastern California. *Tectonics*, 35(11):2564–2608, 2016.

Phillip B Gans and Elizabeth L Miller. Style of mid-tertiary extension in east-central Nevada. *Geological excursions in the overthrust belt and metamorphic core complexes of the Intermountain region: Utah Geological and Mineral Survey Special Studies*, 59:107–139, 1983.

Phillip B Gans, Justin R Newmann, Evan Monroe, and Andrew Kylander-Clark. Orthogonal (N-S) extension at the leading edge of a propagating continental rift: a reassessment of Homer Mountain and environs, lower Colorado River extensional corridor (CREC). *Geological Society of America Abstracts with Programs*, 50(5), 2018. doi: 10.1130/abs/2018RM-313804.

Allen F Glazner and John M Bartley. Timing and tectonic setting of tertiary low-angle normal faulting and associated magmatism in the southwestern United States. *Tectonics*, 3(3):385–396, 1984.

Allen F Glazner, Jane E Nielson, Keith A Howard, and David M Miller. Correlation of the Peach Springs Tuff, a large-volume Miocene ignimbrite sheet in California and Arizona. *Geology*, 14(10):840–843, 1986.

Warren Hamilton. Mesozoic California and the underflow of pacific mantle. *Geological Society of America Bulletin*, 80(12):2409–2430, 1969.

Gregg E Hileman, Calvin F Miller, and Martin A Knoll. Mid-tertiary structural evolution of the Old Woman Mountains area: Implications for crustal extension across southeastern California. *Journal of Geophysical Research: Solid Earth*, 95 (B1):581–597, 1990.

KA Howard, ML Dennis, K Karlstrom, and GA Phelps. Preliminary geologic map of the Little Piute Mountains. *San Bernardino County, California: A Digital Database: US Geological Survey Open-File Report*, pages 97–693, 1997.

Keith A Howard and Barbara E John. Crustal extension along a rooted system of imbricate low-angle faults: Colorado river extensional corridor, California and Arizona. *Geological Society, London, Special Publications*, 28(1):299–311, 1987.

Barbara E John and David A Foster. Structural and thermal constraints on the initiation angle of detachment faulting in the southern basin and range: The Chemehuevi Mountains case study. *Geological Society of America Bulletin*, 105 (8):1091–1108, 1993.

Ronald W Kistler. Phanerozoic batholiths in western North America: A summary of some recent work on variations in time, space, chemistry, and isotopic compositions. *Annual Review of Earth and Planetary Sciences*, 2(1):403–418, 1974.

Martin A Knoll. Tertiary basin evolution, eastern Mojave Desert. *Ph.D. dissertation, University of Texas, El Paso*, 1988.

Gordon S Lister and Gregory A Davis. The origin of metamorphic core complexes and detachment faults formed during tertiary continental extension in the northern Colorado River region, USA. *Journal of Structural Geology*, 11(1-2):65–94, 1989.

Ivo Lucchitta and Neil H Suneson. Timing and character of deformation along the margin of a metamorphic core complex, west-central Arizona. *Geological Society of America Special Papers*, 303:147–170, 1996.

CF Miller, KA Howard, and TD Hoisch. Mesozoic thrusting, metamorphism, and plutonism, Old Woman-Piute Range, southeastern California. *Mesozoic-Cenozoic tectonic evolution of the Colorado River region, California, Arizona, and Nevada: San Diego, California, Cordilleran Publishers*, pages 561–581, 1982.

Jonathan S Miller. The Tertiary volcanic history and petrology of the Old Woman Mountains area, eastern Mojave Desert, California. *M.S. Thesis, Vanderbilt University, Nashville, Tennessee*, 1989.

Jonathan S Miller and Calvin F Miller. Tertiary extension related volcanism, Old Woman Mountains area eastern Mojave Desert, California. *Journal of Geophysical Research: Solid Earth*, 96(B8):13629–13643, 1991.

Jonathan S Miller, Matthew T Heizler, and Calvin F Miller. Timing of magmatism, basin formation, and tilting at the west edge of the Colorado River extensional corridor: Results from single-crystal 40Ar/39Ar geochronology of Tertiary rocks in the Old Woman Mountains area, southeastern California. *The Journal of Geology*, 106(2):195–210, 1998.

DS Musselwhite, DJ DePaolo, and M McCurry. The evolution of a silicic magma system: Isotopic and chemical evidence from the Woods Mountains volcanic center, Eastern California. *Contributions to Mineralogy and Petrology*, 101(1):19–29, 1989.

Jane E Nielson, James G Frisken, Robert C Jachens, and John R McDonnell Jr. Mineral resources of the Fort Piute Wilderness Study Area, San Bernardino County, California. 1987.

John M Proffett Jr. Cenozoic geology of the Yerington District, Nevada, and implications for the nature and origin of basin and range faulting. *Geological Society of America Bulletin*, 88(2):247–266, 1977.

John S Singleton, Daniel F Stockli, Phillip B Gans, and Michael G Prior. Timing, rate, and magnitude of slip on the Buckskin-Rawhide detachment fault, west central Arizona. *Tectonics*, 33(8):1596–1615, 2014.

Jon E Spencer. Role of tectonic denudation in warping and uplift of low-angle normal faults. *Geology*, 12(2):95–98, 1984.

Jon E Spencer. Miocene low-angle normal faulting and dike emplacement, Homer Mountain and surrounding areas, southeastern California and southernmost Nevada. *Geological Society of America Bulletin*, 96(9):1140–1155, 1985.

Jon E Spencer and Stephen J Reynolds. Tectonics of mid-Tertiary extension along a transect through west-central Arizona. *Tectonics*, 10(6):1204–1221, 1991.

John H Stewart. Regional tilt patterns of late Cenozoic basin-range fault blocks, western United States. *Geological Society of America Bulletin*, 91(8):460–464, 1980.

Paul Stone, Keith A Howard, and Warren Hamilton. Correlation of metamorphosed Paleozoic strata of the southeastern Mojave Desert region, California and Arizona. *Geological Society of America Bulletin*, 94(10):1135–1147, 1983.

George A Thompson. Problem of late Cenozoic structure of the basin ranges. *Int. Geol. Cong., XXI Session, Part XVIII*, pages 62–68, 1960.

Barry Alan Walker Jr., CF Miller, L Lowery Claiborne, JL Wooden, and JS Miller. Geology and geochronology of the Spirit Mountain Batholith, southern Nevada: implications for timescales and physical processes of batholith construction. *Journal of Volcanology and Geothermal Research*, 167(1-4):239–262, 2007.

Brian Wernicke and BC Burchfiel. Modes of extensional tectonics. *Journal of Structural Geology*, 4(2):105–115, 1982.

JL Wooden and DM Miller. Chronologic and isotopic framework for early Proterozoic crustal evolution in the eastern Mojave Desert region, SE California. *Journal of Geophysical Research: Solid Earth*, 95(B12):20133–20146, 1990.

Richard A Young and William J Brennan. Peach Springs Tuff: Its bearing on structural evolution of the Colorado Plateau and development of Cenozoic drainage in Mohave county, Arizona. *Geological Society of America Bulletin*, 85(1):83–90, 1974.

Appendix A: Map Unit and Sample Descriptions

Plate 1: Little Piute Mountains

Qal – Quaternary Alluvium

Unconsolidated alluvial deposits containing angular to rounded gravel to cobble size clasts in a sandy matrix. Clasts derived locally and from neighboring Old Woman Mountains. Found in active channels and across alluvial plains.

Qoal – Quaternary Older Alluvium

Moderately consolidated alluvial deposits containing angular to rounded gravel to cobble size clasts in a sandy matrix. Clasts derived locally and from neighboring Old Woman Mountains. Best exposed in walls of active channels and in erosional highlands of alluvial plains. Incised by active channels reflecting drop in drainage system base level.

Tus – Upper Gravel Conglomerate

Lithified coarse sand to coarse gravel conglomerate with pebble to small boulder clasts. Dominated by gravel matrix with thin interbedded finer layers. Conspicuous euhedral feldspars and biotite preservation in matrix indicate local sourcing and minimal transport/reworking. Clasts constitute ~10% of rock, mix of Precambrian to Mesozoic basement material and Cenozoic volcanics including boulders of Peach Spring Tuff and basalt. Clasts apparently mixed source from local exposures and Old Woman Mountains to west.

Tmp – Peach Spring Tuff (undifferentiated)

18.78 ± 0.02 Ma ignimbrite deposit characterized by abundant large (up to 5 mm) and clear chatoyant sanidine phenocrysts. Contains 10–20% phenocrysts overall, dominated by sanidine with lesser plagioclase, biotite, hornblende, titanite, and rare quartz. Displays typical ignimbrite zonation from unwelded base (Tpul) into devitrified, vapor phase altered, and moderately to densely welded interior. Welded portions are erosion resistant and commonly cap ridgelines. Vapor phase crystallization of quartz and chalcedony common.

Tmpu – Peach Spring Tuff (unwelded base)

Base of PST ignimbrite deposit. Composition and phenocrysts same as rest of PST, but with no welding, devitrification, or vapor phase alteration. Characterized by ashy white to pink groundmass and lower total phenocryst percentage. Grades up into basal black vitrophyre of PST. Erodes readily, preserved only beneath resistant outcrops of PST interior. Basal surge deposits rarely observed. Mapped as separate unit where exposed.

Tmba2 – Basaltic andesite lava flows (upper)

Undifferentiated sequence of basaltic andesite lava flows ranging from 1–7 meters thick. Flows form erosion resistant cliffs and are laterally continuous for up to 1 km. Typically contains 5-15% phenocrysts of clinopyroxene, orthopyroxene, plagioclase, Fe-Ti oxides, and minor olivine. Groundmass ranges from hypocrystalline to holocrystalline. Vapor phase alteration increasingly common in upper flows with crystal precipitation in lithophysal cavities. Base of unit defined by transition to cliff forming section and presence of devitrification and vapor phase alteration.

Tmba1 – Basaltic andesite lava flows (lower)

Undifferentiated sequence of basaltic andesite lava flows ranging from 1–3 meters thick. Flows form ledges with intervening slopes. Typically contains 5-10% phenocrysts of clinopyroxene, orthopyroxene, plagioclase, Fe-Ti oxides, and minor olivine. Groundmass ranges from hypocrystalline to holocrystalline. Minimal vapor phase alteration, generally more mafic and crystal poor compared to Tba1.

Tms – Basaltic cinder and scoria

Phenocryst poor basaltic cinder and scoria consisting of vesicular lava fragments ranging from millimeter to meter scale in diameter. Lava bombs sit in matrix of cinder and lava fragments. Blocks up to 35% vesicles with very few phenocrysts. Scoria is heavily oxidized and displays characteristic red color. Deposits are interpreted as eroded remnants of a cinder cone/eruptive center.

Tmc – Red cinder conglomerate and breccia

Pebble to coarse cobble conglomerate composed entirely of volcanic clasts derived from nearby eruptive centers and lava flows. Fragments mostly angular to subangular and poorly sorted.

Tmab – Andesite breccia

Autobrecciated lenses within andesite lavas (Ta), compositionally identical to Ta. Lenses typically thin and discontinuous, ranging from 5–150 m long.

Tma – Andesite lavas

Undifferentiated sequence of andesitic lava flows ranging from 1 to 10 m thick and up to 1 km long. Typically contains 7–15% phenocrysts of plagioclase, clinopyroxene, orthopyroxene, and Fe-Ti oxides. Phenocrysts up to 4 mm. Hypocrystalline groundmass. Forms large green to black cliffs and ridges. Lowest cliff forming rock in section. Ubiquitous flow banding and jointing.

Tmvb – Volcaniclastic breccia

Medium grained breccia dominated by angular basalt and basaltic andesite clasts ranging from pebble to cobble. Angular clast supported horizons. Dark red to brown sand matrix. <10% pre-Miocene basement clasts. Present in northern map area, forms small buttress against p€x. Underlies majority of volcanic sequence.

Tmd – Mafic dikes

Hypabyssal mafic intrusions in lower sedimentary and middle volcanic sections. Range from 1–4 m thick with exposures up 100 m long. Contain <15% phenocrysts of plagioclase and pyroxene. Rare phenocrysts up to 2 cm long, most <1 cm.

Tls3 – Plutoniclastic conglomerate

Plutoniclastic conglomerate composed of granitic detritus from Old Woman Mountain area. Dominated by 1–10 cm subrounded granitic cobble clasts. Clast imbrications indicate transport from west-southwest, toward OWP crest.

Tlb – Basalt lava flows

Basal volcanic rock in Miocene section. Sequence of ~5 basaltic lava flows 1–5 m thick. Diabasic groundmass. 7–13% plagioclase, olivine, and clinopyroxene phenocrysts. Deposited on Tgbc. Top and bottom of lava well exposed, interior recessive.

Tls2 – Granitic boulder conglomerate

Granitic sediments ranging from sandstone to boulder conglomerate. Dominated by coarse conglomerate with granite boulders up to 1.5 m in diameter. Matrix sand to gravel and entirely siliciclastic. Boulders similar in composition to surrounding Cretaceous plutonic exposures. Roughly 10% non-plutonic clasts.

Tls1 – Polymict coarse conglomerate

Basal sediments in section, dominated by Precambrian to Mesozoic clastic pebble to boulder conglomerates. Contains 20–40% clasts with matrix of medium sand. Coarse beds clast supported but mostly matrix supported. Oxidized at base of section directly above Miocene unconformity. Clasts typically subangular suggesting minimal transport distance from local sources.

Kg – Cretaceous Granodiorite

Cretaceous granodiorite pluton exposed around edges of mapping area and present throughout Little Piute Mountains, forms part of Old Woman pluton, dated 74 Ma. Light gray to tan, medium grained with titanite, hornblende, biotite, quartz, and feldspar. Alkali feldspar up to 1 cm across. Miocene sediments deposited unconformably on this unit. Sediments also form buttress unconformity against edge of Kg. Appears to be source for significant portion of Miocene siliciclastic sediments, especially in lower sedimentary section.

p€x – Precambrian crystalline basement

Precambrian metamorphic basement of eastern Mojave Desert region. Foliated with megacrystic K-feldspar and plagioclase plus quartz and biotite. Miocene sediments are deposited unconformably on this unit in the SE corner of map area.

Plate 2: Northwest Piute Mountains

Qal – Quaternary alluvium

Unconsolidated alluvial deposits containing angular to rounded gravel to cobble size clasts in a sandy matrix. Clasts derived locally and from neighboring crystalline core of Piute Mountain block. Found in active channels and across alluvial plains.

Qoal – Quaternary older alluvium

Moderately consolidated alluvial deposits containing angular to rounded gravel to cobble size clasts in a sandy matrix. Clasts derived locally and from neighboring Old Woman Mountains. Best exposed in walls of active channels and in erosional highlands of alluvial plains. Incised by active channels reflecting drop in drainage system base level.

Tcs – Upper coarse siliciclastics

Mixed sandstone and conglomerate deposited on upper PST. Contains roughly 40% PST clasts and 60% pre-Miocene basement, hypabyssal, and other volcanic clasts. Blocks of PST up to 1 m across, other clasts <50 cm.

Tp – Peach Spring Tuff

18.78 ± 0.02 Ma ignimbrite deposit characterized by abundant large (up to 5 mm) and clear chatoyant sanidine phenocrysts. Contains 10–20% phenocrysts overall, dominated by sanidine with lesser plagioclase, biotite, hornblende, titanite, and rare quartz. Subdivided in NWPM map area into six members based on welding, devitrification, and vapor phase alteration. Section in NWPM area is thickest preserved outflow sheet of tuff in Mojave, approaching 140 m. The unit is laterally continuous up to 5 km.

Tpuu – Peach Spring Tuff unwelded upper

Unwelded vitric top of tuff with abundant crystals (20%) but little to no lithic or pumice fragment preservation. Poorly exposed and sometimes not present due to rapid erosion and reworking following deposition. Thickness up to ~15 m but typically less.

Tpdu – Peach Spring Tuff devitrified upper

Devitrified cliff forming upper tuff. Moderate vapor phase alteration and crystallization but not pervasive. Characterized by erosion resistance, often caps PST sections. Dark brown to tan color with heavy desert varnish on exposed ridges. Moderately welded, up to 20 m thick.

Tpi – Peach Spring Tuff interior

Devitrified, heavily vapor phase altered interior of tuff. Abundant lithophysal cavities and vapor phase crystallization, precipitating quartz and chalcedony. Densely welded. Recessive between devitrified upper and lower cliff forming units. Pink to white color on fresh faces. Thickest member unit, up to 60 m.

Tpd – Peach Spring Tuff devitrified lower

Devitrified cliff forming band of lower tuff. Vapor phase alteration present in upper portion of this member. Gradational contact with top of Tpv. Densely welded with fiamme. Most resistant and best exposed member.

Tpv – Peach Spring Tuff vitrophyre

Black to grey moderately welded vitrophyre band in lower PST. Ranges from 3–5 m thick and laterally continuous, although distance above base varies.

Tpul – Peach Spring Tuff unwelded lower

Crystal poor unwelded base of tuff. White to tan with abundant ash to lapilli size pumice and lithic fragments. Typically obscured by erosion resistant colluvial blocks shed from overlying members.

Tpp – Peach Spring Tuff precursor deposits

Ash and lapilli fall and surge deposits predating arrival of PST. Cross bedding and uniform lapilli size fragments in surge layers. Deposits probably sourced from small precursor eruption closer to NWPM area.

Tbc – Boulder conglomerate

Very coarse cobble to boulder conglomerate dominated by pre-Miocene basement and basalt to basaltic andesite clasts. Primarily matrix supported with sub-rounded clasts up to 1.5 m in diameter.

Tss – Coarse sandstone

Coarse sandstone with minor gravel. Composed of approximately 80% quartz, 15% feldspar, and 5% mafic minerals. Average grainsize around 2 mm with moderately abundant pebbles up to 5 mm. Dominated by marble and metamorphic basement likely derived from neighboring Piute Mountain crystalline core. Stratigraphically continuous with Tbc but units never contact each other. Thickness of unit ranges from 10–40 m.

Trc – Dacite conglomerate

Monolithologic conglomerate composed of subangular hypabyssal dacite clasts in a medium grained sandy matrix. Clasts typically 1–25 cm across, up to 20% clasts in coarse beds. Matrix supported. Base of Miocene section, thickness varies throughout map area, mostly exposed in southern portion of map.

Pzm – Paleozoic metasediments

Paleozoic marble and quartzite. Foliated with meter scale folds throughout. Marble varies from grey to white to pink with coarse calcite rhombs. Quartzite uniformly tan-grey. Correlated with rocks of middle Grand Canyon sequence by Fletcher and Karlstrom, 1982.

p€ – Precambrian basement

Precambrian metamorphic basement of eastern Mojave Desert region. Foliated with megacrystic K-feldspar and plagioclase plus quartz and biotite. Miocene sediments are deposited unconformably on this unit throughout the mapping area.

Plate 3: Piute Range

Qal – Quaternary alluvium

Unconsolidated alluvial deposits containing angular to rounded gravel to cobble size clasts in a sandy matrix. Clasts derived locally. Found in active channels and across alluvial plains.

Qc – Quaternary colluvium

Talus and colluvium deposited by rock fall from resistant upslope units, primarily basalt lavas. Commonly obscures less resistant rocks and covers entire hillsides.

Qca – Quaternary caliche

Exposed caliche horizon near west edge of map area. Approximately 2 m thick and flat lying, forming consistent erosion resistant ledge around incised alluvium. Impermeable layer of white calcite precipitates.

QTl – Quaternary lacustrine deposits

Finely laminated silt and clay deposits between old and young alluvium. Approximately 150 m thick section of homogenous brown mud/clay/silt.

QToal – Quaternary older alluvium

Moderately consolidated alluvial deposits containing angular to rounded gravel to cobble size clasts in a sandy matrix. Clasts derived locally and from ranges to the west. Best exposed in walls of active channels and in erosional highlands of alluvial plains. Incised by active channels reflecting drop in drainage system base level.

Tb2 – Basalt lava flows

Undifferentiated sequences of basalt lavas ranging from 1–4 m thick and spanning up to 1 km laterally. Phenocryst content ranges from 2–8% plagioclase and iddingsitized olivine, up to 2 mm long. Groundmass typically glassy. Forms dip slopes and caps ridgelines.

Tvc2 – Intermediate volcaniclastic sediments

Mixed conglomerates and sandstones. Conglomerate dominated by dacitic and granitic rounded pebble to cobble size clasts in coarse sand matrix. Beds typically 15–30% clasts with rare clast supported layers. Interbedded sandstones range from medium to coarse grain, same composition as conglomerates. Abundant orange pumiceous clasts and minor mafic volcanic fragments. Stratigraphically continuous with units from Ta to uppermost Tb, deposited between and against lavas.

Td – Dacite lavas

Light to dark brown cliff forming andesitic to dacitic lavas. Distinguished by color and abundant (up to 10%) hornblende up to 5 mm. Commonly flow banded. Well preserved fault planes throughout. Terminates abruptly laterally indicating unit possibly formed as an effusive dome but contains thin interbedded sediments throughout.

Tav – Andesite vent remnants

Locally erupted lapilli to bomb size rounded fragments of andesitic lava. Mix of scoria, agglutinate, and cinder cone remnants.

Ta2 – Andesite lava flows and breccias

Thick (~100 m) succession of andesite lava flows, breccias, cinder, and Discontinuous pockets of autobrecciated and intensely flow folded lavas. Plagioclase, clinopyroxene, orthopyroxene, Fe-Ti oxides, and trace olivine phenocrysts occupy 8–13% volume. Holocrystalline groundmass with flow aligned plagioclase laths.

Tb1 – Basalt lava flows (lower)

Sequence of 2–6 m thick olivine basalt lava flows which overlie Tvc1 sediments and Ta1 lavas. Contains 5–12% phenocrysts of olivine, plagioclase, and clinopyroxene. Flows have vesicular base and top, cap ridges, form large cliffs.

Ta1 – Andesite lava flows and breccias

Laterally discontinuous andesite lavas and breccias of variable thickness. Flows can exceed 10 m thick and are challenging to differentiate. Discontinuous pockets of autobrecciated and intensely flow folded lavas. Plagioclase, clinopyroxene, orthopyroxene, Fe-Ti oxides, and trace olivine phenocrysts occupy 8–13% volume. Holocrystalline groundmass with flow aligned plagioclase laths.

Tvc1 – Volcaniclastic conglomerate, breccia, and sandstone

Volcaniclastic conglomerate, breccia, and sandstone dominated by basalt and andesite clasts ranging from gravel to small boulder size. Clasts are subangular to subrounded and locally sourced. Beds are laterally discontinuous with irregular thickness, sometimes interbedded with lava flows of similar composition. Bedding thickness ranges from <10 cm to >3 m. Interpreted as debris flow deposits sourced from flanks of neighboring volcanic centers. Unit includes basal basaltic breccia deposited directly on p€x.

p€x – Precambrian crystalline basement

Precambrian metamorphic basement of eastern Mojave Desert region. Foliated with megacrystic K-feldspar and plagioclase plus quartz and biotite. Miocene sediments are deposited unconformably on this unit in the SW corner of map area.

Table 1: Petrographic and Hand Sample Description

Field Area	Sample ID	Lat	Long	Map Symbol	Rock Type	Xtl %	Phase	Pheno/Gmass?	Modal %	Size Range	Groundmass Description	Phenocryst Description	Hand Sample Description
Little Piute Mountains	JN-LP-1	34.62248	-115.073475	Td	Basaltic dike	10	plag olv cpx fe-ti-ox	pg pg g g	5/65 5/2 3 20	0.3-2mm/<300um 0.3-1mm/<300um <300um <50-200um	Holoxtln w/ trachtyic groundmass texture w/heavy clay alteration and calcite + chalcedony alteration throughout.	Clay alteration of olv common, plag has normal zoning	Mafic dike from near vent rock area
	JN-LP-2	34.61155	-115.070331	Ta	Andesite lava flow	5	plag cpx opx fe-ti-ox	pg pg pg g	3/45 1/25 1/5 20	0.5-2.5mm/<500um 0.3-1.2mm/<300um 0.5mm/<300um <100um	Holoxtln w/pronounced flow banding and deflection of gmass grains around phenos. Fresh and unaltered w/abundant oxides.	Tabular plag w/rounded edges and small embayments but solid cores.	Platy andesite from hilltop near southern vent location. Close to breccia body within andesite.
	JN-LP-7	34.609541	-115.062547	Tb	Basalt lava flow	13	plag olv cpx fe-ti-ox	pg p pg g	3/70 4 6/3 14	0.5-3mm/60-500um 0.6-2.5mm 0.5-3.5mm/30-100um <100um	Diabasic groundmass (img 20) w/minor cpx, broad distribution of plag sizes	Plag shows nice sieve texture and reaction rim/possible groundmass growth? Cpx nicely preserved, olv completely clay altered.	Basal basalt for most of map area, sandwiched in Tpc. Sample from bottom of unit. Includes xenolith.
	JN-LP-8	34.613392	-115.066247	Tb	Basalt lava flow	8	plag olv cpx fe-ti-ox	g p pg g	73 5 3/4 15	50-300um 0.5-2mm 0.4-2mm/<150um <80um	Holoxtln plag+cpx+ox groundmass ranging from microxtln to 300um.	Olv pervasively altered to calcite and iddingsite. Cpx shows nice sieve texture but is otherwise unaltered. Distinct lack of plag phenos.	Red weathered pits of olivine (iddingsite) plus fresh cpx. A'a lava flow with rubbly base. Deposited on Ta2px and Tpc.
	JN-LP-9	34.614575	-115.071903	Tba	Basaltic andesite lava flow	8	plag olv cpx opx fe-ti-ox	pg p pg p g	3/48 1 3/4 1 40	0.5-2.5mm/100-500um 3mm 0.5-1.5mm/<150um 2mm <40um	Hypocrystalline groundmass dominated by fe-ti oxides and plag laths. Few small pockets of glass remain. Plag size range continuous from gmass to phenos.	Olv and opx single large xtls. Few large plag.	From first lava flow above cinder, clearly not associated with cone, flowed in from north and covered it up. Very fresh glassy? groundmass. Prismatic opx up to 2mm long, plag up to 1mm
	JN-LP-10	34.615101	-115.072139	Tba	Basaltic andesite lava flow	3	plag cpx fe-ti-ox	pg g g	3/50 2 50	0.5-2mm/<50um-500um <100um <50um	Coarse plag+ox dominated holocrystalline intergranular groundmass. Small euhedral cpx in space between gmass plag.	Nearly aphyric, some plag, some holes in ts inferred to be phenos	From just uphill of 9, not fresh. Apparently flowed in from north.
Piute Range	JN-PR-7	35.091087	-115.013308	Tb1	Basalt lava flow	6	plag olv cpx fe-ti-ox	pg p g g	3/70 3 6 18	0.5-1mm/25-500um 0.5-2mm <100um <60um	Holoxtln diabasic groundmass w/abundant large plag and small intergranular cpx (img 1,2). Variolitic plag.	Olv typically ~0.5mm, pervasively iddingsitized (img 3). Plag size distribution continuous but some large enough to have to be pheno. Distinct plag+olv xtl clot in center of slide.	Diabasic basalt capping section in canyon south of old govt road
	JN-PR-8	35.090893	-115.013243	Ta1	Andesite lava flow	8	plag olv cpx fe-ti-ox	pg p pg g	2/70 1 5/2 20	0.5-2mm/30-500um 0.3-0.7mm 0.3-1mm/<100um <80um	Holoxtln flow aligned gmass w/variably sized plag clearly deflected around phenos (img 1). Ox clots up to 800um across but individual grains mostly 20-80um.	Small cpx, few large plag w/clay alteration, iddingsite rims on olv.	Directly underlies PR-7
	JN-PR-9	35.094206	-115.008528	N/A	Basaltic dike	23	plag olv cpx opx fe-ti-ox	pg p g pg g	14/60 7 1 2/1 15	0.5-3mm/<100um 0.5-3mm <50um 0.5-0.8mm/<50um 20-100um	Holoxtln fine grain plag+ox dom groundmass w/trace pyroxenes.	Blocky euhedral plag w/resorbed and moderately embayed inner rims, sieve textured cores, and clean late stage rim growth. Large subhedral olv completely iddingsitized.	Intruded along fault
	JN-PR-10	35.093306	-115.007633	Tb1	Basalt lava flow	14	plag olv cpx opx fe-ti-ox	pg p pg pg g	4/70 6 1/1 2/4 12	0.5-1.2mm/50-300um 0.4-1mm 0.4mm/<80um 0.3-1mm/<100um <100um	Holoxtln fine grain plag+cpx+opx+ox gmass w/acicular flow aligned plag (img 1)	Olv iddingsitized. Plag elongate and tabular w/simple twinning and weak flow alignment. Pyroxenes small and anhedral.	Iddingsitized olv, depositional on lowest tephra above pC
	JN-PR-11	35.095314	-115.007226	Ta1	2px andesite lava flow	13	plag olv opx fe-ti-ox glass	pg p p g g	7/20 5 1 17 50	0.5-3.5mm/20-200um 0.4-2mm 0.2-0.8mm <30um	Hypoxtln gmass with 60% glass 40% xtls. Fuzzy brown intersertal glass, no fragments (img 15,16). Small abundant oxides and small plag laths throughout. Plag weakly flow aligned, deflects around phenos.	Well formed plag w/simple twinning, eu-subhedral, weak sieve texture in some grains. Individual dispersed grains of olv.	Above red breccia
	JN-PR-12	35.09556	-115.006669	Tb2	Basalt lava flow	14	plag olv opx fe-ti-ox	pg p g g	8/60 6 2 24	0.5-2mm/20-250um 0.3-2mm <40um <40um	Microxtln groundmass of plag+ox+opx (img 1) all gmass xtls <250um.	Olv clotted w/iddingsite rims. Plag normal.	Above 2px andesite